THE INTERACTION OF LIGHT AND MICROWAVES WITH PHOTOSYNTHETIC PIGMENTS

Dit proefschrift met stellingen van

SIEVERT JAN VAN DER BENT

doctorandus in de fysica, geboren te Deventer op 15 januari 1948, is goedgekeurd door de promotor dr. T.J. Schaafsma, hoogleraar in de molecuulfysica.

De Rector Magnificus van de Landbouwhogeschool,

H.C. van der Plas

Wageningen, 13 oktober 1977

S.J. van der Bent

THE INTERACTION OF LIGHT AND MICRO-WAVES WITH PHOTOSYNTHETIC PIGMENTS

proefschrift

ter verkrijging van de graad
van doctor in de landbouwwetenschappen,
op gezag van de rector magnificus,
dr. H.C. van der Plas,
hoogleraar in de organische scheikunde,
in het openbaar te verdedigen
op donderdag 8 december 1977
des namiddags te vier uur in de aula
van de Landbouwhogeschool te Wageningen

ISN = 104048-04

Aan mijn ouders

Aan Else Hans en Steven

VOORWOORD

Dit proefschrift is tot stand gekomen na drie jaar onderzoek waarbij ik van velen op de afdeling Moleculaire Fysica aan de Landbouwhogeschool en velen daarbuiten onmisbare steun heb gehad.

Allereerst wil ik Tjeerd Schaafsma danken voor zijn steun, met name bij het verwerken van de experimenten en het tot stand komen van dit proefschrift. Zijn soms wilde plannen hebben er toe bijgedragen dat de experimenten vaak met succes op voorheen onbegane paden zijn gedaan.

Henny van Beek, Simon Maasland en Adrie de Jager dank ik voor hun hulp bij het opbouwen en indien nodig in bedrijf houden van de meetopstelling. De preparatie van stoffen door Piet Geerse, Willem van Berkel en Henny Zoutendijk is voor het onderzoek onmisbaar geweest. Ik dank ook Willy Seldenrijk-Baas van de afdeling Biofysica in Utrecht voor het afstaan van de algen voor mijn onderzoek.

Ik wil allen danken die gewerkt hebben aan het drukklaar maken van dit proefschrift, in het bijzonder de heer Hoogeveen, die de tekeningen maakte, Tine de Vries en Nel Rozendaal-Pennings die het grootste deel van het typewerk deden.

Ik dank de North-Holland Publishing Company voor hun toestemming het in Chemical Physics Letters gepubliceerde artikel in dit proefschrift op te mogen nemen.

I am grateful to the American Institute of Physics and the Academic Press for their permission to copy articles which were published previously in the Review of Scientific Instruments and the Biochemical and Biophysical Research Communications respectively.

CONTENTS

LIST OF SYMBOLS AND ABBREVIATIONS

A	in formulae: arbitrary constant
$\underline{\underline{A}}$	matrix
A_{ij}	element of matrix $\underline{\underline{A}}$
α	arbitrary constant
Bph	bacteriopheophytin-a
Chl-a	chlorophyll-a
D	zero-field-splitting parameter
DCMU	3- (3,4-dichlorophenyl) -1, 1-dimethyl urea
$\Delta\phi_f$	relative difference between fluorescence-yield for $S_0 \rightarrow S_1$ excitation and $S_0 \rightarrow S_1$ (v) excitation, indicating the deviation from Vavilov's law (chapter 3)
E	zero-field splitting parameter; energy
E_x, E_y, E_z	energies of triplet spin states $\|x\rangle$, $\|y\rangle$, $\|z\rangle$ as referred to molecular axis-system
E_i, E_j, E_k	energies of triplet spin states $\|i\rangle$, $\|j\rangle$, $\|k\rangle$ no reference to axis system
FDMR	Fluorescence Detected Magnetic Resonance
$\mathcal{H}$	Hamiltonian operator
h	Planck's constant h = 6.625 10^{-34} Jsec
I	electric current
I,I'	excitation light intensities
I_f	fluorescence intensity
IC	interconversion
ISC	intersystemcrossing
$\bar{k}$	average decay rate constant as defined by: $\bar{k} = (\sum_m k_m n_m) / \sum_m n_m$
k_i, k_j, k_k	decay rate constant for lowest excited triplet spin state $\|i\rangle$, $\|j\rangle$, $\|k\rangle$ respectively
$k_{\ell\ell'}$	rate constant for transition from level ℓ to level ℓ': $\ell,\ell' = 1\text{-}6$; k_{21} is purely radiative
k_T	mean decay constant for decay from triplet spinstates $\|i\rangle$, $\|j\rangle$, and $\|k\rangle$; $k_T = \frac{1}{3} \sum_m k_m$; m = i,j,k
ℓ,ℓ'	$\ell,\ell' = 1\text{-}6$ labels excited state $\|\ell\rangle$; as a subscript for singlet or triplet states $\ell,\ell' = 0,1,2,\ldots$ e.g. $S_\ell = S_0, S_1, S_2$, etc.
λ	radiation wavelength or eigen value of a matrix

MTHF	3-methyltetrahydrofuran
m,m'	m,m' = i,j,k labels spin levels
$\|m\rangle$, $\|m'\rangle$	In zero magnetic field $\|i\rangle$, $\|j\rangle$ and $\|k\rangle$ correspond to spin states $\|x\rangle$, $\|y\rangle$ and $\|z\rangle$ which are eigenstates of the spin-operators $\underline{S}_x$, $\underline{S}_y$, $\underline{S}_z$, respectively i,j,k are ordered so that $E_i > E_j > E_k$; for $\pi\pi$ triplet states $E_x, E_y > E_z$
N	total number of molecules in a sample
$\vec{n}$	vector
$n_\ell, n_{\ell'}$,	relative population of excited level $\|\ell\rangle$, $\|\ell'\rangle$
$n_m, n_{m'}$,	relative population of triplet spin state $\|m\rangle, \|m'\rangle$
n_T	relative triplet population :$n_T \equiv \sum_m n_m$
ODMR	Optically Detected Magnetic Resonance
P	relative triplet populating rate
P_m	relative triplet populating rate to spin state $\|m\rangle$
Ph-a	pheophytin-a
PS	photosystem
PSU	photosynthetic unit
PTFE	polytetrafluorethylene
p_m	relative triplet populating rate normalized so that: $\sum_m p_m = 1$
$\phi_{TT}^{mm'}$	yield for formation of $T_o\|m'\rangle$ originating from the process $T_0\|m\rangle \rightarrow T_\ell\|m\rangle \dashrightarrow S^* \dashrightarrow T_0\|m'\rangle$
ϕ_T^m	yield of backformation of $T_0\|m\rangle$ following excitation $T_0\|m\rangle \rightarrow T_\ell\|m\rangle$, not including ISC processes
ϕ	general symbol for yield, defined as number of molecules participating in or produced by a particular process, divided by the number of absorbed photons
ϕ_f	fluorescence yield
ϕ_{TT}^m	yield for fluorescence originating from $T_o\|m\rangle \rightarrow T_n\|m\rangle$ absorption
$\bar{\phi}_{fT}$	average value of ϕ^m as defined in Chapter 3
ϕ_{ISC}^m	yield of formation of $T_o\|m\rangle$, following $S_0 \rightarrow S_1$ excitation

ϕ_{ISC}	yield of formation of T_o as defined by $\phi_{ISC} \equiv \sum_m \phi_{ISC}^m$
q_m	relative rate constant for $T_0\|m\rangle \rightarrow T_\ell\|m\rangle$ excitation followed by $T^* \dashrightarrow S^* \dashrightarrow T'^*$ ISC
$r_{mm'}$	relative rate constant for transition $T_0\|m\rangle \dashrightarrow T_0\|m'\rangle$ *via* T-T absorption and $T \dashrightarrow S^* \dashrightarrow T'$ *ISC processes
S_ℓ, S_ℓ',	singlet state with energy increasing when ℓ, ℓ' increases; S_0 = ground state; S_1 = first excited singlet state, etc; Generally ℓ, ℓ' = 0,1,2,3, etc
$\underline{S}_x, \underline{S}_y, \underline{S}_z$	spin operators for spin states $\|x\rangle$, $\|y\rangle$, $\|z\rangle$
S^*, T^*	excited singlet or triplet states
$T_\ell, T_{\ell'}$	triplet states with increasing energy when ℓ, ℓ' increases; T_0 = lowest excited triplet state, T_1 = first excited triplet state, etc; generally ℓ, ℓ' = 0,1,2,3, etc.
τ	lifetime, defined as the time elapsed after a quantity has decreased to 1/e of its original value through exponential decay
X,Y,Z	Energies of triplet spin states $\|x\rangle$, $\|y\rangle$, $\|z\rangle$
x,y,z	define molecular axis-system for porphyrins where x and y are two in-plane axes and z the out-of-plane axis. For dihydroporphyrins the x axis is parallel to the saturated pyrrole C-C bond
ZFS	zero-field-splitting

CHAPTER I

INTRODUCTION

1.1 GENERAL INTRODUCTION

The subject of this thesis is formed by the energy conversion in photosynthetic compounds, with particular emphasis on the energy converting pathways involving the lowest excited triplet state of pheophytins. These compounds can be obtained from the corresponding chlorophylls by replacing the central Mg ion by two protons. As has been shown in a previous study of the triplet state of chlorophylls [1,2], this modification does not essentially alter the kinetic properties of the lowest triplet state; using pheophytins instead of chlorophylls has the main advantage that the former compounds are photochemically more stable; also, thorough studies have been carried out on the triplet state of porphin free base [3-5]. Results of these studies are very helpful for a first interpretation of the spectral properties of pheophytins, for which porphin free base may be considered to be a suitable -although rather primitive- model compound. We have limited this study to two kinds of pheophytins derived from chlorophylls occurring in plants and algae: chlorophyll a and b. Bacteriopheophytins, derived from another important class of photosynthetic pigments, the bacteriochlorophylls,

a

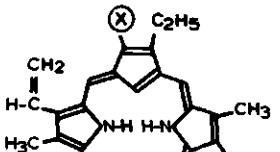

PHEOPHYTIN a: X = CH_3
PHEOPHYTIN b: X = CH_O

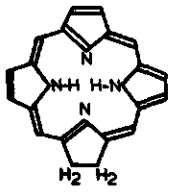

CHLORIN FREE BASE

b

Fig. 1.1.1 Chemical structure of pheophytins-a and b (lefthand side) and chlorin free base (righthand side).

which occur in photosynthetic bacteria [6], have been omitted from this investigation, mainly because they prove to be experimentally more difficult. The chemical structure of pheophytin-a and b is presented in fig. 1.1.1a; it is evident that the chromophoric group can be viewed as a porphin base of which pyrrole ring IV has been reduced. Such a dihydrophorphin, also called chlorin free base, is shown in fig. 1.1.1b. Its spectral properties carry much resemblance to those of pheophytins, although they are not identical. Pheophytin may be considered as a perturbed dihydroporphin free base, and therefore we have carried out a detailed study of the triplet state of this modelcompound of pheophytins, using a recently developed magnetic resonance technique. This technique, zero field optically detected magnetic resonance [7,8] has come out to be very attractive for the study of such complex molecules as pheophytins, and has yielded new and interesting data on a variety of even more complex systems such as enzymes [9], DNA [10], and photosynthetic reaction centers of plants [11], algae [12], and bacteria [13-16]. The potential of this method is only beginning to show as is demonstrated by the rapidly increasing amount of papers, among which are several excellent reviews [17-19]. For more details about ODMR, we refer to section 1.5 below, and Chapter 2,which treats experimental methods, both preparative and instrumental. This chapter partly consists of a reprinted paper from Review of Scientific Instruments. Although at first sight, the study of triplet state properties by ODMR may seem to be a rather limited approach to *in vitro* and *in vivo* energy conversion processes involving several excited states, kinetic and static properties of the triplet state, obtained from such ODMR studies provide information on other excited states and their kinetics as well, as is shown in Chapter 3. Also, slow processes suchs as photoinduced proton translocation in dihydroporphin free base can be followed by ODMR, whereas at the same time interactions of the lowest triplet state with other excited states can be extracted from kinetic ODMR data (Chapter 4 and 5).

Chapter 4 is a reprint of a paper published in Chemical Physics Letters, whereas Chapter 5 has been submitted to the Journal of Chemical Physics.

An outstanding problem in the optical spectroscopy of complexed photosynthetic pigments is the occurrence of multicomponent spectra, resulting from several types of complexed pigments. This occurs with many pigments *in vitro*, but certainly *in vivo*. As is shown in Chapter 6, ODMR is a suitable method for unravelling of such complex optical spectra. This Chapter has been submitted to Chemical Physics Letters. The last Chapter,

partly presented as a reprinted paper, is devoted to the application of ODMR to the study of the triplet state of chlorophyll-a and to what is thought to be its hydrogenated pheophytin derivative in a number of algae. It is the first report of its kind demonstrating the application of ODMR to an *intact* organism. It has been published in Biochemical and Biophysical Research Communications. All symbols, used throughout this Thesis, have been collected in a list, preceding Chapter I, and the less atractive parts of mathematical derivations have been removed from the reader's eye by dumping in an Appenditch.

1.2 RELEVANCE OF PHEOPHYTINS FOR IN VIVO SYSTEMS

The primary photochemical reaction in bacterial photosynthesis is the transfer of an electron from a bacteriochlorophyll complex P to an acceptor X. There is extensive evidence [20-27] that P consists of a bacteriochlorophyll dimer; X has been shown to contain iron chelated with a quinone, very similar to ubiquinone [28-31]. Between P and X, an intermediate I occurs, which is very likely to be bacteriopheophytin as follows from spectroscopic experiments [32,33]. The bacterial reaction center contains four bacteriochlorophylls, two bacteriopheophytins and approximately two equivalents of X [34-37]. The three compounds are thought to be held in place by surrounding proteins and are part of the entire electron-transport system. There is accumulating evidence, that the geometrical arrangement is such that two bacteriochlorophylls are coupled, forming a dimer, the two remaining chlorophylls being at larger distance than the first two, and being located on both sides of the dimer. Bacteriopheophytin is located between X and the chlorophylls. It has been possible to observe the trapped anion radical of bacteriopheophytin by low temperature magnetic resonance [33]. The data suggest considerable orbital overlap between $I^{\cdot-}$ and X^{-}. In bacterial reaction centers where electron tranport through X is blocked, a short lived intermediate state ($t_{\frac{1}{2}} \sim 10$ nsec) has been detected, where one electron finds itself on the (reduced) bacteriopheophytin [38,39]. This intermediate state may decay to the singlet groundstate by recombining both electrons in their singlet state, or to a lower lying triplet state, which has been detected by magnetic resonance both at high field [40-42] and at zero magnetic field [43,44]. The process carries much resemblance to cleavage resulting in radical fragments, originating from excited states, and it is therefore to be expected that magnetic fields may have a profound effect on both triplet

yield and the populating mechanism of this triplet state [45,46].
On the whole, the system represents a case where crucial information on the details of the primary photosynthetic act has been extracted from the unusual triplet state properties, found in these highly organized systems. Although it is clear that bacteriopheophytin participates in the primary photosynthetic act in bacteria, the significance of this observation is not yet fully understood and further studies are necessary to answer important questions concerning the exact geometrical arrangement of pigments, photoinduced potentials, and the excitonic interaction in these reaction centers. The rôle of pheophytins in plants and algae is much less clear. Although these compounds are found in chloroplast or algae preparations, usually one is not certain if they were naturally present or have been produced by chemical treatment. A similar rôle for pheophytins as an intermediate acceptor in chloroplasts has been suggested by van Gorkom [47]. This suggestion appears to be confirmed by luminescence measurements on the algae *Chlorella vulgaris* [48] and a very recent report on the detection of pheophytins in pea chloroplasts [49].

Finally, Mg^{2+} in chlorophylls can be replaced by 2 H^{+} upon irradiation with blue or UV light [50]. It is interesting to note that this phototransformation is inhibited by triplet quenchers, such as carotene and methylred, which has led to the conclusion that photopheophytinisation (!) occurs through the triplet state of the corresponding chlorophyll [50]. Such photoinduced pheophytinisation may be caused by local photoinduced pH gradients across membraned. At low pH, chlorophylls are chemically instable and are converted into pheophytins. Even in the absence of light, pheophytinisation can occur, and is one of the mechanisms causing the seasonal changes of colour in green leaves.

1.3 THE RELEVANCE OF TRIPLET STATE STUDIES ON PHOTOSYNTHETIC PIGMENTS IN RELATION TO PHOTOSYNTHESIS RESEARCH

By now, it has been well established that the triplet state of photosynthetic pigments, among which pheophytins, is not directly involved in the series of events, starting with the absorption of photons in living organisms at ambient temperature, and ending with the transfer of an electron of the reaction center to the electron transport chain. However, by adding an electron transport blocking agent, preventing electron transfer from the primary acceptor to the secondary and subsequent acceptors, the triplet

state of photosynthetic pigments may be trapped and studied at low temperature by magnetic resonance, or at ambient temperature by flash spectroscopy. In this way pheophytins and chlorophylls can be used as natural, non-perturbing probes, sensing the interaction of other parts of the photosynthetic system with the probing triplet. Sofar its use has been rather limited in this respect, but pioneering studies [11-17] have demonstrated that this approach is very fruitful and promising.

1.4 ENERGY CONVERSION IN PHOTOSYNTHETIC PIGMENTS

The most important energy levels involved in (optical) excitation of photosynthetic pigments are shown in fig. 1.4.1. By absorption of red light molecules are transferred from the singlet ground state S_0 into a first excited singlet state S_1 or into a second excited singlet state S_2 by blue light. Following excitation to one of these singlet states, different pathways are possible for deactivation of the excited molecule:

i) intermolecular energy transfer
ii) chemical reactions
iii) internal conversion, vibrational relaxation, and intersystem crossing
iv) radiative decay

The first process is the most important one for the *in vivo* chlorophyll forming the "antenna" [6]. The purpose of this antenna chlorophyll is the transfer of energy originating from absorbed light to an energy trap formed by the reaction center (see section 1.2), where the second process takes place. This reaction center is formed by a specially organized

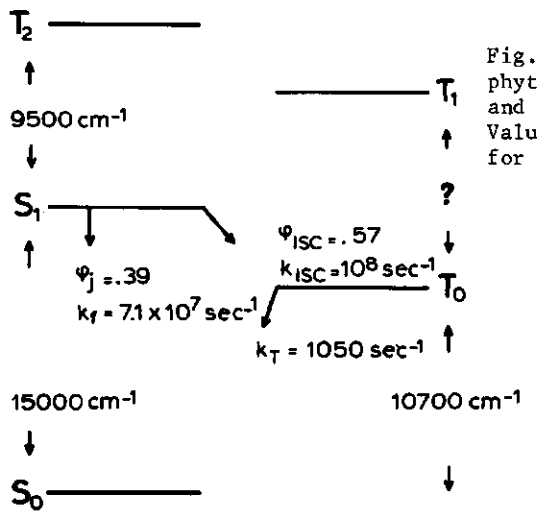

Fig. 1.4.1 Energy level diagram of pheophytin-a; the values of k_f, ϕ_f, k_{ISC}, and ϕ_{ISC} are those for chlorophyll-a. Values of all other parameters are those for pheophytin-a.

assembly of chlorophyll molecules ("special pair") for which the detailed structure may be different for green plants, algae, and photosynthetic bacteria [6,34-37]. At the reaction center the absorbed energy is converted into chemical energy through oxidation of the special pair from which an electron is transferred *via* an intermediate electron acceptor (which is in photosynthetic bacteria bacteriopheophytin [32,33]) to an electron transporting chain of a number of acceptors.

Apart from energy transfer and chemical reactions acting as deactivation processes, there is a possibility of intra molecular processes iii) and iv). These processes lead to losses of the total originally absorbed energy, and are suppressed in natural energy conversion mechanisms.
Although these processes are therefore not of direct importance in natural systems, *in vitro* studies of these intra molecular processes are very useful since a detailed knowledge of the internal energy conversion processes is necessary for an understanding of the naturally occurring processes i) and ii) mentioned above. In this Thesis we will therefore describe processes iii) and iv) within photosynthetic pigments based on results from experiments carried out on pheophytin-a and -b and some of its model compounds.

Let us now consider the nature of these intra molecular processes. As depicted in fig. 1.4.1 a molecule excited into the first or second excited singlet state can decay within the singlet manifold by $S_2 \rightarrow S_1$ (ν) interconversion followed by a fast relaxation process from $S_1(\nu)$ to the vibrationless S_1 state. From the latter the molecule can decay to the S_0 ground state with the emission of a photon (fluorescence) or radiationless by interconversion and vibrational relaxation. Generally, it is found that radiative processes dominate the $S_1 \rightarrow S_0$ decay, and we have therefore only considered the latter type of decay. A third pathway involves intersystem crossing (ISC) to the lowest excited triplet state denoted by T_0. From T_0 a second ISC process takes place to the S_0 ground state;in most photosynthetic pigments the latter process is almost exclusively radiationless; some weak phosphorescence can be found for chlorophylls and pheophytins [51,52].

The lowest excited triplet state has two important features. Firstly it has a relatively long lifetime, for photosynthetic pigments at $T < 77K$ $\sim$ 1 msec. If there is a high exciting light intensity, the molecule can be re-excited by the absorption of a second photon into a higher excited triplet state, the consequences of which are described in detail in chapter

3 for the case that this T-T absorption is not followed by a chemical decomposition of the molecule.

The second important feature of the triplet state is the fact that the three T_0 spinstates (see section 1.5) have different kinetic constants, which can be seen by cooling the sample to liquid the temperature or lower, diminishing the relaxation rate between the spin states. At room temperature the differences between kinetic constants of the various spin levels are dominated by such relaxation however.One of the consequences of this different kinetic behaviour is the larger population of the highest spin states w.r.t. that of the lowest spin state for *in vitro* photosynthetic pigments in model systems (e.g. chlorophylls, pheophytins, chlorin free base, porphin free base). Therefore these compounds can in principle show stimulated microwave emission at frequencies corresponding to the transition frequency between spin states. Thus, in principle, the compounds can be used for masers. A chlorophyll laser has been constructed [53,54].
Fluorescence and ISC yields have been previously measured by Gradyushko *et al* for chlorophyll-a, chlorin and similar compounds [55]. For the pheophytins, however, very little is known about the kinetic behaviour of states other than T_0. Since the effects of replacement of the central Mg^{++}-ion in the chlorophylls by the two central protons are relatively small for the spectroscopic properties, we assume that the yields for fluorescence and ISC ($S_1 \rightarrow T_0$) for chlorophyll-a [55] will be similar to those of pheophytin-a. Fig. 1.4.1 contains typical yields and rates for chlorophyll-a. Summarizing, we have studied those processes, which represent energy losses in the excited states of photosynthetic pigments, such as emission of microwaves, and fluorescence, as well as the generation of heat, causing spin lattice relaxation in the lowest triplet state of pheophytins and their model compounds.

1.5 THE PRINCIPLES OF ZERO FIELD MAGNETIC RESONANCE

An electronic triplet state has three magnetic substates, denoted as spin states; in the absence of an external magnetic field, these three spin states $|x\rangle$ $|y\rangle$ and $|z\rangle$ have energies corresponding to the eigenvalues of the zero field spin Hamiltonian.

$$\mathcal{H} = - (X \underline{S}_x^2 + Y \underline{S}_y^2 + Z \underline{S}_z^2) \qquad (1)$$

$\underline{S}_x$, $\underline{S}_y$, and $\underline{S}_z$ are the spin operators such that the eigen value of $\underline{S}^2$ =

$\underline{S}_x^2 + \underline{S}_y^2 + \underline{S}_z^2$ equals S (S+1) = 2 when expressed in units of $\hbar^2$ and S | > = 0. S (S+1) equals 2 for each of the zero field levels. Microwave induced transitions between spin states can occur when microwaves with frequency ν satisfy the resonance condition

$$\Delta E = \frac{\nu}{c} \tag{2}$$

where c is the velocity of light in cm sec^{-1}, ΔE is expressed in cm^{-1} and

$$\Delta E = |X-Y|, \ |Y-Z|, \text{ or } |X-Z| \tag{3}$$

Since changes induced by microwaves in the populations of spin states lead to small changes in the S_0 ground state population, due to the different decay rate constants of the individual spin states, these changes in the populations of states can be monitored *via* the fluorescence intensity which is coupled to the ground state population. These changes in the fluorescence intensity are in general small (typically $\sim$ 1 - 0.1 %) but detectable due to the high sensitivity of light detectors. For the detailed influence of the microwave irradiation on the fluorescence intensity we refer to previous papers [4, 56] and Chapter 3 of this Thesis.
Since the sum of the energies X + Y + Z equals zero, it is convenient to use the zero-field splitting parameters D and E defined such that

$$D \equiv \tfrac{1}{2} (X+Y)-Z = - 3/2 \ Z \tag{4a}$$

$$E \equiv \tfrac{1}{2} (X-Y) \tag{4b}$$

Then microwave transitions occur at energies 2 E, D-E and D+E (expressed in cm^{-1}), corresponding to the transitions between states |x> $\leftrightarrow$ |y>, |y> $\leftrightarrow$ |z>, and |x> $\leftrightarrow$ |z>, respectively.
In general the notation with x,y and z refers to a molecular axis system, therefore we have denoted the spin states with |i>, |j>, and |k> respectively, ordered by decreasing energy, independent of a molecular axis system. Only when possible, we have made an asignment for i,j, and k in terms of x,y and z.

Selection rules for microwave transitions between spin states |x>, |y>,

and $|z\rangle$ are derived from a perturbation Hamiltonian $\mathcal{H}'(t)$, given by

$$\mathcal{H}'(t) = H_1(t).\underline{S} \qquad (5)$$

where H_1 represents the microwave field, and $\underline{S} = \underline{S}_x + \underline{S}_y + \underline{S}_z$.
For microwave radiation polarized along the x-direction $\mathcal{H}' = H_1^x S_x$ the matrix elements $\langle\zeta|Sx|\zeta'\rangle$ determine the probability for transitions between spin levels $|\zeta\rangle$ and $|\zeta'\rangle$.
Since $S_x|x\rangle = S_y|y\rangle = S_z|z\rangle$ vanish, non-zero matrix elements are only obtained if ζ' is y or z with S_x as the operator. It is readily seen, that this only allows transitions between $|y\rangle$ and $|z\rangle$. Similarly, y polarized radiation induces transitions between $|x\rangle$ and $|z\rangle$, and z polarized radiation between $|x\rangle$ and $|y\rangle$.
At sufficient amplitude, resonant radiation connecting spin states $|\zeta\rangle$ and $|\zeta'\rangle$, equalizes their populations. We have excluded coherent effects occurring at still higher microwave power.
For a more detailed treatment of principles and applications of zero field magnetic resonance, we refer to some recent reviews [17-19,57].

1.6 REFERENCES

1. J.F. Kleibeuker, Thesis, Wageningen, 1977.
2. R.H. Clarke, R.E. Connors, T.J. Schaafsma, J.F. Kleibeuker, and R.J. Platenkamp, J. Am. Chem. Soc., 98 (1976) 3674-4677.
3. W.G. van Dorp, T.J. Schaafsma, M. Soma, and J.H. van der Waals, Chem. Phys. Lett. 21 (1973) 47-51.
4. W.G. van Dorp, W.H. Schoemaker, M. Soma, and J.H. van der Waals, Mol. Phys. 30 (1975) 1701-1721.
5. W.G. van Dorp, M. Soma, J.A. Kooter, and J.H. van der Waals, Mol. Phys. 28 (1974) 1551-1568.
6. Bioenergetics of Photosynthesis, ed. Govindjee (Academic Press, New York, 1975).
7. J. Schmidt, and J.H. van der Waals, Chem. Phys. Lett. 2 (1968) 640-642.
8. D.S. Tinti, M.A. El-Sayed, A.H. Maki, and C.B. Harris, Chem. Phys. Lett. 3 (1969) 343-346.
9. J.U. von Schütz, J. Zuchlich, and A.H. Maki, J. Amer. Chem. Soc. 96 (1974) 714-718.
10. R.J. Hoover, K.F.S. Luk, and A.H. Maki, J. Mol. Biol. 89 (1974) 363-378.
11. A.J. Hoff and J.H. van der Waals, Biochim. Biophys. Acta, 423 (1967) 615-620.
12. S.J. van der Bent and T.J. Schaafsma, Biochem. Biophys. Res. Comm. 71 (1976) 1147-1152.
13. R.H. Clarke, R.E. Connors, and H.A. Frank, Biochem. Biophys. Res. Comm. 71 (1976) 671-675.
14. R.H. Clarke, R.E. Connors, Chem. Phys. Lett. 42 (1976) 69-72.
15. A.J. Hoff, Biochim. Biophys. Acta 440 (1976) 765-771.
16. R.H. Clarke, Proceedings 3-rd. Specialized Colloque Ampere, Dublin, 1977, to be published.
17. A.L. Kwiram, MTP Int. Rev. Sci. Phys. Chem: Ser. One, Volume 4, Butterworths, London, 1972, p. 271.
18. M.A. El Sayed in ref. 17, volume 3, p. 119.
19. H. Maki and J.A. Zuclich in Topics in Current Chemistry, Vol. 54, p. 116-163, Springer Verlag, New York, 1975.
20. F.K. Fong, Appl. Phys. 6, (1975) 151.
21. H. Chow, R. Serlin, and C.E. Strouse, J. Am. Chem. Soc. 97 (1975) 7230.
22. J.J. Katz and J.R. Norris, Current Topics Bioenerg. 5 (1973) 41.

23. G. Feher, A.J. Hoff, R.A. Isaacson, and L.C. Ackerson, Ann. N.Y. Acad. Sci. 244 (1975) 239.
24. E.A. Dratz, A.J. Shultz, K. Sauer, Brookhaven Symp. Biol. 19, (1966) 303.
25. T.G. Ebrey, R.K. Clayton, Photochem. Photobiol. 10 (1969) 109.
26. R.H. Clarke, R.E. Connors, H.A. Frank, and J.C. Hoch, Chem. Phys. Lett. 45 (1977) 523.
27. J.R. Norris, M.E. Druyan, J.J. Katz, J. Am. Chem. Soc. 95 (1973) 1680.
28. D.W. Reed, J. Biol. Chem. 244 (1969) 4936.
29. D.W. Reed, R.K. Clayton, Biochem. Biophys. Res. Comm. 30 (1968) 471.
30. M.Y. Okamura, R.A. Isaacson, G. Feher, Proc. Nat. Acad. Sci. USA 72 (1975) 3491.
31. P.A. Loach, R.L. Hall, Proc. Nat. Acad. Sci USA 69 (1972) 786.
32. J. Fajer, D.C. Brune, M.S. Davis, A. Forman, and L.D.Spaulding, Proc. Nat. Acad. Sci. USA 72 (1975) 4956.
33. D.M. Tiede, R.C. Prince, G. Reed, P.L. Dutton, FEBS Lett. 65 (1976) 301.
34. W.W. Parson, T.G. Monger, Brookhaven Symp. Biol. June 1976, and references cited in this review.
35. P.L. Dutton, K.J. Kaufmann, B. Chance, P.M. Rentzepis, FEBS Lett. 60 (1975) 275.
36. D.W. Reed, G.A. Peters, J. Biol. Chem. 247 (1972) 7148.
37. S.C. Straley, W.W. Parson, D.C. Mauzerall, R.K. Clayton, Biochim. Biophys. Acta 305 (1973) 597.
38. W.W. Parson, R.J. Cogdell, Biochim. Biophys. Acta 416 (1975) 105.
39. R.J. Cogdell, T.G. Monger, and W.W. Parson, Biochim. Biophys. Acta 408 (1975) 189.
40. J.S. Leigh, P.L. Dutton, Biochim. Biophys. Acta, 357 (1974) 67.
41. R.A. Uphaus, J.R. Norris, J.J. Katz, Biochem. Biophys. Res. Comm. 61 (1974) 1057.
42. M.C. Thurnauer, J.J. Katz, J.R. Norris, Proc. Nat. Acad. Sci. USA 72 (1975) 3270.
43. R.H. Clarke, R.F. Connors, and H.A. Frank, Biochem. Biophys. Res. Comm. 71 (1976) 671.
44. R.H. Clarke and R.E. Connors, Chem. Phys. Lett. 42 (1976) 69.
45. A.J. Hoff, Biochim. Biophys. Acta 440 (1976) 765.
46. R.E. Blankenship, T.J. Schaafsma, and W.W. Parson, Biochim. Biophys. Acta, 461 (1977) 297.

47. H.J. van Gorkom, Thesis, University of Leiden, 1976.
48. J.A. van Best, and L.N.M. Duysens, Biochim. Biophys. Acta. 459 (1977) 187.
49. V.V. Klimov, A.V. Klevanik, V.A. Shuvalov, and A.A. Krasnovskii, Symp. Photosynthetic Oxygen Evolution, Tübingen, 1977, ed. H. Metzner, in press.
50. A.A. Krasnovskii and E.V. Pakshina, Dokl. Akad. Nauk. SSSR 148 (1963) 935.
51. A.A. Krasnovskii, V.A. Romanyuk, and F.F. Litvin, Dokl. Biophys. 209 (1973) 51.
52. A.A. Krasnovskii jr., N.N. Lebedev, F.F. Litvin, Dokl. Akad. Nauk SSSR 216 (1974) 1406.
53. J.C. Hindman, R. Kugel, A. Svirmickas, J.J. Katz, Proc. Natl. Acad. Sci. USA 74 (1977) 5.
54. D. Leupold, S. Mory, P. Hoffmann, B. Hieke, R. König, Chem. Phys. Lett. in press.
55. A.T. Gradyushko, A.N. Sevchenko, K.N. Solovyov, and M.P. Tsvirko, Photochem. Photobiol. 11 (1970) 387-400.
56. R.H. Clarke and R.H. Hofeldt, J. Chem. Phys. 61 (1974) 4582-4587.
57. J. Schmidt, Thesis, Leiden 1971.

CHAPTER 2

MATERIALS AND METHODS

Since we have described the preparations of the investigated compounds in other Chapters, we will treat remaining details in this Chapter.

2.1 MODEL COMPOUNDS

Meso-tetraphenylporphin free base (I) was synthesized according to Adler et al [1] I was obtained in almost quantitative yield and purified by sublimation in an oxygen-free nitrogen stream at 350-250 ^{o}C, yielding I as long, pink needles.

Meso-tetraphenylchlorin free base (II) was synthesized following Whitlock et al [2]. II was recrystallized from high purity grade benzene. Mass spectra revealing a dominant m/e = 616 peak were taken at a sample temperature of 100 ^{o}C; at higher sample temperature we have observed a strong increase of the 614 peak at the cost of that at 616, indicating the oxydation of II to I.

Chlorin free base (III) was synthesized following Eisner and Linstead [3]. It turns out that III is obtained in its most pure form if the reaction temperature is taken at 140 ^{o}C, using xylene as a solvent. Yields at 140 and 180 ^{o}C, using xylene and O-dichlorobenzene as solvents, were 0.33 and 0.50 %, respectively. If the reaction is carried out in sealed tubes at 220 ^{o}C [4], using O-dichlorobenzene as a solvent, III is obtained in 1.6 % yield. In addition to the chlorin mass peak at 312 impurities occur at m/e = 326 and 394. The relative amount of these impurities increases with increasing reaction temperature and may amount to - 30 %. The crude fraction obtained at 140 ^{o}C reaction temperature was purified by thin layer chromatography using silicagel as solid medium and benzene-heptane 5 : 1 mixture as an eluent. The visible absorption spectrum of a fraction with R_f = 0.6 agreed satisfactorily with literature data [3]. Purity was further improved by vacuum-sublimation.

2.2 NATURAL COMPOUNDS

The synthesis and sample preparation of pheophytins from chlorophylls is described in Chapter 6 of this Thesis.

2.3 ALGAE

For ODMR experiments on in vivo systems we used the following algae: *Anacystis nidulans, Euglena gracilis, Porphyridium cruentum, Chlorella vulgaris, Synechococcus cedrorum, Phaeodactylum tricornutum,and Visscheria stellata.*

All these algae except *Phaeodactylum tricornutum* were grown in an incubator shaker at 27 ^{o}C with a dark-light cyclus of 14 hrs light, 10 hrs dark. The air was slightly enriched with CO_2.

Phaeodactylum tricornutum was grown at 17 ^{o}C with constant illumination with extra addition of CO_2. All cultures were grafted on fresh medium every 3 or 4 weeks.

Anacystis nidulans was grown following Myers and Kratz [5] .

Euglena gracilis was grown in a 0.5 % solution of pepton Difco in tap-water.

Porphynidium cruentum and Phaeodactylum tricornutum were grown in an artificial sea water medium.

For *Phaeodactylum tricornutum* some waterglass was added.

Synechococcus cedrorum was grown in a solution following Emerson and Lewis [6] .

Chlorella vulgaris was grown in a medium as described in [7] .

Viscberia stellata was grown in a proteose medium: 1 gr Proteose pepton added to 1000 ml Bristol's solution [8] .

For the preparation of the samples we refer to Chapter 7 of this Thesis.

2.4 THE ODMR APPARATUS

Section 2.4.1 consists of a reprint of our paper containing a detailed description of the apparatus. In section 2.4.2 below we describe some recent improvements.

Optical detection and electronic simulation of magnetic resonance in zero magnetic field of dihydroporphin free base*

Sievert J. van der Bent, Adrie de Jager, and Tjeerd J. Schaafsma

Agricultural University, Department of Molecular Physics, De Dreijen 6, Wageningen, The Netherlands

(Received 14 August 1975)

An apparatus for the measurement of optically detected magnetic resonance (ODMR) in zero magnetic field at 4.2 K using commercially available parts is described. A simple electronic analogue device is used to obtain kinetic data from ODMR transients in a fast and reliable way. From these data decay rates of the three spin levels of the lowest molecular triplet state can be obtained, whereas populating rates can be determined within defined limits. Since the apparatus is suited for unguarded operation during long periods of time, signal averaging of weak signals, e.g., from biological molecules, is particularly easy. Kinetic data have been obtained for dihydroporphin, which can be considered as the structural basis for chlorophyll: $k_1 = 121 \pm 12$ sec^{-1}; $k_2 = 277 \pm 28$ sec^{-1}; $k_3 = 22 \pm 2$ sec^{-1}; $0.28 < P_1 < 0.43$; $P_2 = 1$; $P_3 < 0.08$, where k_i and P_i are the decay and populating rates of the ith spin level.

I. INTRODUCTION

Optical detection of magnetic resonance in the lowest molecular triplet state has proved to be a very sensitive and selective method as compared with detection of microwave absorption by diodes or bolometers.[1-3] At low temperature, relaxation between the three triplet spin levels can be slowed down sufficiently such that they can be considered as isolated. Under such conditions intersystem crossing occurs to and from separate spin levels. Microwave absorption resonant with energy separations between spin levels results in a change of spin level populations which can be monitored by the phosphorescence intensity, due to the fact that the spin levels generally have different radiative properties.[3-5] If phosphorescence emission cannot be used to monitor the changes in triplet state population—which is very common for biological molecules—magnetic resonance of the lowest triplet state can be detected by the effect on the $S_0 \leftarrow S_1$ fluorescence intensity.[3,6,7] This is to be expected since a triplet state population perturbation is transmitted to every part of the optical pumping cycle. As an illustration we present in this paper an application of this method to a model compound of a photosynthetic pigment, since for this type of molecule the phosphorescence emission is usually weak or absent, whereas the intersystem crossing is fast.[8-10] This approach provides the experimental basis for the study of more complicated biological systems, such as *in vivo* photosynthetic reaction centers.

II. EXPERIMENTAL

A. ODMR apparatus

For the type of molecule which we have studied, phosphorescence is absent or too weak to be useful in monitoring changes in triplet population. The microwave-induced changes in the fluorescence intensity are usually on the order of 0.1%–1%, which leads to the following instrumental requirements:

(1) Due to the low S/N ratio of the changes in the fluorescence intensity, averaging over many measurements is necessary. Therefore, the instrument must allow long periods of operation (typically 8 h).

(2) Noise from the excitation light source and the photomultiplier must be kept at a minimum.

(3) Since the measurements are carried out over prolonged periods of time, liquid helium losses must be low.

(4) Preferably, the instrument should allow unattended operation.

The experimental setup presented in Fig. 1 meets these requirements. We have replaced the conventional optical cryostat by a superisolated liquid He container: (L'Air Liquide model RS 25), with a capacity of 25 liters. This enables uninterrupted use over periods up to 3 weeks. Liquid He losses other than due to evaporation occur only by sample replacement. Thus the net loss of liquid He is considerably lower than with the filling procedure of conventional cryostats. With the 350–450 nm filtered output of a 200 W Osram superhigh pressure mercury arc focused onto the sample immersed in liquid He and with a microwave input of ~10 mW, the He losses typically amount to 50–60 cm^3/h, which is about twice the "dark" evaporation losses of the container.

For a description of the experimental setup we refer to Fig. 1. Excitation light from an Osram HBO 200 W/2 superhigh pressure mercury arc is passed through bandpass filters and diaphragms and focused onto the top of a quartz light guide (Suprasil, Schott), which

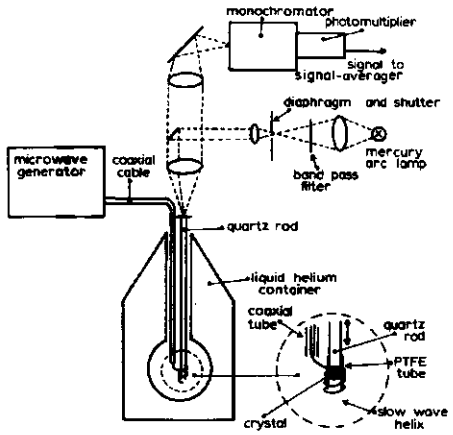

FIG. 1. Outline of ODMR apparatus suitable for long periods of operation. For details see text.

has no coatings. A small Al-coated surface mirror deflects the excitation light to the light guide, but does not obstruct the fluorescence light focused by two collecting lenses and a second mirror onto the slit of a 0.25 m Spex Minimate monochromator, equipped with an EMI 9659 QB extended S20 photomultiplier, thermoelectrically cooled to −35°C. (Products for Research, model TE 104). Microwave power from a Hewlett–Packard 8690B/8699B sweep generator is applied to the sample immersed in liquid He via an RG-213/U Amphenol cable and a coaxial line of stainless steel tubes (outer tube o.d. 8 mm, inner tube o.d. 3 mm; wall thickness of both tubes 0.2 mm). Styrofoam spacers keep the inner tube in position.

The rigid coaxial line terminates in a four-turn slow wave helix (1 mm Cu wire), surrounding a thin-walled Teflon tube containing the sample. The general features of the apparatus are very similar to those described by Schmidt,[3] who used a conventional cryostat. The assembly of light guide and microwave coaxial line fits into the superinsulated liquid He container, which has a 16 mm diam entrance. With −15 V pulses from a Farnell pulse generator, microwave power can be amplitude modulated. Signals are fed into a Hewlett–Packard 5480B signal analyzer for S/N improvement.

B. Equivalent electronic network

The simulation of the measured signals can be understood by noting that the fluorescence intensity is given by the expression

$$I_f(t) = A[N - \sum_{i=1}^{3} n_i(t)], \tag{1}$$

where $I_f(t)$ is the fluorescence intensity, A is a constant, N the total number of solute molecules in the sample, and n_i the number of molecules in the spin levels of the lowest excited triplet state.

A time dependent change $\Delta I_f(t)$ in the fluorescence intensity I_f, induced by a microwave pulse, is given by

$$\Delta I_f(t) = -A \sum_{i=1}^{3} \Delta n_i(t), \tag{2}$$

where $\Delta n_i(t) \equiv n_i(t) - n_i^o$; the superscript o refers to steady state populations under continuous illumination in the absence of microwaves.

When a saturating microwave field resonant with the energy difference between two triplet spin levels is applied, the populations of the two connected spin levels are equalized. In the absence of spin-lattice relaxation, application of resonant microwaves equalizing the populations of the ith and jth spin levels results in a change $\Delta I_f(t)$[7,11]:

$$\Delta I_f(t) = A(k_i - k_j)(n_i^o - n_j^o)(k_i + k_j)^{-1} \times\{\exp[\tfrac{1}{2}(k_i + k_j)t] - 1\}, \tag{3}$$

where $i \neq j = 1,2,3$; total decay constants are denoted by k and comprise both the radiative and the radiationless deactivation. Switching off the microwave field results in a time-dependent change $\Delta I_f(t)$ given by

$$\Delta I_f(t) = A(n_i^o - n_j^o)k_i k_j(k_i + k_j)^{-1} \times[k_i^{-1}\exp(-k_i t) - k_j^{-1}\exp(-k_j t)]. \tag{4}$$

The time-dependent changes in the fluorescence intensity expressed by Eqs. (3) and (4) can be simulated by an equivalent electronic network. We identify the spin level population n_i with an electric charge Q_i, decay constants k_i with $1/R_iC_i$, and populating rates P_i with electric currents I_i. A similar technique has been applied to high-field EPR transients.[12] Figure 2 represents the analogy between the optical pumping cycle involving the lowest molecular triplet state T_0 and the ground and

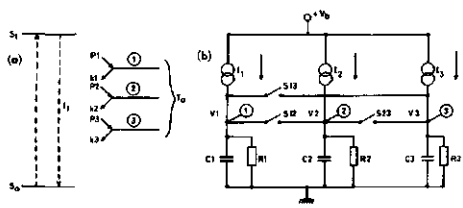

FIG. 2. (a) Optical pumping cycle involving molecular singlet states S_0 and S_1 and the lowest excited triplet state T_0. Dashed arrows refer to absorption and fluorescence; fully drawn arrows to and from triplet spin levels labeled by $i = 1, 2$, and 3 correspond to populating and decay processes with rates P_i and k_i, respectively. (b) Electronic network equivalent to Fig. 2(a) consisting of current sources I_i, capacitors C_i, and resistors R_i. Charges Q_i on C_i are measured by determination of the voltage V_i at points indicated by 1, 2, and 3 corresponding to similar labels in Fig. 2(a). Changes $-\Sigma\Delta V_i$ proportional to a change ΔI_f can be measured following closing and opening of any of the switches S_{ij}; V_b denotes the supply voltage; spin-lattice relaxation can be simulated with three extra resistors added parallel to the switches, not included in the schema. $C_1 = C_2 = C_3 = 0.5\ \mu$F; $R_1, R_2, R_3 = 1$–$100\ k\Omega$, variable, tolerance 1%; S_{12}, S_{23}, S_{13} reed relays (switching time 0.25 msec), Elec-Trol RA 30441051; I_1, I_2, I_3 variable between 100 μA and 10 mA.

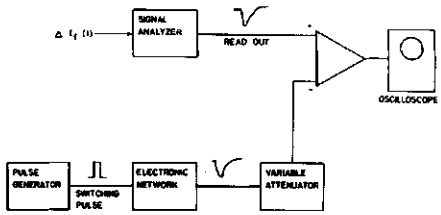

FIG. 3. Experimental setup for the fitting of the measured and simulated ODMR transients using a signal analyzer, a simulating electronic network, and a pulse generator. For details see text.

excited singlet states S_0 and S_1, and—on the other hand—an electronic network containing three current sources, capacitors, and resistors. The part of the network containing I_i, R_i, and C_i corresponds to one triplet spin level.

Applying a resonant microwave field connecting any two triplet spin levels (i) and (j) in Fig. 2(a) corresponds to closing a switch S_{ij} between the points (i) and (j) in the electronic network of Fig. 2(b).

The transient response of the network to closing or opening one of the switches S_{ij} is governed by the values of two feeding currents I_i and I_j and two RC constants $1/R_iC_i$ and $1/R_jC_j$.

According to Eq. (2), the changes in fluorescence intensity are determined by

$$\sum_{i=1}^{3} \Delta n_i,$$

corresponding to

$$\sum_{i=1}^{3} \Delta Q_i$$

in Fig. 2(b). Choosing all capacitors to be equal and noting that

$$\sum_{i=1}^{3} \Delta Q_i = C \sum_{i=1}^{3} \Delta V_i,$$

$\Delta I_f(t)$ is found to be proportional to

$$-\sum_{i=1}^{3} \Delta V_i(t),$$

where $\Delta V_i(t)$ is the change in potential at the points $i = 1$, 2, and 3 of Fig. 2(b).

Experimentally, currents and resistors are adjusted with calibrated ten-turn potentiometers, enabling a direct readout of the values of I and R which can be simply related to the absolute values of k and the relative magnitude of P and n for each spin level. In practice, only the decay rates and relative steady state population differences $(n_i^o - n_j^o)$ are uniquely determined by comparing simulated and experimental transients $\Delta I_f(t)$. This means that without further experimental data, the magnitude of n_i^o is determined up to an unknown additive constant. Then, the relative populating rates P_i can only be defined within certain limits. By introducing the absolute value of the triplet yield or the change in fluorescence intensity immediately after applying an exciting light pulse,[6,7] the relative population numbers and populating rates can be obtained.

The use of fast reed relays allows the simulation of pulsed microwave saturation. Note that the changes $\Sigma_i \Delta V_i$ result only from connecting or disconnecting 1, 2, and 3 and not from a change in the feeding currents I_i. This is analogous to the experimental situation where changes in I_f are observed during continuous optical excitation.

When the experimental $\Delta I_f(t)$ transient is stored in the memory of the analyzer, its output can be compared with that from the equivalent electronic network. The difference between these two transients can be monitored on an oscilloscope, allowing the determination of the values of I and R and giving an optimum fit between the measured and the simulated transient. Typically, the fitting boundaries are ~10% for the slow and ~5% for the fast decay rates. The method is schematically represented in Fig. 3. By inserting the values of R_i and C, the "kinetic" network constants corresponding to k_i can be determined in straightforward fashion, no calibration of the network against a standard compound being necessary. For representative purposes the repetition rate of the pulses entering the electronic network can be chosen different from the cycling time during the accumulation of experimental $\Delta I_f(t)$ transients. Then the simulated and experimental molecular kinetic constants are simply related by a known multiplication factor, i.e., the change in time base.

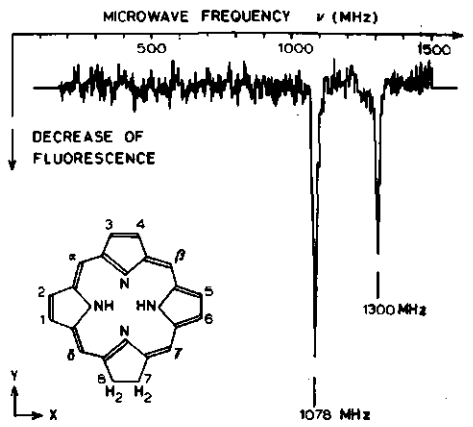

FIG. 4. Zero-field fluorescence detected ODMR spectrum of chlorin free base in a n-octane single crystal at 4.2 K; detection wavelength 635 nm; excitation via the filter combination: Calflex B1/K1 (Balzers), OB 14 (Chance Pilkington), and a 5 cm path length of saturated $CuSO_4$ solution. Microwave sweep 200–1500 MHz; microwave power ≈ 2.5 mW; accumulated over 2^{12} sweeps. Insert: structure of chlorin free base.

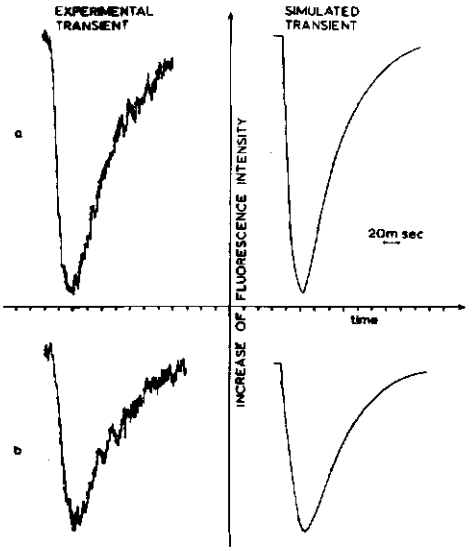

FIG. 5. Experimental and simulated fluorescence detected transients resulting from application of a resonant microwave pulse at (a) 1078 MHz and (b) 1300 MHz. Time scale: 20 msec/div; microwave pulse width: 25 msec. The simulated transients have been obtained by minimizing the voltage difference at all points with the experimental curves (see text).

III. TRIPLET STATE KINETICS OF DIHYDROPORPHIN FREE BASE

We have applied the method outlined before to the compound (chlorin, systematic name: dihydroporphin free base) shown in Fig. 4, which can be considered as the structural basis for chlorophyll. Monitoring the fluorescence $S_{00} \leftarrow S_{10}$ at the origin at 536 nm from a $10^{-6}M$ solution of chlorin free base in a *n*-octane single crystal, and simultaneously sweeping microwaves through the 200–1500 MHz region, results in an ODMR spectrum as shown in Fig. 4. Two transitions at 1078 and 1300 MHz are observed, the third one is absent.[13]

The performance of the apparatus can be estimated by noting that the ODMR spectrum of about 5×10^9 molecules can be detected with an S/N ratio of 20 with 2^{12} accumulated sweeps, using a 200 W Hg arc as an excitation source. For an accurate representation of the line shape in the ODMR spectrum it is necessary to meet the limit,

$$\nu_{rep} < \delta\nu \cdot \Delta^{-1} \cdot k_{min},$$

where ν_{rep} is the repetition rate for accumulation; $\delta\nu$ is the line width at half-height of a transition; Δ is the frequency domain covered in one sweep; and k_{min} is the smallest of all three decay constants. For chlorin free base, this means that with $\Delta \sim 1300$ MHz, $k_{min} \sim 20$ sec^{-1}, and $\delta\nu \sim 10$ MHz, $\nu_{rep} < 0.15$ sec^{-1}. Accounting for 10% dead time between cycles, this results in a total accumulation time of 8 h for 2^{12} sweeps. This time can be shortened to 2 h (2^{10} sweeps) by using a 900 W XBO xenon light source.

Now that the zero-field transition frequencies have been determined, we can apply resonant microwave pulses in order to obtain kinetic data on the populating and depopulating process. Referring to Fig. 5, transients in the fluorescence intensity are observed upon application of saturating microwaves at 1078 and 1300 MHz.

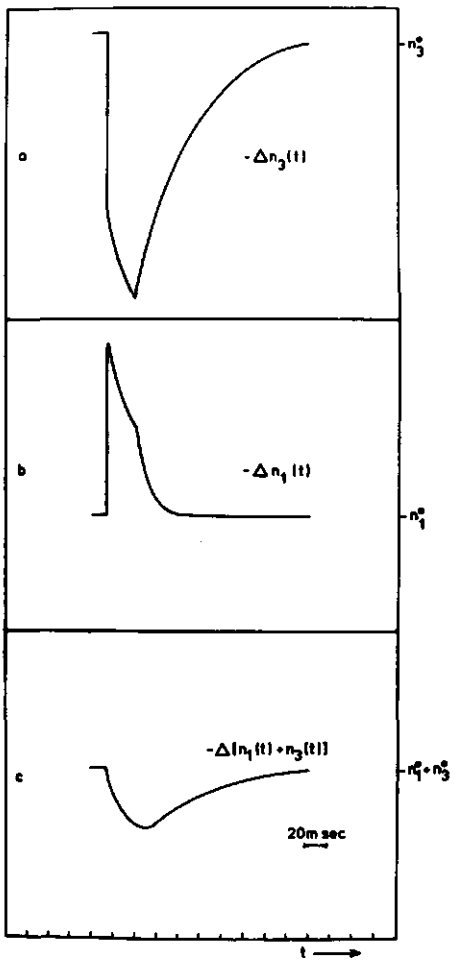

FIG. 6. Simulated time dependence of the population changes $-\Delta n_3(t)$ (a) and $-\Delta n_1(t)$ (b) in spin levels 3 and 1, respectively, resulting from application of a 25 msec duration resonant microwave pulse at 1300 MHz. The sum $-[\Delta n_1(t) + \Delta n_3(t)]$ as shown in (c) is proportional to the simulated change in fluorescence intensity $\Delta I_f(t)$ represented in Fig. 5(b). The upward direction in Fig. 6(a), 6(b), and 6(c) corresponds to a decrease of the populations and an increase of the fluorescence intensity; n_1^0 and n_3^0 represent the steady state populations in the absence of microwave power.

By comparing the output of the electronic equivalent network with the experimental zero-field transients as shown in Fig. 5, we have obtained the following data:

Total decay rates: $k_1 = 121 \pm 12\ \text{sec}^{-1}$; $k_2 = 277 \pm 28\ \text{sec}^{-1}$; $k_3 = 22 \pm 2\ \text{sec}^{-1}$ (estimated error limits including all instrumental inaccuracies).

Relative steady state population differences: $(n_2^0 - n_1^0) : (n_2^0 - n_3^0) : (n_1^0 - n_3^0) = 0.18 : 0.5 : 0.32$ ($\pm 10\%$). From the sign of $\Delta I_f(t)$ for transitions $1 \leftrightarrow 3$ and $2 \leftrightarrow 3$ and the values of k_1, k_2, and k_3 we find $n_3^0 < n_1^0$, n_2^0.

For the two extreme situations, (a) $n_3^0 = 0$; $n_1^0 \neq n_2^0 \neq 0$ and (b) $n_1^0 \approx n_2^0 \approx n_3^0$ one can calculate the relative values of the populating rates P_i, which are found to be within the limits $0.28 \leq P_1 \leq 0.43$; $P_3 \leq 0.08$ choosing $P_2 = 1$, and using $n_i^0 = P_i/k_i$.

In the absence of heavy atoms, such as in aza-aromatics and analogues of free base porphin, a parallelism is to be expected (and found) between populating and decay rates.[14] This means that the real situation mostly resembles (b), resulting in $P_1 : P_2 : P_3 \approx 0.29 : 0.66 : 0.05$.

It should be pointed out that an additional check of correct fitting is contained in the fact that a particular set of kinetic constants should lead to a simultaneous fitting to all three experimental transients, both with respect to their shape and their amplitude.

It is interesting to note that such a fit of the simulated to the experimental transients at 1078 and 1300 MHz results in a very small amplitude of the third simulated transient at 222 MHz, typically less than 10% of the amplitude of the other two transitions, corresponding to the fact that this transition was found neither in the ODMR spectrum nor as a transient.

By measuring the voltage at the points 1, 2, and 3 in the equivalent network of Fig. 2 separately, we are able to follow the time evolution of the populations in the three spin levels, even if we are not able to measure these changes in the zero-field experiment. As an illustration, Fig. 6 depicts the time-dependent changes in the populations of spin levels 1 and 3, as follows from the simulated curves. Note that these changes have been drawn to scale, illustrating that the change in the sum of two populations generally is smaller than that in the populations separately.

This can be expected since upon microwave saturation of a transition $i \leftarrow j$ the changes $\Delta n_i(t)$ and $\Delta n_j(t)$ are of opposite sign. Therefore, in the sum $\Delta n_i(t) + \Delta n_j(t)$ there is always partial cancelling of the two effects. If phosphorescence can be used to monitor the microwave-induced changes Δn_i and Δn_j, this may result in a more favorable sensitivity since in that case the change in signal intensity is proportional to $k_i^r \Delta n_i(t) + k_j^r \Delta n_j(t)$, where $k_{i,j}^r$ are generally different, radiative decay constants of spin levels i and j.

The straightforward method described above appears to provide a valuable tool for elucidating the energy conversion in photosynthetic pigments, both *in vitro* and *in vivo*.

ACKNOWLEDGMENTS

We are indebted to the staff of the physical chemistry machine shop for technical assistance and to P. Geerse for supplying us with a sample of chlorin free base.

* This research was supported in part by a NATO grant no. 921.

[1] C. P. Poole, *Electron Spin Resonance* (Interscience, New York, 1967), Chap. 11.
[2] *Electron Paramagnetic Resonance*, edited by S. Geschwind (Plenum, New York, 1972).
[3] J. Schmidt, Ph.D. thesis (University of Leiden, 1971).
[4] D. S. Tinti, M. A. El-Sayed, A. H. Maki, and C. B. Harris, Chem. Phys. Lett. **3**, 343 (1969).
[5] J. Schmidt and J. H. van der Waals, Chem. Phys. Lett. **2**, 640 (1968).
[6] W. G. van Dorp, T. J. Schaafsma, M. Soma, and J. H. van der Waals, Chem. Phys. Lett. **2**, 47 (1973).
[7] W. G. van Dorp, Ph.D. thesis (University of Leiden, 1975).
[8] G. P. Gurinovich, A. N. Sevchenko, and K. N. Solovyov, *Spectroscopy of Chlorophyll and Related Compounds* (Science and Engineering Publishing, Minsk, USSR, 1968), Chap. 7. (English translation by Natl. Techn. Inform. Service, Springfield, VA 22151).
[9] A. T. Gradyushko, A. N. Sevchenko, K. N. Solovyov, and M. P. Tsvirko, Photochem. Photobiol. **11**, 387 (1968).
[10] A. A. Krasnovskii, N. N. Lebedev, and F. F. Litvin, Dokl. Akad. Nauk. SSSR **216**, 1406 (1974). [English translation Dokl. (Biophysics) **216**, 39 (1974).]
[11] R. H. Clarke and R. H. Hofeldt, J. Chem. Phys. **61**, 4582 (1974).
[12] J. F. Kleibeuker and T. J. Schaafsma, Chem. Phys. Lett. **29**, 116 (1974).
[13] S. J. van der Bent and T. J. Schaafsma, Chem. Phys. Lett. **35**, 45 (1975).
[14] D. Antheunis, Ph.D. thesis (University of Leiden, 1974).

2.4.2. IMPROVEMENTS IN ODMR APPARATUS

In order to improve the S/N ratio we have replaced the 200 w mercury are lamp by a 900 w Xenon arc lamp (Osram XBO 400 w/r.) For the irradiation of the sample with two resonant microwave frequencies we used the following set-up:
The output from two sweep-generators (Hewlett-Packard 8620C/86220A and 8690B/8699B), was seperately amplified using an Avantek AMP 200 amplifier for the 1-2 GHz region and an Avantek UA 405 amplifier for the 20-1000 MHz region. After amplification the two frequencies were coupled via an Anzac H-183-4 "Hybrid T", preventing one microwave frequency to influence the source of the other microwave frequency. It turned out to be important to amplify the microwaves before mixing , since addition before amplification may result in harmonic distortion yielding not only the two original frequencies, but also sum and difference frequencies. The power was monitored at one of the parts of the Hybrid T using a Hewlett-Packard 423A detector. If necessary, attenuators (Hewlett-Packard 8491A series) were used to prevent overloading of the amplifiers.

2.5 OPTIMIZING SIGNAL TO NOISE RATIO

For most of the measurements reported in this Thesis, we have employed a signal analyzer for signal-to-noise (S/N) improvement, with such a device one feeds noisy signals periodically into a digital memory.
For the special case of light-induced decomposition of the sample material, as occurs in algae (see Chapter 7), it is necessary to determine the total period of accumulation for which maximum S/N of the recorded signal is obtained. With a first-order decomposition process, characterized by a rate-constant k_d, it can be easily derived that

$$S/N(t) = S/N(0)\ k_d^{-1} t^{-\frac{1}{2}} [1-e^{-k_d t}] \quad \text{for } t > 0 \qquad (1)$$

The maximum S/N ratio is found for an accumulation period $t \sim k_d^{-1}$.

2.6 FITTING EQUATIONS TO DATA

For single-exponential fitting of experimental transients, as described in Chapters 4-6 and using equations represented in Chapter 3, we have made use

of a program of Daniel and Wood [9] after lineairization of exponential decaycurves. Double exponential fitting was carried out using an algorithm described by Fiacco and McCormick [10] and applied in the optimization package OPTPAC III, obtained from Corporate ISA's SCA-group of N.V. Philips Gloeilampenfabrieken, Eindhoven, The Netherlands.

2.7 REFERENCES

1. A.D. Adler, F.R. Longo, J.D. Finarelli, J. Goldmacher, J. Assour, and J. Korsakoff, J. Org. Chem. 32 (1967) 476
2. H.W. Whitlock, R. Hanauer, M.Y. Oester, and B.K. Bower, J. Amer. Chem. Soc. 91 (1969) 7485
3. U. Eisner and R.P. Linstead, J. Chem.Soc. (1955) 3742-3754
4. G.D. Egorova, K.N. Solovev, and A.M. Shulga, Zhurnal Obsh. Khim. 37 (1967) 357
5. J. Myers and W.A. Kratz, J. Gen. Bot. 39 (1955) 11
6. J. Emerson and S. Lewis, J. Gen. Physiol. 25 (1942) 579
7. Zur Beitrage zur Physiologie und Morphologie der Algen (G. Fisher Verlag, Stuttgart, 1962) p. 157.
8. Starr, The Culture of Algae at Indiana University.
9. C. Daniel and F.S. Wood, Fitting Equations to Data (Wiley-Interscience, New York, 1971).
10. A.V. Fiacco and P.G. McCormick, Programming under non-linear constraints by unconstrained minimization: A primal dual method (Research analysis Corp. R.A.C.-T.P., Bethesda , N.D., 1963).

CHAPTER 3

KINETIC THEORY OF ODMR

3.1 INTRODUCTION

In this chapter we will derive rate-expressions for the kinetics for populating and decay of the electronically excited triplet (sub]states relevant for optical detection of magnetic resonance of nonphosphorescing molecules. Part of the expressions which are important for our work have been reported in literature [1-3].

In this study we will emphasize on the effects of T-T absorption, spin-lattice relaxation (SLR), and high light intensity on kinetic equations. A similar study has been carried out by Clarke *et al.* [4], neglecting SLR. Most of the experiments described in Chapters 5-7 are carried out at 4.2 K, where spin-lattice relaxation between triplet spinlevels cannot be neglected, in particular for *in vivo* systems; furthermore, for reasons of sensitivity it is necessary to employ considerable light intensity for excitation. Under these conditions, T-T absorption cannot always be avoided in particular for porphyrins and chlorins, which have overlapping S-S and T-T bands. The kinetic equations derived in this Chapter provide the necessary framework for understanding the experimental results. Auxiliary mathematics which are helpful in deriving and understanding the equations are presented in Appendix I.

3.2 DISTRIBUTION OF MOLECULES OVER ENERGY LEVELS AS A FUNCTION OF LIGHT INTENSITY

Figure 3.2.1 represents the most important energy levels, participating in the optical pumping cycle of an ODMR experiment, including both $S_0 \rightarrow S_2$ and $T_0 \rightarrow T_n$ excitations. For convenience the electronic levels have been numbered by ℓ ,ℓ' = |1> through |6>, such that excitation-, interconversion-, and ISC rate constants are given by $k_{\ell\ell'}$, (ℓ,ℓ' = 1-6). These constants include both radiative and radiationless transitions. Optical excitations take place at a rate $I(\lambda)\, k_{\ell\ell'} n_{\ell}$ from state $|\ell>$ to state $|\ell'>$ where $I(\lambda)$ denotes the excitation light intensity at wavelength λ and n_{ℓ} is the population of state $|\ell>$; $I(\lambda)$ and

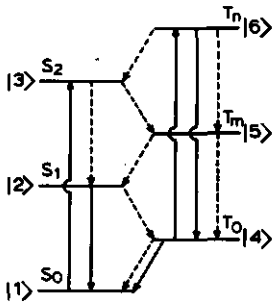

Fig. 3.2.1.
Level diagram of the relevant singlet states S_0, S_1, S_2, triplet states T_0, T_m, T_n, and deactivation pathways involved in an optical pumping cycle; levels are numbered |1> through |6>; fully drawn lines denote optically allowed transitions; dashed lines mark radiationless transitions.

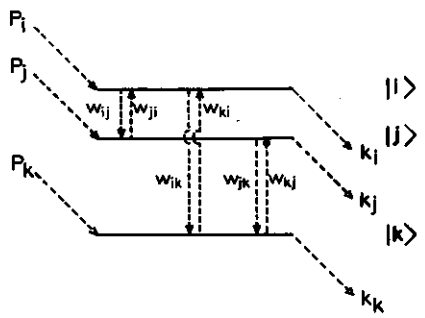

Fig. 3.2.2.
$T_0|m>$ spin states, populating rates P_m, decay rate constants k_m and relaxation rate constants $w_{mm'}$, where m,m'=i,j,k.

I'(λ) are taken to be dimensionless and correspond to $S_0 \rightarrow S_2$ and $T \rightarrow T_n$ excitations, respectively.

Defining the fraction of molecules in each level |1> through |6> by n_1 through n_6 such that $\sum_{\ell=1}^{6} n_\ell = 1$, the molecular kinetics follow from the set of differential equations for $\dot{n}_\ell \equiv \frac{dn_\ell}{dt}$

$$\dot{n}_1 = -Ik_{13}\, n_1 + k_{21}\, n_2 + k_{41}\, n_4 \tag{1a}$$

$$\dot{n}_2 = -(k_{21} + k_{24})\, n_2 + k_{32}\, n_3 + k_{52}\, n_5 \tag{1b}$$

$$\dot{n}_3 = Ik_{13}\, n_1 - (k_{32} + k_{35})\, n_3 + k_{63}\, n_6 \tag{1c}$$

$$\dot{n}_4 = k_{24}\, n_2 - (k_{41} + I'k_{46})\, n_4 + k_{54}\, n_5 + k_{64}\, n_6 \tag{1d}$$

$$\dot{n}_5 = k_{35}\, n_3 - (k_{52} + k_{54})\, n_5 + k_{65}\, n_6 \tag{1e}$$

$$\dot{n}_6 = I'k_{46}\, n_4 - (k_{63} + k_{65} + k_{64})\, n_6 \tag{1f}$$

For these differential equations the following assumptions have been made:

(i) Only one S-S and one T-T excitation is considered; $S_0 \rightarrow S_1$ excitation is disregarded.

(ii) The triplet state is regarded as a single level, i.e. the presence of three spinlevels is ignored.

(iii) Excitation into vibronic levels is taken to be equivalent to excitation directly into the vibrationless state.

Concerning assumption (i), we note that usually kinetics are measured using $S_0 \rightarrow S_2$ excitation. As will be subsequently shown, this does not make any difference for the determination of the kinetic constants of the lowest triplet state.

Considering the three spinstates of an electronic triplet state as a single state, results in simplified kinetic equations.
Since always

$$\dot{n}_T = \dot{n}_i + \dot{n}_j + \dot{n}_k \tag{2}$$

where n_m denotes the fraction of the total number of molecules N, occupying the spinstate $|m\rangle$ of the electronic triplet state (m = i,j,k) and n_T defines the *total* fraction of molecules occupying all three spin states $|m\rangle$ (see fig. 3.2.2).

We can now define an *effective* decay constant k_{eff} by writing

$$\dot{n}_T = - k_{eff}\, n_T + \sum_m \sum_\ell k_{\ell 4}^m\, n_\ell^m - \sum_m I' k_{46}\, n_m \tag{3a}$$

$$\dot{n}_T = \sum_m k_m\, n_m + \sum_m \sum_\ell k_{\ell 4}^m\, n_\ell^m - \sum_m I' k_{46}\, n_m \tag{3b}$$

Combining (3a) and (3b) defines k_{eff}:

$$k_{eff} \equiv \frac{1}{n_T} \sum_m k_m\, n_m \tag{4}$$

where m = i,j,k labels spinstates; $\sum_\ell$ includes sommation over all triplet spin states or singlet states from which the triplet state $T_0|m\rangle$ is populated at a rate $k_{\ell 4}^m\, n_\ell^m$; k_m is the total decay rate constant of the spin state $|m\rangle$. As will be shown in the following, eqns. (1 a-f) can be simplified in this manner. Note however, that k_{eff} cannot be considered to be a molecular constant, since we can change its value by varying the temperature or by applying a resonant microwave field connecting spin levels.
For high temperature when SLR dominates triplet decay rates

$$k_{eff} = \frac{1}{3} \sum_m k_m \tag{5}$$

We are interested in the change of the fluorescence intensity I_f and the fractional lowest triplet state population n_T (= n_4) caused by connecting two or three T_0 spin levels by resonant microwaves. The expression for I_f as a function of the constants $k_{\ell\ell'}$, ($\ell,\ell' \neq 4,1$) and the variables I,I', and k_{eff} (= k_{41}) for the steady state situation (i.e. $\dot{n}_\ell = 0 (\ell = 1\text{-}6)$) is given by

$$I_f = \frac{I\, k_{13}\, k_{21}\, (1-\Delta\phi_f)\, (k_{41} + I' k_{46} \bar{\phi}_{fT}) + I\, k_{13}\, I' k_{46} \bar{\phi}_{fT}\, (k_{24} + \Delta\phi_f k_{21})}{I\, k_{13}\, (k_{24} + \Delta\phi_f\, k_{21}) + (k_{21} + k_{24})\, (k_{41} + I'\, k_{46} \bar{\phi}_{fT})} \qquad (6)$$

where I_f is expressed in number of photons emitted per molecule per second. We define

$$\Delta\phi_f \equiv \sum_m \frac{k^m_{35}\; k^m_{54}}{(k_{32} + k_{35})(k^m_{54} + k^m_{52})} \qquad (6a)$$

and:

$$\bar{\phi}_{fT} \equiv \sum_m \left[\frac{k_{21}}{k_{21}+k_{24}} \; \frac{k^m_{63}\, \Delta\phi_f}{k^m_{63}+k^m_{64}+k^m_{65}} + \frac{k^m_{65}\; k^m_{52}}{(k^m_{63}+k^m_{64}+k^m_{65})(k^m_{54}+k^m_{52})}\; n_m \cdot n_T^{-1} \right] \qquad (6b)$$

Defining the fluorescence yield $\phi_f\ (S_0 \rightarrow S_n)$ as the number of fluorescence quanta emitted per second divided by the number of excitations per second for the $S_0 \rightarrow S_n$ transition *in the absence of T-T absorption* ($I' = 0$), we find

$$\Delta\phi_f = \frac{\phi_f(S_0 \rightarrow S_2) - \phi_f(S_0 \rightarrow S_1)}{\phi_f(S_0 \rightarrow S_2)} \qquad (7)$$

$\Delta\phi_f$ is thus the relative difference in the fluorescence yield for $S_0 \rightarrow S_2$ and $S_0 \rightarrow S_1$ excitation caused by ISC directly from $S_2 \rightarrow T_m$.
$\bar{\phi}_{fT}$ is the fraction of $T_0 \rightarrow T_m$ excitations resulting in deactivation through the pathways:
$T_n \dashrightarrow S_2 \dashrightarrow S_1 \rightarrow S_0$, $T_n \dashrightarrow T_m \dashrightarrow S_1 \rightarrow S_0$, and $T_n \dashrightarrow S_2 \dashrightarrow T_m \dashrightarrow S_1 \rightarrow S_0$.
The value of both $\Delta\phi_f$ and $\bar{\phi}_{fT}$ is between 0 and 1, and depends on the type of molecule and its surroundings.

In deriving (6), two assumptions have been made:

(i) k_{21} is purely radiative as found for porphyrins, chlorins, chlorophyll and pheophytins [5];

(ii) the probability for finding a molecule in a state other than S_0 or T_0 is taken to be so small that to a high degree of accuracy $n_1 + n_4 = 1$ (see Appendix I).

Eqn (6) is only valid in the absence of energy transfer or photochemical decomposition.

As is evident from (6), I_f is non-linear in the excitation light intensity I, but *in the absence of T-T absorption* there is a linear dependence of I_f^{-1} vs I^{-1}; then

$$I_f^{-1} = \frac{k_{24} + \Delta\phi_f k_{21}}{k_{21}(1-\Delta\phi_f) k_{41}} + \frac{k_{21} + k_{24}}{k_{21}(1-\Delta\phi_f)} \cdot \frac{1}{I k_{13}} \qquad (8)$$

The slope of the linear plot of I_f^{-1} *vs* I^{-1} is given by $\frac{k_{21} + k_{24}}{k_{21}(1-\Delta\phi_f)}$ i.e. ϕ_f^{-1} $(S_0 \rightarrow S_2)$.

Figure 3.2.3 represents a plot of the fluorescence intensity I_f as a function of excitation rates Ik_{13} and $I'k_{46}$, with ϕ_{fT} as a parameter. We have taken $\Delta\phi_f$ to be zero and have adopted values for $k_{\ell\ell}$, which are common to porphyrin-like molecules. These values have been used throughout Chapter 3, so that calculated curves in different sections of this Chapter can be compared.

We will now consider possible spin-effects on the processes involving T-T absorption and ISC crossing from $T_n|m\rangle$ to $S_n(v)$. In the most general case (i), $\bar{\phi}_{fT}$ is spin-dependent and no spin-flip is assumed during the spin-selective $T_0|m\rangle \leftrightarrow T_n|m'\rangle$ T-T absorption- and IC processes. Relaxing the spin-selection w.r.t. $T_n|m'\rangle \rightarrow S_n(v)$.ISC results in a spin-independent $\bar{\phi}_{fT}$ and a spin-selective T-T process (case ii). Finally, we may conceive that both $T_n|m'\rangle \rightarrow S_n(v)$ ISC and T-T processes are totally spin-independent (case iii).

It depends on the type of molecule (through factors such as density of states at T_n, ISC matrix coupling elements, etc.) which of these cases applies.

For large molecules the most likely case appears to be (iii) because of a physical argument: such molecules generally are expected to have relatively small ZFS values and short spin state lifetimes of T_n. Then, lifetime broadening of all T_n spin states removes spin-dependency from $T_n|m'\rangle \rightarrow S_n(v)$ and $T_0|m\rangle \leftrightarrow T_n|m'\rangle$ processes. This means that in all equations following this section the index m can be dropped from the equations defining $r_{mm'}$ and q_m (17a,d etc.).

Fig. 3.2.3 has been calculated for case (ii). It turns out that the results obtained for case (i) and (ii) are very similar because of mathematical reasons: The yield $\phi_{ISC}^{'m}$ for the ISC process $T_n|m\rangle \dashrightarrow S^*$ is given by

$$\phi_{ISC}^{'m} = \frac{k_{ISC}^m}{k_{ISC}^m + k_{IC}^m} \qquad (9)$$

Clearly, when $k_{IC}^m << k_{ISC}^m$, where k_{ISC}^m is the rate constant for ISC from $T_n|m\rangle$ to $S_n(v)$, and k_{IC}^m is the rate constant for IC from $T_n|m\rangle$ to $T_0|m\rangle$, $\phi_{ISC}^{'} = 1$ and spin-independent. This situation corresponds to curve a in fig. 3.2.3. In the other extreme, i.e. $k_{IC}^m >> k_{ISC}^m$ we have no noticeable ISC from $T_n|m\rangle$ to S , then $\phi_{ISC}^{'} = 0$ and again we have a spin-independent case. The intermediate situation could give rise to different results depending on whether we take $\bar{\phi}_{fT}$ to be

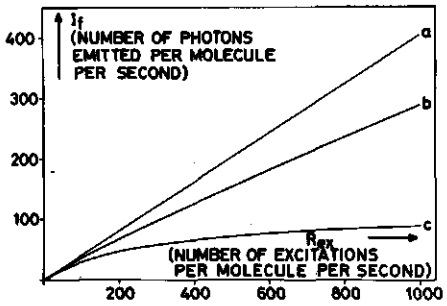

Figure 3.2.3.
Calculated fluorescence intensity I_f (in number of photons emitted per molecule per second) as a function of excitationrate, $R_{ex} \equiv Ik_{13}$ expressed in number of excitations per molecule per second . For all curves the rate of $S_0 \rightarrow S_2$ absorption (Ik_{13} in eqn.(6)) is taken to be equal to the rate of $T_0 \rightarrow T_n$ absorption (Ik_{46} in eqn.(6)). Furthermore $k_{21}.(k_{21}+k_{24})^{-1} = 0.4$, $k_{41} = 169.2$ sec^{-1}, and $\Delta\phi_f = 0$. The value of $\overline{\phi}_{fT}$ in eqn.(6) is taken to be 0.4, 0.2, and 0 for curves a, b, and c, respectively; for the calculated curves in this figure $\overline{\phi}_{fT}$ has been taken to be spin-independent.

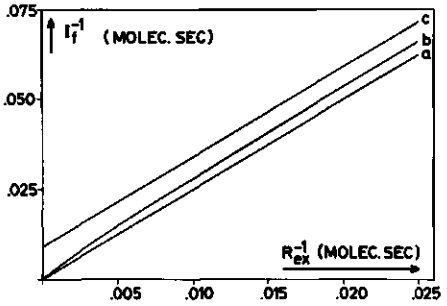

Figure 3.2.4.
Reciprocal plot of the fluorescence intensity I_f^{-1}, expressed in (number of emitted photons per molecule per second)$^{-1}$ vs. the reciprocal rate of excitation $R_{ex}^{-1} \equiv (Ik_{13})^{-1}$, expressed in (number of excitations per molecule per second)$^{-1}$. We have taken $Ik_{13} = I'k_{46}$; all other parameters are taken to be equal to those in fig. 3.2.3. a-c: curve a: $\overline{\phi}_{fT} = \phi_f = 0.4$; curve b: $\overline{\phi}_{fT} = 0.2$; curve c: $\overline{\phi}_{fT} = 0$.

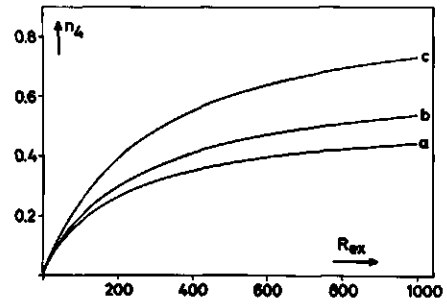

Figure 3.2.5.
Calculated steady state fractional population of $T_0(n_4)$ vs. the rate of excitation R_{ex}.
Conditions as in fig. 3.2.3.; curve a: $\overline{\phi}_{fT} = 0.4$; curve b: $\overline{\phi}_{fT} = 0.2$; curve c: $\overline{\phi}_{fT} = 0$.
Note that n_4 expresses the fraction of the total number of molecules present in T_0.

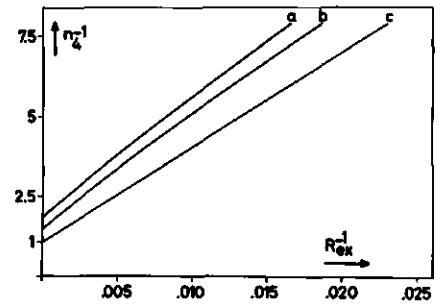

Figure 3.2.6.
Reciprocal plot of steady state triplet population n_4^{-1} vs. R_{ex}^{-1}. For symbols and conditions, see fig. 3.2.4.

dependent on spin or not. We have carried out a calculation, assuming that the ratio's between k_{ISC}^{m} for different spinlevels $T_n|m\rangle$ is equal to the ratio's for the k_m, describing the ISC process $T_0|m\rangle \dashrightarrow S_0$.
Furthermore, it was assumed in this calculation that IC rate constants were spin-independent. It turns out that curve b of fig. 3.2.3 is almost insensitive for inclusion of the abovementioned spin-effects.

A final comment on the boundary conditions of fig. 3.2.3 should be made. For all calculations - and this holds throughout Chapter 3 - we are at low enough excitation rates, so that induced singlet emission can be excluded.
For the compounds in which we are interested, the triplet yield is relatively high, and the radiative decay rate for the process $T_0 \rightarrow S_0$ is very small. Stimulated emission from T_0 does not have to be considered.
Saturation phenomena readily occur, however, as is apparent from curve c in fig. 3.2.3. This curve reflects the build-up of triplet-population at increasing $S_0 \rightarrow S_2$ excitation rate, even in the presence of T-T absorption proceeding at the same rate. Saturation occurs because there is no possibility for ISC from highly excited triplet states.
As soon as the latter process is allowed, no saturation occurs anymore, at least in the regime which is of interest to us.

A plot of I_f^{-1} *vs.* $(Ik_{13})^{-1}$ is presented in fig. 3.2.4 using the same parameters as in fig. 3.2.3; we note that no linear plot is obtained when T-T absorption is included and $0 < \bar{\phi}_{fT} < \phi_f$ (curve b). Furthermore we obtain a linear reciprocal plot which does not pass through the origin when $\bar{\phi}_{fT} = 0$ *or* when T-T absorption is absent. Experimentally we may meet three situations if we make a reciprocal I_f^{-1} *vs.* I^{-1} plot:
A linear plot as represented by fig. 3.2.4c allows one to conclude that *either*

$\bar{\phi}_{fT} \approx 0$; no conclusion about T-T absorption is possible

or

$\bar{\phi}_{fT} \neq 0$; T-T absorption absent.

In both cases the triplet state kinetics *are not affected by T-T absorption*, as will be shown in the next section.
If one finds a reciprocal plot of the type shown in fig. 3.2.4b, one may conclude that

$0 < \bar{\phi}_{fT} < \phi_f$; T-T absorption present

whereas curve a corresponds to

$\bar{\phi}_{fT} = \phi_f$; T-T absorption present.

Physically, the latter situation corresponds to a 100% effective ISC process $T_n \dashrightarrow S$ ($\phi'_{ISC} = 1$), so that all molecules which are excited into higher triplet states, are transferred to the singlet manifold.

From the abovementioned results, it is evident that a reciprocal plot of I_f^{-1} *vs.* $(Ik_{13})^{-1}$ (where Ik_{13} is proportional to the experimental excitation light intensity) is helpful in deciding whether there is an effect of T-T absorption on the triplet state kinetics. Another useful piece of information can be extracted from a non-zero value of I_f^{-1} at infinite excitation rate, i.e. at $(Ik_{13})^{-1} = 0$, and the slope of the (linear) plot. We will show that these data allow an absolute scaling of experimental reciprocal plots of I_f^{-1} *vs.* $(Ik_{13})^{-1}$ in terms of number of emissions or excitations per molecule per second, provided the values of ϕ_{ISC}, ϕ_f and k_{41} are known. (Usually, it is sufficient to know only ϕ_f and k_{41}, since $\phi_f \approx 1 - \phi_{ISC}$ for many compounds.)

From eqn. (8) it follows that for $(Ik_{13})^{-1} = 0$

$$I_f^{-1} = \frac{k_{24} + \Delta\phi_f k_{21}}{k_{21} k_{41} (1 - \Delta\phi_f)} \tag{10}$$

As follows from eqns (18) and (22) in Appendix I, I_f^{-1} can also be expressed as

$$I_f^{-1} = \phi_{ISC} \phi_f^{-1} k_{41}^{-1} \tag{11}$$

for $(Ik_{13})^{-1} = 0$

From eqn. (11) it is clear that the experimental values of I_f^{-1} (expressed in a reciprocal signal amplitude, usually $(\text{Volts})^{-1}$) can be expressed in (number of emissions per molecule per second)$^{-1}$. From the slope of I_f^{-1} *vs.* $(Ik_{13})^{-1}$ we may also obtain an absolute scaling of the $(Ik_{13})^{-1}$ axis.

In fact all excitation and emission rates are expressed relative to the measurable triplet decay rate k_{41}.

A second relevant parameter is the total T_0 population n_4 as a function of I, I' and k_{41}: we find (see Appendix I)

$$n_4 = \frac{I\, k_{13}\, (k_{24} + \Delta\phi_f k_{21})}{I\, k_{13}\, (k_{24} + \Delta\phi_f k_{21}) + (k_{21} + k_{24})\, (k_{41} + I'\, k_{46}\, \bar{\phi}_{fT})} \tag{12}$$

Figure 3.2.5 represents the dependence of the *fractional* T_0 population on the rate of excitation under different conditions (curves a-c). Again, in all cases we have allowed T-T absorption to occur. In curve c, however, there is no possibility of ISC from a higher excited triplet state, resulting in a rather

high fractional T_0 population (n_4) under steady state conditions and high excitation rate. In the limit of infinite excitation rate, n_4 approaches 1, i.e. all states except T_0 are depleted and almost all molecules are transferred to T_0. If ISC from T_n or T_m is allowed, n_4 drops of course. Saturation of T_0 is observed in all three cases, as is evident from fig. 3.2.6, where we have plotted n_4^{-1} *vs.* R_{ex}^{-1}. Note also that curve c in fig. 3.2.6 is linear whereas a and b are not.

As a final point regarding fig. 3.2.5 we observe that n_4 continuously increases with R_{ex}. As we will see in section 3.3 this is not necessarily so for the steady-state populations of the individual spinlevels of T_0.

3.3 EFFECTS OF T-T ABSORPTION, SLR, AND LIGHT INTENSITY ON TRIPLET STATE KINETICS

3.3.1 General theory

In this section we will demonstrate how the time dependence of the populations of the three triplet spin states can be detected via changes in the fluorescence intensity induced by microwaves. Similar studies have been published by van Dorp *et al.* [1] and Clarke *et al.* [3]. We pay particular attention to the influence of T-T absorption as well as spin lattice relaxation (SLR) in the presence of a relatively high optical excitation rate on triplet state kinetics. The relevant pathways for excitation, decay, ISC and relaxation and their parameters have been presented in figs. 3.2.1 and 3.2.2.

Let us follow the fase of a molecule, residing in the spin state $|m\rangle$ of the lowest triplet state T_0 and subjected to SLR, T-T absorption, and ISC at the level $T_n|m'\rangle \dashrightarrow S_n(v)$. Spin-lattice relaxation tends to transfer molecules from spin states $T_0|m\rangle$ preferentially to states $T_0|m'\rangle$ with *lower* ZFS energy, until Boltzmann equilibrium is reached: then $n_k > n_j > n_i$. If heating occurs, due to Stokes-losses in a solid host with a low heat conductivity, increasing the intensity of the exciting light may result in a rise in temperature and an increase in SLR rates. Thus, one may approach Boltzmann-equilibrium by increasing the exciting light intensity.

As will be shown in section 3.4.1 T-T absorption followed by ISC, both from $T_n|m\rangle$ to $S_n(v)$ and from S_1 to $T_0|m'\rangle$ results in a transfer of molecules from the least active level (having the smallest populating rate constant for the $S_1 \dashrightarrow T_0|m\rangle$ process (see 17a-d)) to the more active levels, when the exciting light intensity is increased. For photosynthetic pigments and aromatic molecules,

this implies *depletion* of the lowest spin-state with increasing exciting light intensity.

Finally, if no $T_n|m\rangle \dashrightarrow S_n(v)$ ISC or SLR occurs, there may still be transfer of molecules from $T_0|m\rangle$ to $T_0|m'\rangle$ under the action of light by T_0-T_n absorption, if we assume that the higher excited triplet state T_n is life time broadened (case iii, section 3.2). Then we have complete loss of spin-memory in T_n. By returning to T_0, the molecule, which has started in $T_0|m\rangle$, may end up in any spin state $|m'\rangle$ of T_0 with equal probability, thus *equalizing* populations of all three spin states of T_0. There are few experimental data [6] allowing one to decide which of these mechanisms is the most significant one. Zero-field ODMR may be an attractive means to settle this question, which appears to be very important for photochemical studies. If SLR becomes dominant at increasing exciting light intensity, we predict for photosynthetic pigments that D+E and D-E signal amplitudes *vanish after changing sign from negative to positive* (section 3.4.2, fig. 3.4.2.1 and Chapter 6). With $T_0 \rightarrow T_n$ followed by $T_n \dashrightarrow S_n(v)$ we predict a considerable *increase of signal amplitudes* with increasing light intensity for the D+E and D-E transitions. With only $T_0|m\rangle \leftrightarrow T_n|m'\rangle$ processes, allowing spin-flip, but no $T_n|m'\rangle \dashrightarrow S_n(v)$, we expect the D+E and D-E signal amplitudes to approach zero without changing sign, with increasing exciting light intensity. Thus, it appears, that ODMR provides a means to distinguish between these rather subtly different cases.

Before describing the kinetics of triplet spinstates $|m\rangle$ (m=i,j,k) in more detail, we make the following assumptions:

(i) If molecules are excited from the lowest triplet state T_0 to any higher lying triplet state T_ℓ, or when molecules in T_ℓ return to T_0 by interconversion there occurs no change of spin direction, i.e. the excitation and decay processes can be expressed as $T_0|m\rangle \overset{\longleftarrow}{\rightarrow} T_\ell|m\rangle$. As has been noted before, this condition can be further relaxed by assuming life time broadening of $T_n|m\rangle$ states, wiping out all spin dependence of $T_n \rightarrow S_n$ and $T_n \leftrightarrow T_0$ processes.

(ii) Without further approximations, a description of the excited state kinetics of a molecule including $T_0 \rightarrow T_n$ and $S_0 \rightarrow S_2$ absorption, as well as $T_n \dashrightarrow S_2$, $T_m \dashrightarrow S_1$, $S_1 \dashrightarrow T_0$, $S_2 \dashrightarrow T_m$, and $T_0 \dashrightarrow S_0$ ISC processes and radiationless transitions within the singlet- and triplet manifolds, would involve at least 12 coupled differential equations.
Therefore, we make a further simplifying assumption by noting that the lifetimes of S_0 and $T_0|m\rangle$ are at least four orders of magnitude larger than those

of all other states. This means that we may take all $k_{\ell\ell'}$ except k_{13},k_{46}, and k_{41}^{m} (m = i,j,k) as infinite; k_{46} does not carry a spin-index m, because of assumption (i). In Appendix I it is shown that the abovementioned approximation is justified.

The yields $\phi_f(\ell)$, $\phi_{ISC}^{m}(\ell)$, $\phi_{fT}^{m}(\ell)$, $\phi_{ISC}^{mm'}(\ell)$ and $\phi_{TT}^{m}(\ell)$ are defined in Appendix I. Furthermore we define

$$\phi_{ISC}(\ell) \equiv \sum_{m} \phi_{ISC}^{m}(\ell) \tag{13}$$

and note that for most tetrapyrrole pigments the relation

$$\phi_{ISC}^{(\ell)} + \phi_f(\ell) \approx 1 \tag{14}$$

is valid.

In the absence of photochemistry, and assuming (14) to be valid, the following relation can be shown to hold:

$$\sum_{m,m'} \phi_{ISC}^{mm'}(\ell) + \phi_{TT}^{m}(\ell) + \phi_{fT}^{m}(\ell) = 1 \tag{15}$$

Triplet state kinetics are not expected to be affected by taking the lifetime of all states except those of S_0 and $T_0|m\rangle$ to be zero, *provided that the quantum-yields defined in Appendix I are kept constant.* This also implies that $n_1 + n_4 \approx 1$, i.e. on a time-scale relevant for our measurements ($\sim k_{41}^{-1}$ sec), the populations of all other states except T_0 and S_0 can be neglected.

For the general relations between these yields and the kinetic constants $k_{\ell\ell'}$, we also refer to Appendix I.

With the aforementioned assumption, the kinetics of the four states S_0,$T_0|i\rangle$,$T_0|j\rangle$, and $T_0|k\rangle$ are described by the set of coupled differential equations:

$$\dot{n}_m = -\{k_m + \sum_{m' \neq m} w_{mm'} + (1 - \phi_{TT}^{m})\, I'k_{46}\}\, n_m + I'k_{46} \sum_{m'} \phi_{ISC}^{m'm}\, n_{m'} + \sum_{m' \neq m} w_{m'm}\, n_{m'} + Ik_{13}\, \phi_{ISC}^{m}\, n_1 \tag{16a}$$

and

$$\dot{n}_1 = \sum_{m} (k_m + I'k_{46}\, \phi_{fT}^{m})\, n_m - Ik_{13}\, \phi_{ISC}\, n_1 \tag{16b}$$

Eqns. (16a,b) can be rewritten using physically significant rates

$$r_{mm'} \equiv \frac{I'}{I} k_{46} \phi_{ISC}^{mm'} \tag{17a}$$

$$P_m \equiv k_{13} \phi_{ISC}^{m} \tag{17b}$$

$$P \equiv \sum_m P_m \tag{17c}$$

$$q_m \equiv \frac{I'}{I} k_{46} (1 - \phi_{TT}^{m}) \tag{17d}$$

resulting in

$$\dot{n}_m = - (k_m + \sum_{m' \neq m} w_{mm'} + I q_m) n_m + I \sum_{m'} r_{m'm} n_{m'} + \sum_{m' \neq m} w_{m'm} n_{m'} + IP_m n_1 \tag{18a}$$

and

$$\dot{n}_1 = \sum_m (k_m + I' k_{46} \phi_{fT}^{m}) n_m - IP n_1 \tag{18b}$$

For all eqns. (16a,b), (17), and (18a,b) m,m' = i,j,k.

We can give the following meaning to the rates $r_{mm'}$, P_m, and q_m: $r_{mm'}$ is the rate constant of the process by which molecules are transferred by $T_0|m\rangle \rightarrow T_n|m\rangle$ excitation from spinlevel $T_0|m\rangle$ to $T_0|m'\rangle$ via ISC to and from the singlet manifold; P_m is the populating rate constant for formation of the spinlevel $T_0|m\rangle$ by excitation $S_0 \rightarrow S_2$ and ISC from the singlet manifold, and q_m is the rate constant for the process by which molecules are transferred from the $T_0|m\rangle$ state to the singlet manifold via $T_n|m\rangle$.

Eqns. (18a,b) can be solved using the expression

$$\dot{\vec{n}} = - \underline{A} \vec{n} \tag{19}$$

where

$$\vec{n} \equiv \begin{bmatrix} n_i \\ n_j \\ n_k \\ n_1 \end{bmatrix} \tag{20}$$

and

$$\underline{\underline{A}} \equiv \begin{bmatrix} k_i+w_{ij}+w_{ik}+Iq_i-Ir_{ii} & -w_{ji}-Ir_{ji} & -w_{ki}-Ir_{ki} & -IP_i \\ -w_{ij}-Ir_{ij} & k_j+w_{ji}+w_{jk}+Iq_j-Ir_{jj} & -w_{kj}-Ir_{kj} & -IP_j \\ -w_{ik}-Ir_{ik} & -w_{jk}-Ir_{jk} & k_k+w_{ki}+w_{kj}+Iq_k-Ir_{kk} & -IP_k \\ -k_i-I'k_{46}\phi_{fT}^{i} & -k_j-I'k_{46}\phi_{fT}^{j} & -k_k-I'k_{46}\phi_{fT}^{k} & IP \end{bmatrix} \qquad (21)$$

Since all excitation- and deactivation pathways form closed cycles, the sum of each column in $\underline{\underline{A}}$ vanishes and $\underline{\underline{A}}$ has an eigenvalue equal to zero. Then, the solutions of (19) are given by

$$n_\nu(t) = a_0^\nu + a_1^\nu e^{-\lambda_1 t} + a_2^\nu e^{-\lambda_2 t} + a_3^\nu e^{-\lambda_3 t} \qquad (22)$$

where ν = i,j,k, or 1, and λ_μ (μ=1,2,3) are representing the non-zero eigenvalues of $\underline{\underline{A}}$.

We are interested in the values of λ_μ and the steady state solutions of (19). Before presenting these values it is important to note that we can distinguish three different conditions:

(i) No microwaves resonant with any transition between spinlevels $T_0|m\rangle$ are present; this situation is denoted as the 'free system' (FS).

(ii) Saturating microwaves are present inducing transitions between one pair of spinlevels of T_0. This situation can also be described by replacing *one* set of relaxation rate constants $w_{mm'}$ and $w_{m'm}$ by $w_{mm'} + b_{mm'}$ and $w_{m'm} + b_{m'm}$, respectively; $b_{m'm} = b_{mm'}$ is the rate constant for transitions between spin states $|m\rangle$ and $|m'\rangle$ induced by a microwave field. Under saturating conditions we may seek solutions in the limit $b_{mm'} \to \infty$. We denote this situation as a 'single resonance system' (SRS).

(iii) The solution for the situation where *two* pairs of spin levels are connected by saturating microwaves can be found analogously to case (ii). We denote this situation as a 'double resonance system' (DRS).

The cases (i) through (iii) will be discussed below in sections 3.3.2 through 3.3.4 and their subparagraphs.

For each case we may choose our remaining conditions - presence or absence of T-T absorption and/or SLR, low or high light intensity - in several ways, as summarized in Table I.

Table I. Guide for sections 3.3.2 - 3.3.4.

		I	II	III	IV	V	VI	VII
TT	a)	+	+	+	0	+	0	0
SLR	a)	+	+	0	+	0	+	0
L	b)	+	0	+	+	0	0	+

a) + and 0 denote the presence and absence of T-T absorption and/or spin-lattice relaxation, respectively.
b) + and 0 denote the inclusions of the light-dependence and the limit of $I \to 0$, respectively.

For cases VI and VII we can refer to published expressions [1-3]. The previously reported results follow from the general solution (case I) by substituting $I = 0$ (case VI) and $w_{mm'} = q_m = r_{mm'} = 0$ (case VII) into (21). Cases II and V are irrelevant, since taking $I \to 0$ eliminates T-T absorption as well. We will treat the remaining cases I, III, and IV in the following sections.

3.3.2 The free system (FS)

Since one of the eigenvalues of $\underline{\underline{A}}$ in (21) equals zero, we want to apply a similarity-transformation [7] so that the transformed matrix contains one row of zero's. Then, the 3 x 3 part of this matrix which is necessary for calculating the non-zero eigenvalues, is given by

$$\underline{\underline{A}}' = \begin{bmatrix} k_i+w_{ij}+w_{ik}+I(P_i+q_i-r_{ii}) & -w_{ji}+I(P_i-r_{ji}) & -w_{ki}+I(P_i-r_{ki}) \\ -w_{ij}+I(P_j-r_{ij}) & k_j+w_{ji}+w_{jk}+I(P_j+q_j-r_{jj}) & -w_{kj}+I(P_j-r_{kj}) \\ -w_{ik}+I(P_k-r_{ik}) & -w_{jk}+I(P_k-r_{jk}) & k_k+w_{ki}+w_{kj}+I(P_k+q_k-r_{kk}) \end{bmatrix} \quad (23)$$

A non-oscillating solution of the eigenvalues of $\underline{\underline{A}}'$ is obtained under the condition that

$$\sum_{i<j} A'_{ii} A'_{jj} - A'_{ij} A'_{ji} < \frac{1}{3} \left(\sum_i A_{ii}\right)^2 \quad (24)$$

where A'_{ij} are elements of $\underline{\underline{A}}'$; the eigenvalues of $\underline{\underline{A}}'$ are given by

$$\lambda_1 = 2\sqrt{-q} \cos \frac{1}{3}\alpha - \frac{c_2}{3} \quad (25a)$$

and

$$\lambda_{2,3} = -\sqrt{-q}\ \cos\tfrac{1}{3}\alpha - \frac{c_2}{3} \pm \sqrt{-3q}\ \sin\tfrac{1}{3}\alpha \qquad (25b,c)$$

where $\lambda_1 > \lambda_2 > \lambda_3$

$$q \equiv \frac{c_1}{3} - \frac{c_2^2}{9} \qquad (26a)$$

$$r \equiv \frac{1}{6}(c_1c_2 - 3c_0) - \frac{1}{27}c_2^2 \qquad (26b)$$

$$\alpha \equiv \arccos\left(\frac{r}{\sqrt{-q^3}}\right) \qquad (26c)$$

and $c_0 \equiv \det \underline{\underline{A}}'$ (27a)

$$c_1 \equiv \sum_{i<j} (A'_{ii}\,A'_{jj} - A'_{ij}\,A'_{ji}) \qquad (27b)$$

$$c_2 \equiv \mathrm{Tr}\ \underline{\underline{A}}' \qquad (27c)$$

The solutions given by (25a-c) are exact provided we may assume that the populations of all levels except S_0 and T_0 can be neglected on a timescale comparable to the lifetime of T_0, which is in the msec range for the compounds which we have studied.

Eqns. (25-27) are not very helpful when we want to have a quick idea about the behaviour of λ_μ as a function of the relevant parameters. Therefore, we use a perturbation approach in order to obtain simpler expressions in the limit $Ik_{13} \to 0$ and $I'k_{46} \to 0$.

As long as non-diagonal elements of $\underline{\underline{A}}'$ are small compared to the difference between diagonal elements we may write in a good approximation for the eigenvalues of $\underline{\underline{A}}'$

$$\lambda_i = k_i + w_{ij} + w_{ik} + I(P_i + q_i - r_{ii})$$

$$+ \frac{[w_{ji} + I(P_i - r_{ji})][w_{ij} + I(P_j - r_{ij})]}{(k_i - k_j) + (w_{ik} - w_{kj}) + I(P_i - P_j + q_i - q_j + r_{ii} - r_{jj})}$$

$$+ \frac{[w_{ki} + I(P_i - r_{ki})][w_{ik} + I(P_k - r_{ik})]}{(k_i - k_k) + (w_{ij} - w_{jk}) + I(P_i - P_k + q_i - q_k + r_{ii} - r_{kk})} \qquad (28)$$

and similiar expressions for λ_j and λ_k, where we have assumed $w_{mm'} = w_{m'm}$ where $m,m' = i,j,k$; this means that we still have an isotropic relaxation whereas the small Boltzmann factor is neclected. In the limit $Ik_{13} \to 0$ where $w_{mm'} = 0$ and $q_m = 0 \quad \lambda_m = k_m$.

From these expressions it is evident that in the absence of T-T effects ($q_m = 0$, $r_{mm'} = 0$) the slope of $\lambda_m(I)$ for $I = 0$ approaches P_m. It is important to note that as soon as $q_m = 0$ for $m = i,j,k$ all $r_{mm'}$ vanish as follows from (17a,d) and the sumrule (14) in Appendix I, and the roots become independent of T-T absorption, whether T-T absorption is present or not. Physically this means that the measured decay constants only depend on T-T absorption when ISC from the excited triplet state to the singlet manifold can occur.

Eqn. (28) is valid in the region of low excitation rates: with the set of parameters used throughout this Chapter, this region is limited to $Ik_{13} \lesssim 70\ sec^{-1}$.

Figs. 3.3.2.1-3.3.2.3 represent a collection of calculated curves λ_μ (μ=1,2,3) *vs.* I with various choices of parameters corresponding to cases I, III, and IV of table I. For all curves we have taken the same parameters as used in figs. 3.2.3-3.2.6. For further details we refer to the figure captions.

Fig. 3.3.2.1 represents the most general case (case I) for the free system. We have plotted λ_μ (μ=1,2,3) in the order $\lambda_1 > \lambda_2 > \lambda_3$ as a function of excitation rate R_{ex} for $w = 100\ sec^{-1}$ ($w_{mm'} = w$) and $\bar{\phi}_{fT} = 0.2$. The cases $w = 100\ sec^{-1}$, $\bar{\phi}_{fT} = 0$ or 0.4 have been omitted from this figure, since the behaviour of the roots λ_μ can be easily derived by comparison with figs. 3.3.2.2 and 3.3.2.3. Generally, our results allow the following conclusions:

a) In the absence of T-T absorption, independent of the presence of SLR, the largest root continuously increases with R_{ex} (at high R_{ex} $\lambda_1(R_{ex})$ is linear), whereas the middle and smallest roots (λ_2, λ_3) asymptotically approach a plateau at high values of R_{ex}.

b) In the presence of T-T absorption effects all roots continuously increase with R_{ex}, with (fig. 3.3.2.1) or without SLR (fig. 3.3.2.2.).

In the presence of both T-T absorption and $w = 100\ sec^{-1}$ it appears that at high excitation rates a crossing of λ_1 and λ_2 may occur. This crossing is not shown in fig. 3.3.2.1, but may be anticipated from the relative slopes of λ_1 and λ_2 vs. R_{ex}.

Fig. 3.3.2.2 represents a less general, but more easily understandable situation: T-T absorption is present but no SLR. Apart from the trends already observed in

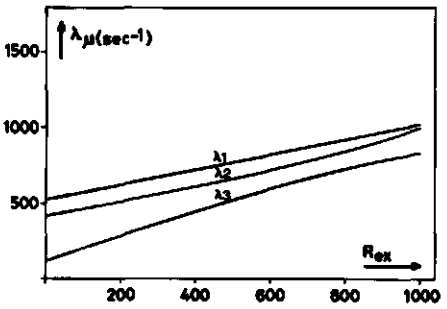

Fig. 3.3.2.1.
Calculated decay rate constants λ_μ for the free system, representing the eigenvalues of matrix (23) as a function of excitation rate R_{ex} ($= Ik_{13} = I'k_{46}$), $w = w_{mm'} = 100\ sec^{-1}$ and $\phi_{fT} = 0.2$. Decay rate constants for $T_{0-1}|m\rangle$ have been chosen as $k_i = 180\ sec^{-1}$, $k_j = 250\ sec^{-1}$, $k_k = 20\ sec^{-1}$, $p_i = .34$, $p_j = .63$, $p_k = .03$. Further choice of parameters as in figs. 3.2.3-3.2.6.

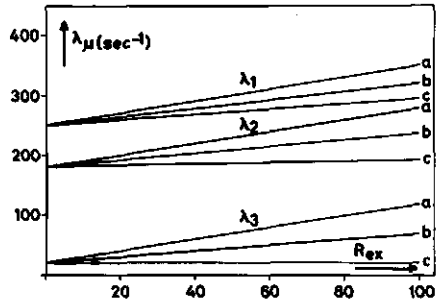

Fig. 3.3.2.2.
Calculated decay rate constants λ_μ for the free system, representing the eigenvalues of matrix (23) as a function of excitation rate R_{ex} ($= Ik_{13} = I'k_{46}$), $w_{mm'} = 0$, and $\phi_{fT} = 0.4$ (a), $\phi_{fT} = 0.2$ (b), and $\phi_{fT} = 0$ (c). Choice of remaining parameters as in figs. 3.2.3 and 3.3.2.1.

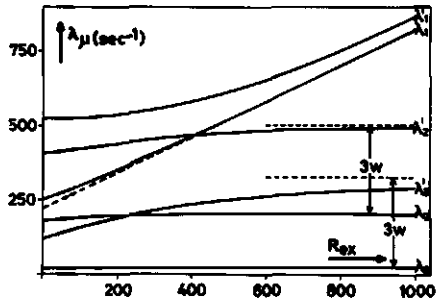

Fig. 3.3.2.3.
Calculated decay rate constants λ_μ, λ'_μ for the free system as a function of R_{ex}, for $\phi_{fT} = 0$, $w = 0$ (unprimed rate constants), $w = 100\ sec^{-1}$ (primed rate constants). Further details as in previous figures.

the previous figure, we note also that with increasing $\bar{\phi}_{fT}$ all slopes approach the same value. This is not unexpected since we have assumed that no spin-effects are present in the process $T_0 \rightarrow T_n \dashrightarrow S^*$ (see section 3.2). Whereas this did not lead to significant effects on the I_f vs. R_{ex} curves (figs. 3.2.3 and 3.2.4) the neglect of spin-effects can be significant for the shape of the λ_μ vs. R_{ex} curves, i.e. the slopes of λ_1, λ_2, and λ_3 can be different if we allow spin-effects to occur in $\bar{\phi}_{fT}$. Due to lack of data we have not pursued this case.

There is a clear message in the curves of fig. 3.3.2.2 - and also in fig. 3.3.2.3 - which is valid independent of the assumption of a spin-independent $\bar{\phi}_{fT}$. In the presence of T-T absorption (or SLR) the slopes of the λ_μ vs. R_{ex} curves do not represent a straightforward measure of the populating rates of the individual spin levels. This straightforward relation only holds when no SLR or T-T effects are present in the limit $I \rightarrow 0$, as has been shown in our discussion of the matrix $\underline{\underline{A}}'$, eqn. (23).

In fig. 3.3.2.3 a plot is presented of λ_μ vs. R_{ex} (μ=1,2,3) for w = 0 (λ_1, λ_2, λ_3) and w = 100 (λ_1', λ_2', λ_3').
There are two striking features:

a) as has already been observed before, the largest root (λ_1) keeps increasing with increasing R_{ex}, whereas the other roots become independent of R_{ex};
b) at high excitation rates λ_1' approaches λ_1, in contrast with the behaviour of the other two roots.

The properties a) and b) can be understood as follows:
The matrix $\underline{\underline{A}}'$ of eqn. (24) takes the form

$$\underline{\underline{A}}' = \begin{bmatrix} k_i + 2w + IP_i & -w + IP_i & -w + IP_i \\ -w + IP_j & k_j + 2w + IP_j & -w + IP_j \\ -w + IP_k & -w + IP_k & k_k + 2w + IP_k \end{bmatrix} \qquad (29)$$

if we take $w_{mm'} = w$, i.e. SLR is assumed to be isotropic.

Via a similarity transformation all large terms containing I can be transferred to the diagonal of $\underline{\underline{A}}''$:

$$\underline{\underline{A}}'' = \frac{1}{P} \begin{bmatrix} (P_j+P_k) & -P_i & -P_i \\ 1 & 1 & 1 \\ -P_k & -P_k & (P_i+P_j) \end{bmatrix} \cdot \underline{\underline{A}}' \cdot \begin{bmatrix} 1 & P_i & 0 \\ -1 & P_j & -1 \\ 0 & P_k & 1 \end{bmatrix} \tag{30}$$

resulting in

$$\underline{\underline{A}}'' = \begin{bmatrix} \frac{k_i(P_j+P_k)+k_jP_i}{P} + 3w & \frac{P_iP_j(k_i-k_j)+P_iP_k(k_i-k_k)}{P} + (3P_i-P)w & \frac{(k_j+k_k)}{P} \\ \frac{k_i-k_j}{P} & \frac{k_iP_i+k_jP_j+k_kP_k}{P} + IP & \frac{k_k-k_j}{P} \\ \frac{(k_j-k_i)P_k}{P} & \frac{P_iP_k(k_k-k_i)+P_jP_k(k_k-k_j)}{P} + (3P_k-P)w & \frac{k_k(P_i+P_j)+k_jP_k}{P} + 3w \end{bmatrix} \tag{31}$$

We note several interesting features in $\underline{\underline{A}}''$:

Firstly, *there is only one element containing a dependence on* I, namely A''_{22}. The value of A''_{22} approaches the measured value at high excitation rates, since all off-diagonal elements are independent of I, only contain *differences* of decay constants, and thus are expected to be small.

By contrast, the elements A''_{11} and A''_{33} are *independent* of I and thus we have demonstrated that one root (i.e. one measured decay constant) varies linearly with I at high excitation rate, whereas the other two reach a plateau. The asymptotic values of λ_i and λ_k are given by

$$\lambda_2 = \lambda_i = \frac{k_i(P_j+P_k) + P_ik_j}{P} + 3w \tag{32a}$$

and

$$\lambda_3 = \lambda_k = \frac{k_k(P_i+P_j) + P_kk_j}{P} + 3w \tag{32b}$$

This is borne out by the simulated curves λ_2, λ'_2 and λ_3, λ'_3 in fig. 3.3.2.3. The linearly extrapolated value of $\lambda_1 = \lambda_j$ for $I \to 0$ is given by taking $I = 0$ in A''_{22}:

$$\lambda_j \ (I \to 0) = \frac{\Sigma k_m P_m}{P} \tag{32c}$$

Note that the intersection of λ_j (dashed line in figure 3.3.2.3) with the vertical axis is not equal to k_j. This, of course, is due to the contribution of non-diagonal terms to λ_j in the limit $I \to 0$.
Finally, we note from $\underline{\underline{A}}''$ that the presence of SLR, proceeding at a rate w, adds exactly 3w to the measured value of λ_i and λ_k in the plateau region of fig. 3.3.2.3, whereas the value of λ_j is not affected for high excitation rates by the presence of SLR.
This explains why the curves of the largest root (λ_1 in fig. 3.3.2.3) with and without SLR approach each other at high excitation rate.
One may wonder why the *largest* root ($\lambda_1 = \lambda_j$) behaves differently from the other two, as is evident from $\underline{\underline{A}}''$. As is clear from the form of A''_{22}, this element is insensitive for permutation of i, j and k. The off-diagonal elements, however, are changed by such permutation. By taking a similarity-transformation the element A'_{22}, which was assumed to be the largest element of $\underline{\underline{A}}'$, does not change position. By doing this, we also ascertain that the off-diagonal terms make a minimal contribution.

Finally, we want to make some comments: firstly, on the existence of complex eigenvalues of $\underline{\underline{A}}'$, resulting in fluorescence- and population-oscillations, and secondly, on the existence of $T_n \to S_n(v)$ ISC.
Oscillations may occur, if

$$\sum_{i<j} \left(A'_{ii}\, A'_{jj} - A'_{ij}\, A'_{ji}\right) > \frac{1}{3} \left(\sum_i A_{ii}\right)^2 \qquad (33)$$

This can only occur when $A'_{ij}\, A'_{ji}$ is negative, thus when non-diagonal elements at opposite positions have different signs. Therefore it is necessary that $I(P_m - r_{m'm})$ has the opposite sign of $I(P_{m'} - r_{mm'})$. Since in general

$$P_{mm'} = \frac{I'k_{46}}{I\,k_{13}} \left(1-\phi_{TT}^{m}\right) P_{m'} \qquad (34)$$

one of the abovementioned non-diagonal terms can be negative if

$$\frac{I'k_{46}}{Ik_{13}} \left(1 - \phi_{TT}^{m}\right) P_{m'} > P'_m \qquad (35a)$$

or

$$\frac{I'k_{46}}{Ik_{13}} \left(1 - \phi_{TT}^{m'}\right) P_m > P_m \qquad (35b)$$

This means $I'k_{46} > Ik_{13}$ in order to satisfy this condition. Secondly, ϕ_{TT}^{m} must be different from $\phi_{TT}^{m'}$ in order to obtain oscillation-behaviour. Therefore

oscillation may only occur in molecules with high spin-selective ISC rates for the processes T_m or T_n --→ S when the T-T excitation rates are larger than the S-S excitation rates. W.r.t. $T_n \rightarrow S_n(v)$ ISC Keller 8,9 has shown this process to occur for a limited number of compounds, but with a very low yield ($< 10^{-6}$). This does not imply, that such a process cannot be important for compounds with strong T-T absorption and/or with a large number of hetero-atoms, such as in photosynthetic pigments. In addition, Keller performed his measurements on relatively low-lying excited triplet states. In triplet ODMR studies on photosynthetic pigments one should be aware, however, of the fact that excitation in the 400 nm region excites T_0 to $T_2(v)$ or higher. Then, ISC coupling to the singlet manifold may be much more effective than in Keller's case. It is interesting to note, that Keller's results suggest that the $S_n(v) \rightarrow T_n$ process is much less important than the reverse pathway. This implies that we can still assume $\Delta\phi_f$ in eqn. (6) to vanish, whereas ϕ'_{ISC} (eqn. (9)) is non-zero.

3.3.3 Single resonance system (SRS)

In this Section we will treat the case, where two spinlevels are connected by resonant microwave radiation. The parameters used for the calculation of kinetic constants λ_μ under various conditions (presence or absence of T-T absorption and/or SLR) are the same as in the previous Section. The expressions in this Section for λ_μ have been derived assuming the presence of a *saturating* microwave field, i.e. a field of such amplitude that the transition rate constant $b_{mm'} >> k_m, k_{m'}$, resulting in $dn_m/db_{mm'} = dn_{m'}/db_{mm'} = 0$. This means that a further increase of $b_{mm'}$, which is linearly dependent on microwave power does not lead to a change of the populations n_m and $n_{m'}$ of the connected spinlevels $|m\rangle$ and $|m'\rangle$.
Furthermore, we assume that $b_{mm'} = b_{m'm}$, implying that we have excluded the possibility of population inversion between levels $|m\rangle$ and $|m'\rangle$ by application of a very strong microwave field. This case has been treated by Schmidt [12].

There are two methods in use for the determination of decay constants λ_μ (μ = i,j,k), which we will denote as method I, devised by van Dorp *et al.* [1] and method II used by Clarke *et al.* [3]. Both methods are essentially different; in method I a microwave *pulse* (short compared with the smallest λ_μ^{-1}) disturbs the steady-state populations of a pair of spinlevels connected by the resonant pulse. After termination of this pulse, the system behaves as a free system and decays back to the original situation, the time dependence of this process revealing the various decay constants of T_0 spinlevels through the timedependent fluorescence-intensity.

In method II a *long* microwave pulse (long as compared with the value of $2(k_j + k_k)^{-1}$ if $|j\rangle$ and $|k\rangle$ are the connected levels) is applied to the sample and $I_f(t)$ is measured just after applying the pulse as well as at long time after the microwave field has been switched off.

The advantage of method I is its independence of the presence of saturating microwaves: any disturbance, saturating or not, will cause the desired effect; its disadvantage is the possible occurrence of triple exponentials (see Section 3.3.2) in $I_f(t)$, which are cumbersome for computer fitting.

The advantage of method II is the less complicated time-dependence of $I_f(t)$: at most there are two exponentials present in the $I_f(t)$ curve just after the microwave-field has been switched on. One is much more dependent on the condition of sufficient saturation, however. A considerable amplitude of microwave radiation is needed to ascertain such saturation. A test of maximum saturation from a constant amplitude of the zero-field resonance signal with increasing microwave-amplitude seems to be a rather primitive criterion. One can show (see Section 3.3.5) that undersaturation can result in measured decay constants which deviate from their values under saturating conditions.

We can transform $\underline{\underline{A}}'$ (see Section 3.3.2) via a properly chosen similarity transformation, so that all terms containing the microwave rate constant $b_{mm'}$ are on the diagonal of the transformed matrix. From the three eigenvalues λ_μ, one contains terms with $b_{mm'}$ and thus approaches an infinite value in the limit $b_{mm'} \to \infty$; the other two are the eigenvalues calculated for the remaining 2 x 2 matrix. These λ_μ's are sufficiently accurate as long as all terms in $\underline{\underline{A}}'_{SRS}$ are small compared to $b_{mm'}$. With a microwave field connecting levels $|j\rangle$ and $|k\rangle$, $\underline{\underline{A}}'_{SRS}$ is given by

$$\underline{\underline{A}}'_{SRS} = \begin{bmatrix} k_i + I(P_i + q_i - r_{ii}) + w_I & -\tfrac{1}{2}I(r_{ij} + r_{ik}) + IP_i - \tfrac{1}{2}w_I \\ -I(r_{ji} + r_{ki} - P_j - P_k) - w_I & \tfrac{1}{2}\{k_j + k_k + w_I + I(2P_j + 2P_k + q_j \\ & + q_k - r_{kj} - r_{jk} - r_{jj} - r_{kk})\} \end{bmatrix} \tag{36}$$

where

$$w_I \equiv w_{ij} + w_{ik} = w_{ji} + w_{ki} \tag{37}$$

The second equality is only true if $e^{-\Delta E/kT} \approx 1$, where ΔE amounts to the energy difference between spin-states. At 4.2k and a typical ΔE of 0.03 cm^{-1}, the difference $|e^{-\Delta E/kT} - 1| \approx 0.01$. As long as relaxation does dominate other kinetic

processes in T_o, the approximation (37) does not have any significant effect on the calculated value of λ_μ.
Note that all terms with indices jk or kj have disappeared from $\underline{\underline{A}}'_{SRS}$ since these terms correspond to processes parallel to the microwave transition containing b_{jk} or b_{kj} terms, which are taken to be infinite.
The eigenvalues of $\underline{\underline{A}}'_{SRS}$ are given by

$$\lambda_{\pm} = \frac{a+d}{2} \pm \tfrac{1}{2}\sqrt{(a-d)^2 + 4bc} \tag{38}$$

with

$$a = k_i + w_I + I(P_i + q_i - r_{ii}) \tag{39a}$$

$$b = -\tfrac{1}{2} I(r_{ij} + r_{ik} - 2P_i) - \tfrac{1}{2}w_I \tag{39b}$$

$$c = - I(r_{ji} + r_{ki} - P_j - P_k) - w_I \tag{39c}$$

$$d = \tfrac{1}{2} \{k_j + k_k + w_I + I(q_j + q_k + 2P_j + 2P_k + r_{kj} + r_{jk} - r_{jj} - r_{kk})\} \tag{39d}$$

When the term a-d is small and bc is negative ($|bc| > \frac{(a-d)^2}{4}$ and $bc<0$) we obtain complex roots; physically this means that the populations of the excited states of the molecule oscillate in time. For a given molecule, the oscillation frequency is a function of the exciting light intensity and is given by

$$\omega = -(a-d)^2-4bc \tag{40}$$

For microwave transitions between levels $|i\rangle$ and $|j\rangle$ or $|i\rangle$ and $|k\rangle$ the solutions are obtained by permutation of levels in eqns. (36-39).
With the set of parameters (k_m, P_m, $w_{mm'}$, q_m, $r_{mm'}$,) used in our SRS calculations the results of which are shown in figs. 3.3.3.1 and 3.3.3.2 we do not meet the oscillatory situation.
The curves shown in these figures represent the eigenvalues of $\underline{\underline{A}}'$ (eqn. 23) with $w_{ik} = w_{ki} = 10^5 sec^{-1}$ thereby simulating a D + E transition (fig. 3.3.3.1) and with $w_{jk} = w_{kj} = 10^5 sec^{-1}$, simulating a D - E transition (fig. 3.3.3.2).

We will discuss for each of these transitions the situations w = 0, q = 0 and w = 100, q = 0, where $q = q_i = q_j = q_k$. Figures 3.3.3.1 and 3.3.3.2 also contain simulated curves of $\lambda_\mu(I)$ in the presence of T-T absorption effects. Since these curves (nrs. 3, 4, 7, and 8 of figs. 3.3.3.1 and 3.3.3.2, corresponding to w = 0, q = 0.5 and w = 100, q = 0.5) do not show any remarkable

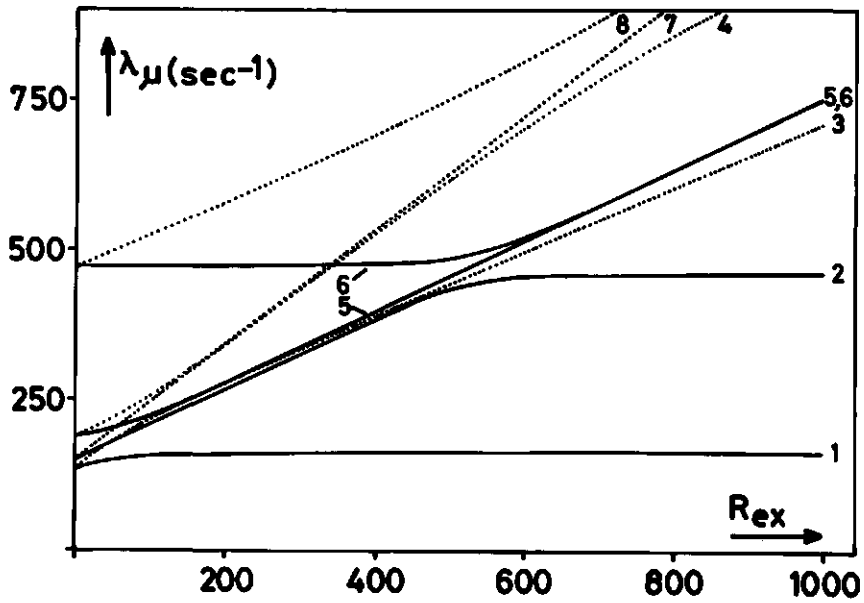

Fig. 3.3.3.1 Calculated decay rate constants λ_- (1-4) and λ_+ (5-8) as a function of R_{ex} for the single resonance system (D+E transition). Choice of parameters:
w=0, q=0 (1,5); w=100 sec^{-1}, q=0 (2,6); w=0, q=0.5 (3,7); w=100 sec^{-1}, q=0.5 (4,8). Choice of remaining parameters as in figs. 3.2.3 and 3.3.2.1.

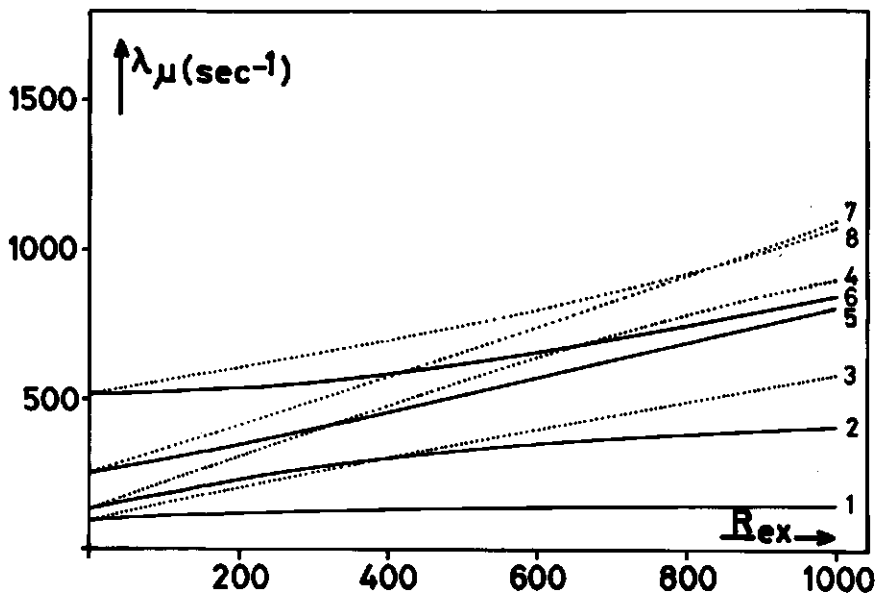

Fig. 3.3.3.2 As previous figure, for D-E transition.

behaviour as compared with the similar situation of the free system (figs. 3.3.2.1 and 3.3.2.3), we will not discuss these curves in further detail.

Referring to fig. 3.3.3.1 curves 1 and 5, we note that in this case spinlevels $|i\rangle$ and $|k\rangle$ have been connected by saturating microwaves following method II. This results in a maximum of two different values for λ_μ for each excitation-rate, denoted with λ_+ as in eqn. (39). Experimentally, of course, one measures a composite timedependence $\Delta I_f(t)$ in principle containing two exponentials. It is helpful to make use of the *amplitude* of both exponentials since in general one of both is dominating, so that a single exponential analysis is sufficient.

The amplitudes of the exponentials $\exp(-\lambda_+ t)$ and $\exp(-\lambda_- t)$, where λ_+ and λ_- are given in (39), are given by

$$\begin{aligned}\Delta I_f(t) &\sim \Delta n_T \\ &= e^{-\lambda_+ t}\ (e+h)(n_+^o - n_+^\infty) - (f+g)(n_-^o - n_-^\infty) \\ &+ e^{-\lambda_- t}\ -(f+h)(n_+^o - n_+^\infty) + (e+g)(n_-^o - n_-^\infty)\end{aligned} \tag{41}$$

Where

$$e = \tfrac{1}{2} + \tfrac{1}{2}(a-d)\left[(a-d)^2 + 4bc\right]^{-\frac{1}{2}} \tag{42a}$$

$$f = -\tfrac{1}{2} + \tfrac{1}{2}(a-d)\left[(a-d)^2 + 4bc\right]^{-\frac{1}{2}} \tag{42b}$$

$$g = -b\left[(a-d)^2 + 4bc\right]^{-\frac{1}{2}} \tag{42c}$$

$$h = c\left[(a-d)^2 + 4bc\right]^{-\frac{1}{2}} \tag{42d}$$

and a, b, c, and d are the elements of $\underline{\underline{A}}_{SRS}$ as defined in (39).
If $a - d > 0$, n_+ is the population of the non-connected level (e.g. n_i for a D - E transition, connecting $|j\rangle$ and $|k\rangle$); n_- is the sum of the populations of the connected levels. If $a - d < 0$, the labels + and - of n_+ and n_- are reversed w.r.t. the previous situation.
Continuing our discussion of curves 1 and 5 of fig. 3.3.3.1, we find that at $I \to 0$, only the exponential with $\lambda_- = \frac{1}{2}(k_i + k_k)$ is present, where as the exponential with $\lambda_+ = k_j$ has a vanishing amplitude. Thus for low excitation light intensity the smallest eigenvalue (λ_-) represented by curve 1 in fig. 3.3.3.1 is the only one which is found from a computer-simulation of $\Delta I_f(t)$. For high excitation light intensity, however, the amplitude of the exponential

with λ_+ is at least 10 times larger than that of the exponential with λ_-. This implies that at high excitation rates λ_+ represented by curve 5 in fig. 3.3.3.1 is dominating in $\Delta I_f(t)$.
Thus, a curve fitting of $\Delta I_f(t)$ at low light intensity for the D + E transition, using a single exponential, yields a reliable value of $\frac{1}{2}(k_i + k_k)$, but not of k_j.
Considering curves 2 and 6 in fig. 3.3.3.1 with an SLR rate constant $w = 100\ sec^{-1}$, again we find that at low excitation rates the exponential with λ_- is strongly dominating the exponential with λ_+. At high excitation rates, however, the amplitude of the exponential with λ_+ is $\sim$ 10 times larger than that of the exponential with λ_-.

It can be shown, that at I = 0 the contribution of SLR to the observed value of $\lambda_- = \frac{1}{2}(k_i + k_k)$ is very small as compared to the contribution to λ_+. This fortunate circumstance can be explained when considering expression (38) at I = 0 and writing out the full expressions for a, b, c, and d. Then we find

$$\lambda_- (I = 0) = \frac{1}{2} k_j + \frac{1}{2}(k_i + k_k) + \frac{3}{2} w - \sqrt{\{k_j - \frac{1}{2}(k_i + k_k) + \frac{1}{2} w\}^2 + 2w^2} \qquad (43)$$

A quadratic term in w under the square root cancels with $\frac{3}{2} w$, whereas the remaining contribution of w consists of crossterms containing no higher powers of w than $w^{\frac{1}{2}}$.

Fig. 3.3.3.2 represents the dependence of the eigenvalues λ_+ and λ_- on I when levels $|j>$ and $|k>$ are connected by saturating microwaves, i.e. the D-E transition is saturated. The behaviour of curves 1, 5, 2, and 6 is completely analogous to those discussed before for the D+E transition: without SLR, the exponential with λ_- (curve 1) is exclusively present at I = 0, yielding $\frac{1}{2}(k_j + k_k)$. At high I curve 5 takes over with λ_+. For curves 2 and 6 we have similar behaviour, except for a less dominating rôle of λ_+ at high excitation rates as compared with fig. 3.3.3.1, curves 2 and 6.
Also for the D-E transition the contribution of w turns out to be small for λ_- at I = 0, as compared to its contribution to λ_+.

What do we expect to find when we try a single exponential curve fitting to $\Delta I_f(t)$ as obtained from experiment? For both D-E and D+E transitions, such fitting is predicted to produce for w = 0 values of λ closely following curves 1 for low I and gradually approaching curves 5 at high I. In the presence of SLR, the previous analysis implies that λ first follows curves 2 at low I and proceeds to follow curves 6 at high I. In fact, this means a continuously increasing λ with increasing I. This is particularly true for curves 2 and 6 of fig. 3.3.3.2.

3.3.4 The double resonance system (DRS)

With two microwave fields simultaneously present, inducing transitions between two sets of spinlevels, we have *only one* finite eigenvalue λ, as follows from a proper similarity transformation of $\underline{\underline{A}}'$ (23), leaving us with a 1 x 1 matrix. This eigenvalue is given by

$$\lambda = \frac{1}{3} \sum_m \{k_m + I(q_m - r_{mm} - \sum_{m' \neq m} r_{m'm}\} + IP \qquad (44)$$

where $m \neq m' = i,j,k$.
Using (15) and (17a,d) λ can be rewritten as

$$\lambda = k_T + IP + I' k_{46} \sum_m \phi_{fT}^m \qquad (44a)$$

Of course, there are no oscillatory solutions. Trivially, for $I = 0$ $\lambda = k_T$.

In the presence of very fast SLR, which occurs at "high" temperature, e.g. 77 K, or when electron-phonon coupling with the lattice is strong, such as may occur in biological material (see Chapters 6 and 7), the rôle of microwave induced transitions between all three levels, is taken over by SLR, which can be considered to cause exactly the same behaviour of λ as saturating microwave radiation.

Thus, (44) also represents the light-dependence of the triplet decay constant k_T, a fact which is often overlooked in previously reported studies [10] .

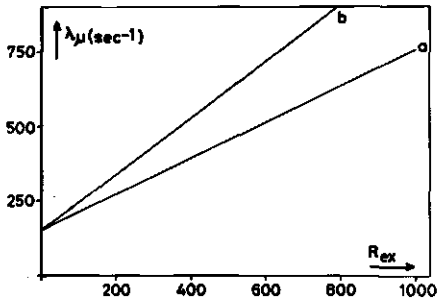

Fig. 3.3.4.
Calculated decay rate constant λ as a function of R_{ex} for the double resonance system. Choice of parameters q=0 (a) q=.5 (b). Choice of remaining parameters as in figs. 3.2.3 and 3.3.2.1.

For a reliable measurement of k_T it is necessary to extrapolate the measurements to I = 0. The extrapolation is particularly simple since (44) shows it to be linear for all values of I.

Figs. 3.3.4a and b represent $\lambda(I)$ in the absence and presence of T-T absorption effects, respectively.

In principle double resonance measurements, where two spin levels are continuously connected and the third level is connected to the other two via a microwave pulse according to method I or II, provide a means to determine relaxation rates $w_{mm'}$, separately from the decay constant k_m. Züchlich *et al.* [2] have treated this case in the limit $I \to 0$.

3.3.5 Effects of non-saturating microwaves on triplet state kinetics

Applying a non-saturating microwave field, it is not allowed to use eqns. (36)(SRS) or (44)(DRS) for calculating decay constants. Rather, we have to use eqn. (23), yielding *three* roots for both the SRS and DRS system. Generally, all three roots will be different from the values obtained under saturating conditions.

The effects of microwave under-saturation on measured decay constants can be easily calculated using (23) and substituting $b_{mm'} + w_{mm'}$ for $w_{mm'}$ and $b_{m'm} + w_{m'm}$ for $w_{m'm}$, where $|m\rangle$ and $|m'\rangle$ are the connected states in the SRS system. For the DRS system a similar procedure can be followed.

From these calculations, inserting the standard set of kinetic constants, used in this chapter, we find that at a microwave power level, where populations of two connected states are equal to within 1 part in 10^3, rate constants may deviate up to 10% from the value at complete saturation. Although this deviation depends on the numerical values of the kinetic constants and thus may be less serious in other cases, it signals a danger in taking the "constant" ODMR amplitude as the criterion for obtaining kinetic constants under saturating conditions.

Since the available amount of microwave power per triplet molecule depends on the total number of triplet state molecules produced in the sample by photoexcitation, the phenomenon of undersaturation may occur at high optical excitation rate, even when sufficient microwave saturation is observed at low optical excitation rate. This may introduce an added source of systematic errors in the measurement of light intensity-dependent decay-constants.

Since in method I no triplet decay occurs in the presence of microwaves, this method is not subject to this source of errors.

3.4 THE AMPLITUDE AND SIGN OF THE FLUORESCENCE DETECTED MAGNETIC RESONANCE SIGNALS

3.4.1 Steady state populations of spin levels

In order to determine the sign and amplitude of ODMR signals in the presence of saturating microwave radiation, we are interested in the solutions of the sets of equations (19): $\dot{\vec{n}} = -\underline{\underline{A}}\vec{n}$ when $\dot{\vec{n}} = 0$ $\underline{\underline{A}}$ can be the orginal (21) or one of its transformed matrices. From n_m, ϕ_{fT}^m, and ϕ_f we can calculate the absolute fluorescence intensity using (18) from Appendix I:

$$I_f = Ik_{13}\phi_f(1-n_T) + I'k_{46}\sum_m \phi_{fT}^m n_m \tag{45}$$

When also $\vec{n}$ is known for the case where one or more spin levels are connected via a microwave field, we can calculate the difference in the fluorescence intensity between situations where microwaves are on and off.
The populations n_i, n_j, and n_k follow from

$$\begin{bmatrix} n_i \\ n_j \\ n_k \end{bmatrix} = (\underline{\underline{A}}')^{-1} \begin{bmatrix} IP_i \\ IP_j \\ IP_k \end{bmatrix} \tag{46}$$

For single resonance (D-E), the populations are found from

$$\begin{bmatrix} n_i \\ n_j+n_k \end{bmatrix} = (\underline{\underline{A}}'_{SRS})^{-1} \begin{bmatrix} IP_i \\ I(P_j+P_k) \end{bmatrix} \tag{47}$$

and similarly for the D+E transition, by permutation of i and j.
For double resonance

$$n_T = \sum_m n_m = IP\lambda^{-1} \tag{48}$$

Where λ is given by (44) and populations are normalized for (46) through (48) by $\sum_m n_m + n_1 = 1$; $\underline{\underline{A}}'$ and $\underline{\underline{A}}'_{SRS}$ are given in (23) and (36), respectively.
It is clear that all effects including T-T absorption can only be calculated quantitatively with the help of a computer. In practice we are interested in trends, e.g. what will happen in the limit $I \to 0$ with increasing $w_{mm'}$, or with increasing T-T absorption in the absence of SRL and in the limit $I \to 0$. In those

cases the expressions for n_m (m=i,j,k) become much simpler.
We will discuss in some detail the results obtained for the light-dependence of the steady state populations n_m for the following cases:
(i) all $w_{mm'} = 0$, no T-T absorption effects (case VII of Table I)
(ii) $w_{mm'} = 0$, T-T absorption present (case III of Table I)
(iii) increasing $w_{mm'}$, no T-T absorption effects (cases IV and VI of Table I).

For case (i), $I \to 0$, we have the familiar situation where

$$n_m = IP_m k_m^{-1} \tag{49}$$

for the free system.
For $I \neq 0$

$$n_m = k_{m'}k_{m''}IP_m \left[k_m k_{m'} k_{m''} + k_m k_{m'} IP_{m''} + k_m k_{m''} IP_{m'} + k_{m'} k_{m''} IP_m \right]^{-1} \tag{50}$$

where $m \neq m' \neq m'' = i,j,k$; (49) is the limiting case of (50) for $I \to 0$. Fig. 3.4.1.1 curves a-c represent a plot of n_m for m = i,j,k, respectively, as a function of the excitation rate $R_{ex} = Ik_{13}$. The ratio $n_i:n_j:n_k$ is independent of I, since the denominator of n_m is invariant for permutation of labels m, m' and m''. Saturation phenomena at high R_{ex} have been discussed in section 3.2.
For case (ii), fig. 3.4.1.1 curves d-f and g-h represent $n_m(R_{ex})$ when SLR is absent for increasing amount of T-T absorption effects (ϕ_{fT} = .2 and .4, respectively).
There are some striking features in these curves: first, the level |k> is depleted at increasing R_{ex}; secondly, for $\phi_{fT} = 0.2$, curve e demonstrates that n_j can even increase in the presence of T-T absorption effects w.r.t. curve b, where such effects are absent.
Previously, we have already shown that T-T absorption effects decrease the total triplet state population n_T, at the same value of R_{ex}. Apparently, the drop of n_k in curve f is so large that n_j (curve e) can still increase when n_T decreases. The relative ordering of $n_j > n_i > n_k$ is not affected by T-T absorption effects and remains unchanged even at high R_{ex}, but the ratio $n_i:n_j:n_k$ does not remain constant at increasing R_{ex}, in contrast with case (i), where T-T absorption was absent. In fact, one can show that the ratio $n_i:n_j:n_k$ is only dependent on R_{ex} if T-T absorption effects are present; *both* for $w_{mm'} = 0$ and $\neq 0$.
Case (iii) can be illustrated by working out (46), setting all q_m, $r_{mm'} = 0$ in $(\underline{\underline{A}}')^{-1}$ (cf. (23)), and taking SLR to be isotropic ($w_{mm'} = w$); for |i> we obtain

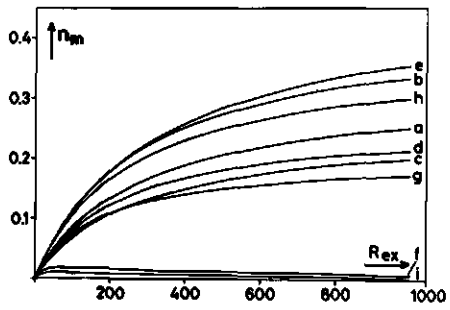

Fig. 3.4.1.1 Populations of spin states $T_0|m>$ as a function of R_{ex}; m=i (a,d,g); m=j (b,e,h); m=k (c,f,i); ϕ_{fT}=0 (a,b,c); ϕ_{fT}=0.2 (d,e,f); ϕ_{fT}= 0.4 (g,h,i); w_{mm}'=0; all other parameters as in fig. 3.3.2.1.

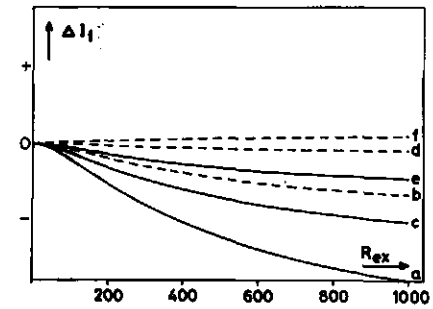

Fig. 3.4.2.1 Change of fluorescence intensity ΔI_f between free system and single resonance system as a function of R_{ex}; D-E transition: curves a,c,e; D+E transition: curve b,d,f; w_{mm}'=w; w=0 (a,b); w=10 sec^{-1} (c,d); w=50 sec^{-1} (e,f); ϕ_{fT}=0 for all curves; The other parameters are as in fig. 3.3.2.1.

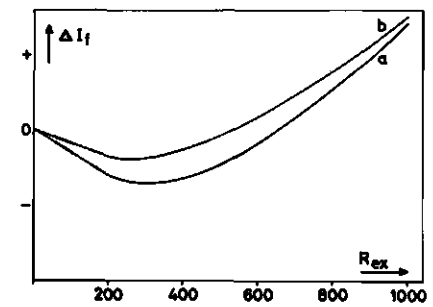

Fig. 3.4.2.2 Change of fluorescence intensity ΔI_f between free system and single resonance system as a function of R_{ex}; D-E transition: curve a; D+E transition: curve b; w_{mm}=0; ϕ_{fT}=0.4; all remaining parameters as in the previous figures.

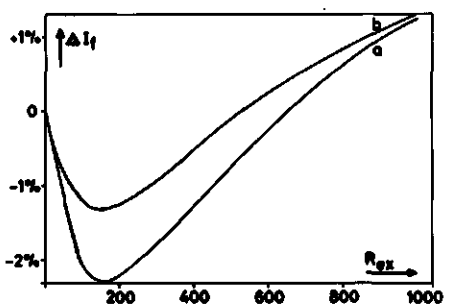

Fig. 3.4.2.3 As 3.4.2.2 for the *relative* change of fluorescence intensity $\frac{\Delta I_f}{I_f}$ as a function of R_{ex}.

$$n_i = |\underline{\underline{A}}'|^{-1} \cdot [k_j k_k P_i + 3w^2 P + 2w(k_j + k_k)P_i + wk_k P_j + wk_j P_k] \qquad (51)$$

and similar expressions for n_j and n_k by permutation of i, j, and k. At high R_{ex} this equation yields equal values for all n_m due to the terms containing w^2. As has been noted already for case (ii) the ratio $n_i:n_j:n_k$ does not depend on the excitation rate $R_{ex} = Ik_{13}$, since I is a factor common to all n_m's.

3.4.2 Single resonance amplitudes

In this section we will discuss some relevant features of the ODMR amplitudes, derived from expressions and calculated $n_m(R_{ex})$ curves, presented in the previous section. Again, we will discuss three cases in fig. 3.4.2.1 through 3.4.2.3, in accordance with our discussion in the previous section. For case (i), ($w_{mm'} = 0$, *no T-T absorption*), curves a and b in fig. 3.4.2.1 represent plots of the magnitude of ΔI_f(D-E) and ΔI_f(D+E), respectively, as a function of R_{ex}. The ratio of both amplitudes is independent of R_{ex}, as follows from the constant ratio $n_i:n_j:n_k$. If one is mainly interested in observing ODMR spectra with favourable signal-to-noise ratio, these plots show that such measurements can best be carried out at high R_{ex}.

For case (ii) ($w_{mm'} = 0$, T-T absorption effects present), fig. 3.4.2.2, curves a and b, represent plots of ΔI_f(D-E) and ΔI_f(D+E), respectively, as a function of R_{ex}. As one would suspect already from (45), the terms containing $(1-n_T)$ and $\sum_m \phi_{fT}^m n_m$ have opposite dependence on $R_{ex} = Ik_{13} = I'k_{46}$. Therefore one expects a sign change of both transitions at increasing R_{ex}, as is also found in the computed curves a and b in fig. 3.4.2.2. Note also that these curves do not show a levelling-off as found for ΔI_f(D+E) and ΔI_f(D-E) *vs.* R_{ex} in the absence of T-T absorption effects. Also the ratio of both amplitudes does not remain constant with increasing R_{ex}, *which is so characteristic of T-T absorption accompanied by spin-selective re-feeding of T_0 via S , that a light-dependent ratio of the amplitudes of the D+E and D-E amplitudes provides a simple test for the presence of such mechanisms.*

We have not observed significant light-dependent changes of ΔI_f(D-E) vs. ΔI_f(D+E) for the compounds which we have studied.

In this case, it is of interest to calculate the dependence of the *relative* change in I_f on R_{ex}, for both transitions. Fig. 3.4.2.3, curves a and b represent plots of ΔI_f(D-E)/I_f and ΔI_f(D+E)/I_f, respectively. We observe at moderate values of R_{ex} a maximum relative change of I_f when saturating the D-E transition of $\sim$ 2%, which is significantly lower than the calculated relative change at the same value of R_{ex} for case (i).

Finally, for case (iii) ($w_{mm'} \neq 0$, no T-T absorption effects], we return to fig. 3.4.2.1, curves c-f. There are two main effects of increasing SLR on the amplitudes.
First, we observe a decrease with increasing w; secondly, the weakest transition (D+E) *changes sign* at increasing SLR. Such a case has been treated in Chapter 6 for pheophytin-a in n-octane and has also been found for chlorophyll-a in the same solvent [11].

3.4.3 Double resonance amplitudes

The application of double resonance to ODMR spectroscopy has been rather limited so far. Yet there are some very useful features, which make it an attractive technique. Apart from the determination of kinetic parameters, including SLR rate constants [2], one can make use of double resonance to increase the amplitude of otherwise non-detectable transitions; we have applied double resonance to dihydroporphin free base, which lacks a 2E transition under single resonance conditions (see Chapter 5).
Generally, a CW saturating microwave field at $\nu^{mm'}$ causes this transition to be absent if a second microwave field is frequency-swept through the ODMR spectrum, whereas the transitions at $\nu^{mm''}$ and $\nu^{m'm''}$ attain the same amplitudes.
A second application of double resonance provides a test to decide which transitions in an ODMR spectrum containing several sets of transitions or in inhomogeneously broadened spectra, belong to the same species. Except for some special pathological cases, generally the irradiation at one transition produces changes of the amplitudes of the remaining two transitions, belonging to the same species.

3.5 REFERENCES

1. W.G. van Dorp, W.H. Schoemaker, M. Soma, and J.H. van der Waals, Mol. Phys. 30 (1975) 1701-1721.
2. J. Zuclich, J.U. von Schütz, A.H. Maki, Mol. Phys. 28 (1974) 33-47.
3. R.H. Clarke, R.H. Hofeldt, J. Chem. Phys. 61 (1974) 4582-4587.
4. P.A. Chika, R.H. Clarke, J. Magn. Res., to be published.
5. A.T. Gradyushko, A.N. Sevchenko, K.N. Solovyov, and M.P. Tsvirko, Photochem. Photobiol. 11 (1970) 387-400.
6. S.K. Lower, M.A. El-Sayed, Chem. Rev. 66 (1966) 199-236.
7. S. MacLane and G. Birkhoff, Algebra (Macmillan Cy, New York, 1967).
8. R.A. Keller, Chem. Phys. Lett. 3 (1969) 27-29.
9. R.A. Keller in: Proc. Intern. Conf. Molecular Luminescence, Loyola University 1968 (ed. Lim,Benjamin inc., New York, 1969).
10. W.W. Parson and T.G. Monger, Brookhaven Symposium in Biology, Brookhaven National Laboratory, Upton, N.Y. 1976 and references cited in this paper.
11. R.P.H. Kooyman, T.J. Schaafsma, and J.F. Kleibeuker, Photochem. Photobiol. in press.
12. J. Schmidt, Thesis, Leyden University, 1971.

CHAPTER 4

ZERO FIELD OPTICALLY DETECTED MAGNETIC RESONANCE (ODMR)

Sievert J. VAN DER BENT and Tjeerd J. SCHAAFSMA
Laboratory of Molecular Physics, Agricultural University, Wageningen, The Netherlands

Received 7 April 1975

ZFS parameters and kinetic constants of the lowest triplet state of chlorin and tetraphenylchlorin free base in *n*-octane have been determined by fluorescence-detected ODMR at 4.2 K. These compounds can be considered as model compounds for pheophytin, a compound of biological interest. For both compounds the *middle* spin-level is the most active one in the populating and depopulating pathway. In the lowest triplet state the NH–NH axis in both chlorins is probably fixed to one orientation not involving the reduced ring, and no evidence was found for the occurrence of two tautomeric forms as in the corresponding porphyrins.

4.1

1. Introduction

Pheophytins can be derived from the chlorophylls by substituting the central Mg^{2+} ion by two protons. They are probably part of the photo-synthetic system of some bacteria and algae, but their rôle in higher plants is not clear [1–3]. A study of the excited states of pheophytins and their model compounds is essential to elucidate the function of the Mg^{2+} ion in chlorophylls for the photosynthetic energy conversion. Furthermore, characterization of the lowest triplet state of pheophytins in vitro by their zero-field splittings and kinetic constants provides the necessary basis for the detection of small amounts of these compounds for in vivo systems.

Recently, very selective and sensitive methods have been developed, for the study of small amounts of photo-excited triplets employing the effect of microwave induced transitions between the triplet state spin-levels on the fluorescence emission [4,5]. We have applied these methods to the lowest triplet state of chlorin free base (H_2PH_2), tetraphenylchlorin free base (H_2TPPH_2) and tetraphenylporphin (H_2TPP). Results on H_2PH_2 are compared with those for porphin free base (H_2P), obtained by van Dorp et al. [4,6].

The main purpose of this investigation was to determine the effects of reduction and methine-carbon substitution of porphin free base on the ZFS and kinetic constants of the lowest triplet state, and to interpret any systematic changes in terms of an electronic perturbation.

4.2

2. Experimental

Porphin (Calbiochem, high purity grade) was purified by chromatography, whereas the other compounds were synthesized as described in the literature [7]. Purification of H_2TPPH_2 and H_2TPP involved entrained sublimation on an all-glass high vacuum line. Purity was checked by mass-spectrometry and TLC. Single crystals of *n*-octane (Baker), purified by chromatography [8], and containing small ($\approx 10^{-6}$ M) amounts of the compounds were grown by slowly lowering the solution, contained in a thin-walled Pyrex tube, into liquid nitrogen. Samples were placed at the end of a quartz light-pipe, immersed in liquid helium and surrounded by a slow-wave structure, conducting microwave-radiation from a Hewlett–Packard 8690B sweeper to the sample. Blue light (λ = 350–450 nm) from a stabilized 200 W super-high-pressure mercury arc was focused onto the top of the light-pipe, whereas fluorescence from the sample was collected onto the entrance-slit of a 0.25 m Jarrell–Ash monochromator, and detected by an EMI 9659QB cooled photomultiplier.

Table 1
Zero-field transitions and parameters

Level scheme [a]	Compound	$(D+E)_{obs}$ (MHz)	$(D-E)_{obs}$ (MHz)	$2E_{obs}$ (MHz)	$D \times 10^4$ cm^{-1}	$E \times 10^4$ cm^{-1}
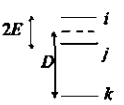	H_2P [b]	1494	1114	380	435	63
		1527	1110	417	440	70
	H_2PH_2	1300 ± 2	1078 ± 2	–	397 ± 1	37 ± 1
	H_2TPP	1370 ± 30 [c]	830 ± 20 [c]	–	367 ± 4	90 ± 4
	H_2TPPH_2	1293 ± 2	900 ± 2	–	364 ± 1	64 ± 1

a) $i, j, k = y,x,z$ for H_2P [6]; other compounds: $k = z$, and i,j refer to the unassigned in-plane molecular axes x or y.
b) See ref. [4].
c) This transition appears to contain more than one component.

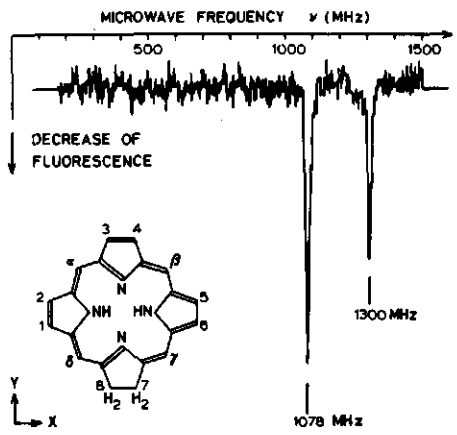

Fig. 1. Zero-field fluorescence detected magnetic resonance spectrum of chlorin free base in an *n*-octane single crystal at 4.2 K; detection wavelength 635 nm. Labelling of atoms in chlorin free base (see insert) according to ref. [18]; x and y axes refer to the assignment of van Dorp et al. [6] for porphin free base, whereas the location of the reduced ring is taken from this work (see text). The spectrum is the accumulated result of 2^{12} scans.

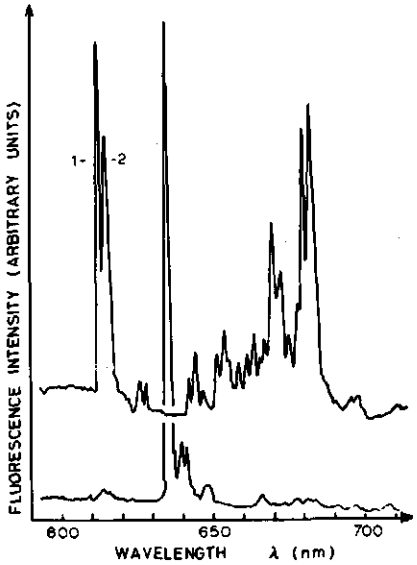

Fig. 2. Fluorescence spectra of porphin (upper trace) and chlorin free base (lower trace) in *n*-octane single crystals at 4.2 K. Excitation at 350–450 nm; bandwidth: 2nm. Tautomer components of the 0–0 transition of porphin free base have been indicated by 1 and 2.

We used a superinsulated Dewar equipped with light pipes resulting in very low losses of liquid helium. Fluorescence-detected ODMR signals and transients were averaged over $2^{15} - 2^{19}$ sweeps, such that the signal-to-noise ratio typically amounts to ≈ 20:1. All experiments were carried out at 4.2 K.

4.3

3. Results

A typical ODMR spectrum of chlorin free base detected at the 0–0 $S_0 \leftarrow S_1$ transition at 635 nm is shown in fig. 1.

Table 2
Kinetic constants of the lowest triplet state [a]

Compound	$k_i(s^{-1})$	$k_j(s^{-1})$	$k_k(s^{-1})$	P_i	P_j	P_k
H_2P [b]	80	250	6	0.4	1	<0.02
H_2PH_2	150 ± 45	260 ± 40	24 ± 2	<0.6	1	<0.09
H_2TPP [b]	168	692	50	>0.24	1	>0.07
H_2TPPH_2	199 ± 20	445 ± 90	40 ± 6	<0.44	1	>0.08

a) For definition of axes i, j, k, see table 1.
b) Values for kinetic constants k and P are taken for comparison from ref. [6] for H_2P and from ref. [10] for H_2TPP (k only). Lower limits on P_λ for H_2TPP have been calculated from published k-values [10] and data reported in this work (see text).

For both H_2P and H_2PH_2 zero-field transitions at $D+E$ and $D-E$ (see insert table 1) correspond to a decrease of the fluorescence intensity I_f ($\Delta I_f < 0$) whereas for the tetraphenyl compounds $\Delta I_f > 0$. The linewidth $\Delta\nu$ of both transitions is less than 7 MHz, for H_2TPP and H_2TPPH_2 $\Delta\nu \approx 50$ MHz. The $2E$ transition was observed for both porphins, but not for the chlorins, despite considerable effort.

In contrast to porphin free base, a single set of zero-field transitions is observed, corresponding to a single 0–0 $S_1 \leftarrow S_0$ transition, as shown in fig. 2. ZFS parameters of chlorin free base were not affected by monitoring the fluorescence at transitions in the vicinity of the 0–0 wavelength, demonstrating that the low-temperature-fluorescence spectrum of chlorin free base originates from one species and not from two tautomeric forms as in porphin free base [4].

By applying saturating microwaves at the $D+E$ and $D-E$ transitions, the fluorescence intensity I_f changes by an amount ΔI_f to a new steady-state value. When the microwaves are switched off, I_f returns to its original value. Kinetic constants (see table 2) were derived from the shape of $\Delta I_f(t)$ after microwaves are switched on and off. We checked for saturation by monitoring ΔI_f as a function of microwave power: a 10 dB reduction of microwave power did not result in a measurable change of ΔI_f. Generally, the shape of the observed transient $\Delta I_f(t)$ is similar to that published in ref. [4] for porphin free base.

4.4

4. Discussion

From the kinetic equations, governing the populations of the ground and first excited singlet states and the magnetic sublevels of the lowest triplet state the following expressions can be derived relating $\Delta I_f(t)$ to the change in the total population $\Sigma_\lambda n_\lambda$ (where $\lambda = i, j, k$ labels the spin levels of the lowest triplet state) [9], when microwaves at the resonance frequency ν_{ij} are switched on or off and the system is continuously irradiated with exciting light.
Microwaves on:

$$\Delta I_f(t) = \alpha(k_i - k_j)(n_i^0 - n_j^0)(k_i + k_j)^{-1} \times \{\exp[-\tfrac{1}{2}(k_i + k_j)t] - 1\} . \quad (1)$$

Microwaves off:

$$\Delta I_f(t) = \alpha k_i k_j (n_i^0 - n_j^0)(k_i + k_j)^{-1} \times [k_i^{-1}\exp(-k_i t) - k_j^{-1}\exp(-k_j t)] , \quad (1a)$$

and similarly for transitions $i \leftrightarrow k$ and $j \leftrightarrow k$; i, j refer to two arbitrary in-plane axes and k to the out-of-plane axis (see table 2).

In (1) and (1a) n_λ^0 denotes the steady state population of the lowest triplet state spin level λ with a decay constant k_λ; α is a proportionality constant containing instrumental parameters and kinetic constants of the $S_0 \leftrightarrow S_1$ process. It is assumed that (a) the intensity of the exciting light is sufficiently low to linearize the kinetic equations and (b) that the microwave power is sufficiently high to warrant complete saturation. Since $n_\lambda^0 = P_\lambda k_\lambda^{-1}$, where P_λ is the relative populating rate of level λ, knowledge of n_λ^0 and k_λ determines P_λ. By fitting experimental transients to (1) and (1a), the values of k_λ were determined for the chlorins. They are presented in table 2, which also contains published data on H_2TPP [10] and H_2P [6] for comparison.

Since the transient-decay at $D+E$ and $D-E$ transitions for chlorin free base contains only one expo-

nential, eq. (1a) tells us that the common decay constant k_k is much smaller than k_i and k_j. This argument has to be handled with care, however, since the slowest exponential has the highest weight in the sum of exponentials due to the factor k_k^{-1} in (1a). Therefore, k_λ values of both chlorins were determined by least-square fitting using a computer.

The sign of $\Delta I_f(t\to\infty)$ in the presence of saturating microwaves contains another piece of information. If in the presence of microwaves at transitions $D+E$ and $D-E$, $\Delta I_f(\infty)$ is negative, corresponding to a decrease of fluorescence intensity when microwaves are switched on, (1) leads to

$$(k_j-k_k)(n_j^0-n_k^0)>0, \qquad (k_i-k_k)(n_i^0-n_k^0)>0\,.$$

This is the case for porphin and chlorin free base. With $k_k<k_i,k_j$ we find

$$n_i^0,\, n_j^0 > n_k^0 \qquad \text{and thus } P_i,P_j \gg P_k\,.$$

Since no $2E$ transition for the chlorins can be observed and yet $k_i\neq k_j$, we are led to conclude that the in-plane spin levels have a very small population difference. Furthermore, under slow passage conditions, the intensity ratio of the zero-field transitions at $D+E$ and $D-E$ are given by

$$\frac{I(D+E)}{I(D-E)}=\frac{\Delta I_f(D+E)}{\Delta I_f(D-E)}=\frac{(k_i-k_k)(k_j+k_k)(n_i^0-n_k^0)}{(k_j-k_k)(k_i+k_k)(n_j^0-n_k^0)}\,,$$

which follows from (1). With known values of k_λ ($\lambda = i,j,k$) and noting for chlorin free base that $n_k^0<n_i^0,\, n_j^0;\, n_i^0\approx n_j^0$, the ratio n_i^0/n_j^0 can be determined; for the relative populating rates P_λ limits can be defined.

Previous work on porphyrins and photosynthetic pigments incorporated in an *n*-alkane matrix [9,11] has shown that in these matrices, spin-levels at 4.2 K can be considered as isolated. We therefore believe that our kinetic data, obtained at 4.2 K, are not severely contaminated by a relaxation contribution. The distinct differences between the decay constants of the various spin-levels provide other evidence that this assumption is justified.

The contents of table 2 have been illustrated in fig. 3, showing that for all four compounds the middle spin-level is the most active in the populating and depopulating process. Reduction of one ring causes the in-plane kinetic constants to become less different

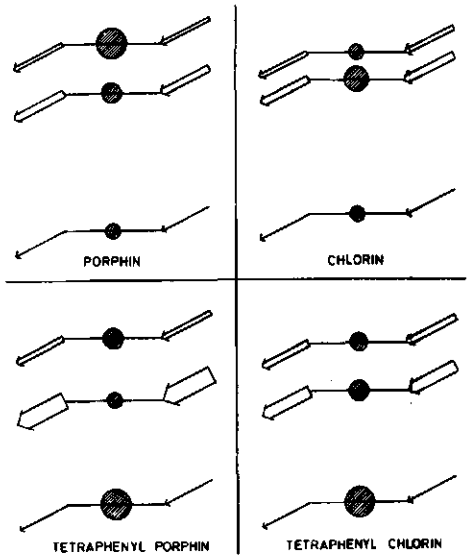

Fig. 3. ZFS diagrams and kinetic data of (tetraphenyl) porphin and (tetraphenyl) chlorin free base. Separation between ZFS levels is drawn to scale; furthermore, adjacent pairs of porphin and chlorin diagrams have a common point of gravity on the (vertical) energy scale, corresponding to $\frac{1}{3}(X+Y+Z)=0$, where X,Y,Z refer to ZFS energies of spin levels $|x\rangle$, $|y\rangle$ and $|z\rangle$, respectively. Arrows entering and leaving spin levels have widths corresponding to their relative magnitudes. Hatched circles represent relative steady-state population numbers; their differences are heavily exaggerated to illustrate the relative ordering of their magnitudes.

than in the porphyrins; also $n_j^0 \gtrsim n_i^0$, where the $\gtrsim$ sign follows from the intensity ratio $\Delta I_f(D+E)/\Delta I_f(D-E)$, in agreement with the absence of a transition at $2E$; $>$ expresses the fact that n_j^0 is near but slightly larger than n_i^0. Although the population differences are not expected to be large, due to a roughly parallel behaviour of k_λ and P_λ, they do determine the signs of the transitions. Thus, introduction of methine-phenyl groups reverses the sign of ΔI_f for the $D-E$ and $D+E$ transitions, apparently because $n_k^0>n_i^0,n_j^0$ in contrast to the unsubstituted compounds. The intersystem crossing rates P_λ can be qualitatively understood by noting that the spin ⊗ orbital symmetries of the in-plane spin levels are A_u and B_{1u}, whereas $|k\rangle$ has total symmetry B_{2u} or B_{3u}

depending on whether the electronic symmetry of the lowest triplet level is B_{3u} or B_{2u}. The in-plane spin levels can derive their activity from first-order spin–orbit coupling with singlet $n\pi^*$ levels or with excitations involving the σ-electrons. The spin-level $|k\rangle$, however, can only couple to $\pi\pi^*$ singlet states which are symmetric with respect to reflection in the molecular plane. This coupling has been shown to be weak [12] which explains why $P_k \ll P_i, P_j$. Phenyl substitution on the methine carbons results in mixing of the B into Q singlet states [13,14] and thus leads to increased $|k\rangle$ activity. Direct contribution to P_k from $\pi\pi^*$ excitation of the phenyl-groups which are rotated out-of-plane by $\approx 50°$ may also be significant.

The systematic changes in ZFS energies, as shown in fig. 3 can be rationalized by considering the reduction of one pyrrole ring as an electronic perturbation $\mathcal{H}'$ resulting in a mixing of other one-electron triplet excitations into the lowest triplet state of porphin free base, which has been demonstrated to have $^3B_{2u}$ ($b_{3g} \leftarrow b_{1u}$) symmetry [6]. If we assume the ring perturbation to be located in such a way that the NH–NH axis is parallel to the 7–8 bond (see fig. 1) then the chlorin perturbation has $A_g + B_{2u}$ symmetry in the D_{2h} group representation. The totally symmetric part of the perturbation mixes ($b_{2g} \leftarrow a_u$) excitations into the lowest triplet state B^0_{2u}, whereas it has also non-zero diagonal matrix elements $\langle B^0_{2u}|\mathcal{H}'|B^0_{2u}\rangle$.

The B_{2u} part of $\mathcal{H}'$ can only mix higher excited states of A_g symmetry into B^0_{2u} and its contribution is assumed to be smaller.

Taking only the A_{g_0} perturbation into consideration one expects the spin density distribution of B^0_{2u} to change by (a) a multiplication of all spin densities by the same factor and (b) a mixing of the B_{2u} ($b_{2g} \leftarrow a_u$) state into B^0_{2u}. If in the latter state $E < 0$*, the superposition of both perturbations can be shown to result in a decrease of the top levels, for porphin assigned [6] as $|y\rangle$, and an increase of $|x\rangle$, the middle level. Thus, the result will be a decrease of E, as is observed in fig. 3. This change can also be pictured as a partial restoration of D_{4h} symmetry by applying a perturbation in a direction perpendicular to the NH–NH axis. In the other configuration (NH–NH ⊥ 7–8 bond) a large *increase* of E is predicted, contrary to observation. This means, that in the lowest triplet state of both chlorins the NH–NH axis is probably parallel to the 7–8 bond, similar to the ground state configuration which is favored by a large electron density on the pyrrole rings containing carbon atoms 1,2 and 5,6 (see fig. 1) [14,15].

Our data do not confirm the tunnelling model proposed by Ponte Gonçalves [16] for the motion of the inner protons in H_2TPP, since even a small perturbation of the 4-fold symmetry of the TPP^{2-} skeleton would result in a sharp decrease of tunnelling rates [17]. The in-plane decay constants of H_2TPP_2 are close to those of H_2TPP, however.

4.5

5. Conclusions

From a comparison of new and published experimental data on ZFS and kinetic constants of H_2P, H_2PH_2, H_2TPP and H_2TPPH_2, we conclude: Ring reduction causes a change in spin density distribution corresponding to a *decrease* of the top level ZFS energy and an *increase* in the middle level position, resulting in a smaller E-value; the kinetic scheme is not essentially altered: the middle spin level is the most active one in the populating and depopulating pathway, whereas the changes of the decay constants are relatively small.

Introduction of methine-phenyl groups results in increased activity of the out-of-plane spin level, a decrease of D and an increase of E.

Our results indicate that in the lowest triplet state of both chlorins, the NH–NH axis is favored to be parallel to the 7–8 direction of the reduced ring. At low temperature, experimental data suggest that in the triplet state neither chlorin nor tetraphenylchlorin free base is present in two tautomeric forms.

Acknowledgement

We want to thank Mr. P. Geerse, for synthesis and purification of compounds, and Dr. D. de Bie for his support in these matters. We are indebted to Mr. J. Meuleman for assistance in computing and to Mr. P.A. de Jager and the Physical Chemistry Machine Shop staff for technical assistance.

* Calculated, using a point-dipole approximation and ground-state MO coefficients of porphin according to Knop, as published in ref. [6].

References

[1] C.L. Greenblatt and J.A. Schiff, J. Protozoölogy 6 (1959) 23.
[2] S.C. Straley, W.W. Parson, D.C. Mauzerall and R.K. Clayton, Biophys. Biochim. Acta 305 (1973) 597.
[3] C.J.P. Spruit, private communication.
[4] W.G. van Dorp, T.J. Schaafsma, M. Soma and J.H. van der Waals, Chem. Phys. Letters 21 (1973) 221.
[5] R.H. Clarke and R.H. Hofeldt, J. Am. Chem. Soc. 96 (1974) 3005.
[6] W.G. van Dorp, M. Soma, J.A. Kooter and J.H. van der Waals, Mol. Phys. 28 (1974) 1551.
[7] U. Eissner and R.P. Linstead, J. Chem. Soc. (1956) 3742.
[8] E.C. Murray and R.N. Keller, J. Org. Chem. 34 (1969) 2234.
[9] R.H. Clarke and R.H. Hofeldt, J. Chem. Phys. 61 (1974) 4582.
[10] R.H. Clarke and R.E. Connors, J. Chem. Phys. 62 (1975) 1600.
[11] I.Y. Chan, W.G. van Dorp, T.J. Schaafsma and J.H. van der Waals, Mol. Phys. 22 (1971) 741, 753.
[12] D.S. McClure, J. Chem. Phys. 20 (1952) 682.
[13] M. Gouterman, J. Mol. Spectry. 6 (1961) 138; J. Chem. Phys. 30 (1959) 1139.
[14] C. Weiss, H. Kobayashi and M. Gouterman, J. Mol. Spectry. 16 (1965) 415.
[15] J.O. Alben, S.S. Choi, A.D. Adler and W.S. Caughey, in: The chenical and physical behaviour of porphyrin compounds and related structures, Vol. 206, ed. A.D. Adler(New York Acad. Sci., New York, 1973) p. 278.
[16] R.P. Burgner and A.M. Ponte-Gonçalves, J. Chem. Phys. 60 (1974) 2942.
[17] E.F. Caldin, Chem. Rev. 69 (1969) 135.
[18] J.E. Falk, Porphyrins and metalloporphyrins (Elsevier, Amsterdam, 1964) p. 4.

CHAPTER 5

ZERO FIELD OPTICALLY DETECTED MAGNETIC RESONANCE OF MODELCOMPOUNDS FOR PHEOPHEOPHYTINS

S.J. van der Bent and T.J. Schaafsma

(Submitted for publication in J. Chem. Phys.)

5.1 INTRODUCTION

Following a preliminary study of chlorin free base [1] (systematic name: dihydroporphin free base) as a model compound of pheophytin we present in this paper a more detailed account of some new experimental results of the kinetics of the lowest triplet T_0 state of this compound. By improving the ODMR spectrometer w.r.t. a previous version [4] we could measure at higher optical excitation rate resulting in a higher S/N ratio, and allowing kinetic data to be determined over a range of light intensities. This enabled extrapolation of experimental decay constants to zero excitation rate, which is necessary for a precise determination of the correct decay constants of the T_0 spin states [2,3] .

In addition, we have obtained reliable values for the relative populating--rates of the three spin states of T_0. Such measurements are of importance since they provide kinetic and static parameters of T_0, bridging the gap between porphin free base, which has been thoroughly studied [3,6-8], and natural photosynthetic pigments, which are far less understood w.r.t. their electronic structure.

Similarly to what has been found in porphin free base [3,8] chlorin free base exhibits a photoinduced rearrangement of the two central protons. There are interesting differences with porphin-behaviour, however, due to the asymmetric potential inside the chlorin ring, since this compound has one saturated pyrrole ring. (Fig. 5.1.1).

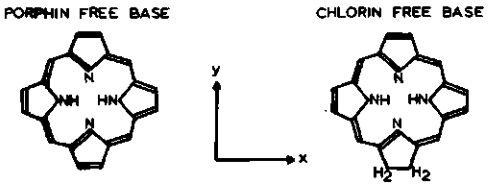

Fig. 5.1.1.
Skeleton of porphin free base and chlorin free base. x,y,z defines the molecular axis-system.

5.2 EXPERIMENTAL

Most of the experimental details have been described in previous papers [3,4]. Some modifications will be described in this section. Unless stated otherwise, all experiments were carried out at 4.2 K.

For optimum S/N ratio we have used a 900 W Xenon arc (Osram XBO 900 W/2) as an excitation source and a dichroic mirror (Schott type 311) for the separation of the blue excitation and red emission light. The ODMR transitions are detected by monitoring the dihydroporphin 0-0 fluorescence emission at 635 nm. [5,6] For the selection of the blue excitation light we used either a combination of a 12 cm cuvette containing water and a Balzers interference filter (Filtraflex B 40) transmitting at 403 nm (bandwidth: 15 nm) or a 12 cm cuvette containing a $CuSO_4$ solution combined with Schott BG 12 and GG 395 filters. The latter combination has a bandwidth of 80 nm.

Two methods were used to determine the kinetics of the spin states of the lowest excited triplet state:

(i) Following Clarke [5], we used a microwave pulse long compared to the mean triplet state lifetime k_T, resulting in a simpler exponential curve fitting, but requiring saturating microwave pulses.

(ii) The second method is due to Van Dorp *et al.* [3] who used a relatively short (i.e. short compared to the lifetime of the fastest decaying T_0 spin state) microwave pulse; this method requires no saturating microwaves, but leads to a more complicated exponential curve fitting [2].

In order to determine the mean triplet state decay constant we used fluorescence onset experiments at 77 K without microwaves or at 4.2 K with CW irradiation at two resonant microwave frequencies as described by Van Dorp *et al.* [3]. To switch the light on and off we used a Vincent Associates Uniblitz model 225 electronic shutter.

For those ODMR transitions, which were strong enough, frequencies were determined as follows: the change of fluorescence intensity $\Delta I_f(t)$ for both transitions was measured while stepwise varying the frequency in a small region ($\sim$ 10 MHz) around the frequencies which were already approximately known using pulsed microwaves following Clarke [5]. The frequency where the amplitude $\Delta I_f(t)$ had a maximum was taken to be the frequency of the ODMR transition. In the following we will refer to this method as the "maximum response" method. The frequency of the microwavesource was measured with a Systron-Donner 1017 series frequency meter with a model 1292A plug-in. In this way, sizeable errors due to

non-linear calibration and systematic errors in markers produced by the swept microwavesource, are avoided.

5.3 RESULTS

5.3.1 ODMR and optical spectroscopy

ODMR spectra of chlorin in n-octane at 4.2 K are presented in fig. 5.3.1.1 A-C, where fig. 5.3.1.1 A is in close agreement with a previously published spectrum with lower S/N ratio [1] in which the transitions marked by 2 through 4 in the D+E region of fig. 5.3.1.1 were not visible.
Anticipating a discussion of spectra A-C, we assign transitions 1-4 to four physically different species 1-4, each with its own D+E and D-E transition. For the D-E region all species have their resonance within one ODMR peak, whereas in the D+E region they are resolved.

The spectra A-C are shown in the order of increasing time of exposure to exciting light in a band centered at 410 nm and halfwidth of $\sim$ 30 nm. We did not carry out an accurate analysis of the slow changes of the ODMR spectra with time during continuous irradation. Spectrum A was taken of a sample for which the product of excitation rate and exposure time was much smaller than for spectra

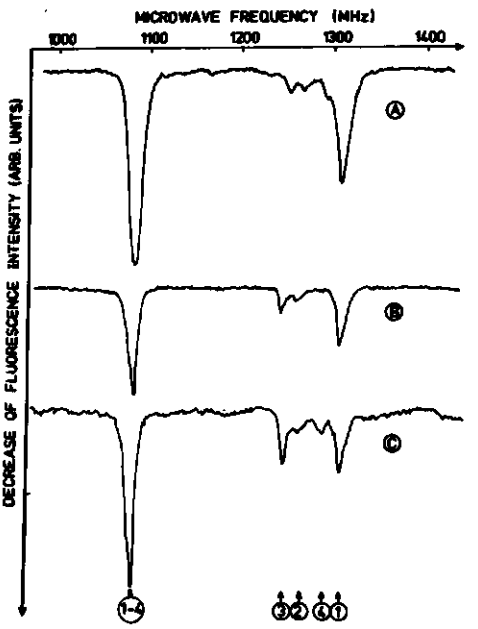

Fig. 5.3.1.1.
Zerofield ODMR spectra of chlorin free base in n-octane single crystal at 4.2 K. Spectra A was taken < 1 hr after starting irradiation; B and C are taken 24 hrs apart. Detection wavelength/bandwidth: A: 635/1; B: 635/1; C: 635/10 nm. Microwavepower: A: 50; B: 10; C: 50 mW. Sweeprate: A: 80; B: 40; C: 40 MHz/sec. Number of accumulated transients: A: 2^9; B: 2^{14}; C: 2^8. Labels 1-4 refer to D+E resonances, mentioned in text. A,B,C have been recorded at different gain.

B and C, which were taken ∿ 24 hrs apart, whereas the excitationrate is estimated to be $R_{ex} \sim 500\ sec^{-1}$ per molecule. A fourth spectrum taken 24 hrs after spectrum C was recorded, did not show detectable differences with spectrum C, all experimental conditions being identical. The spectra A-C have not been recorded at identical experimental conditions (see captions of fig. 5.3.1.1 A-C). It was checked however, that these differences did not affect our conclusions: microwavepower is ∿ 3 times higher for spectrum A than for B and C but this does not cause changes in the relative intensities of any transitions. Some power broadening is noticeable comparing the spectra A with B or C. The optical detection bandwidth of C is much smaller (1 nm) than that for A and C (20 and 10 nm, respectively).

We have compared spectrum B with those observed at various detection wavelengths around the maximum of the 0-0 fluorescence band; no significant changes in relative intensity of transitions 1-4 were observed in the (D+E) region for different wavelengths within the 0-0 band, except for a small (∿5%) contribution at the red edge assigned to species 5. The latter is detected with a relative intensity of the D+E transition of ∿ 50% w.r.t. the species 1 resonance, when detecting the 0-0 fluorescence band on the red edge at 635.8 nm with a 1 nm slitwidth. At lower optical resolution (10-20 nm), monitoring the total 0-0 fluorescence band, species 5 is barely detected and has a maximum relative intensity of < 10% of the total D+E resonance intensity. In view of its slightly red shifted fluorescence maximum (1-2 nm w.r.t. species 1-4) and by analogy with similar shifts in pheophytin-a [9], which is a side-chain substituted chlorin, species 5 may be assigned as chlorin in a n-octane crystal site, where it is near a polar impurity. We will further ignore the presence of species 5, which did not interfere with our measurements.

It turns out that the ratio of the integrated total intensities in the D+E region 1-4 and the D-E integrated intensity does not vary in time within our accuracy of measurement between spectra A, B and C, despite the major changes observed in the shape of the spectra in the D+E region: transitions of species 1 and 2 decrease in amplitude after prolonged irradiation, whereas 3 and 4 simultaneously increase.

The 2E transition is not visible using single resonance ODMR; thus we used double resonance with CW irradiation at ν(D+E) and sweeping through the region 10 - 1200 MHz. Fig. 5.3.1.2 represents such a doubleresonance spectrum for species 1.

The amplitudes of the D-E and 2E transitions in fig. 5.3.1.2 are not equal, as they should be when the D+E transition is completely saturated, due to inhomo-

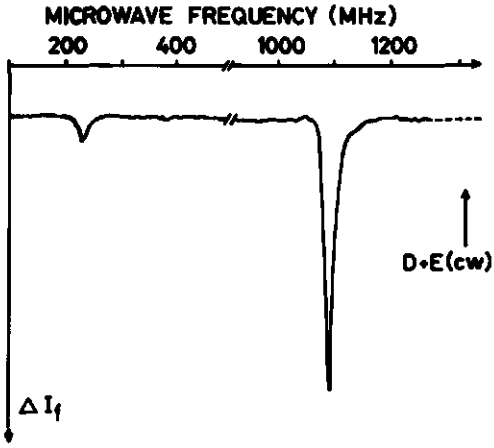

Fig. 5.3.1.2.
Double resonance zerofield ODMR spectra of chlorin free base in a n-octane single crystal at 4.2 K, observed during continuous irradiation at 1308 MHz and 50 mW microwavepower. Detection wavelength/bandwidth 635/20 nm. Sweeprate: 2600 MHz/sec. Number of accumulated spectra 2^{12}; 1308 MHz radiation was unmodulated.

geneous broadening of the D+E transition. This is expected in the absence of FM modulation of the D+E resonance frequency.

Only for the transitions of species 1 we have used double-resonance as an additional check for the determination of $\nu(2E)$; for all observed species $\nu(2E)$ was determined from the difference between $\nu(D+E)$ and $\nu(D-E)$.

The frequencies for species 2 through 5 were obtained by interpolation between $\nu_1(D+E)$ and $\nu_1(D-E)$, where the subscript 1 refers to species 1; these frequencies were determined accurately as described in the previous section. The data are collected in Table I.

TABLE I Frequencies of chlorin ODMR transitions in n-octane/4.2K

Species	$\nu(D+E)$ (MHz)	$\nu(D-E)$ (MHz)	$\nu(2E)$ (MHz)
1	1308±2	1085±2	223±3 [a]
2	1262±3	1085±2	174±4
3	1246±3 [b]	1085±2	161±4
4	1289±3	1085±2	204±4
5	1302±4	1079±4	223±4

a also determined by double resonance (fig. 5.3.1.2) to be 228±5 MHz
b also determined with the maximum response method to be 1249±2 MHz.

Note

The values of $\nu(D+E)$ and $\nu(D-E)$ of species 1 are somewhat (7 MHz) higher than previously reported [3], due to a systematic error in marker frequencies in the older measurements.

TABLE II Experimental and calculated excitation wavelengths (nm) for chlorin in n-octane/4.2 K

λ(calc)[a]	λ(exp)[b]	λ(calc)[a]	λ(exp)[b]	λ(calc)[a]	λ(exp)[b]
635	635	607	608	584	585
631		602	603	580	
628		599	599	578	578
622	623	595		576	
613		591	590	567	568
612		588	588	564	
				561	562

a. Calculated from fluorescence emission wavelengths, assuming identical vibrational progressions for the ground- and first excited singlet states.
b. Experimental fluorescence-excitation wavelengths.

TABLE III Kinetic constants of the lowest excited triplet spin states of chlorin free base in n-octane/4.2 K.[a]

	Decay rate constant (sec^{-1})	Method		Relative populating rates (%)	Method
k_i	174 ± 33	b	p_i	36 ± 8	c
	172 ± 11	c			
k_j	464 ± 60	b	p_j	62 ± 13	c
	406 ± 33	c			
k_k	23.9 ± 2.9	b	p_k	2 ± .5	c
	23.4 ± 0.7	c			
k_T(4.2 K)	221 ± 23	b		Steady state population	
	200 ± 12	c			
	370 ± 19	d	n_i	.47 ±.09	f
			n_j	.34 ±.06	f
k_T(77 K)	325 ± 17	e	n_k	.19 ±.04	f

a. Spinstates are labeled $|i\rangle$, $|j\rangle$, and $|k\rangle$ in decreasing order of zero field energy; subscripts i, j, and k attached to the symbols k, p, and n, refer to these spin states; k_m (m=i,j,k) is the total decay rate constant (almost entirely being of non-radiative character) of spin state $|m\rangle$; similarly p_m and n_m refer to relative populating rates and steady state populations of $|m\rangle$.
b. Determined following van Dorp's method [3].
c. Determined following Clarke's method [5].
d. Determined from fluorescence onset at 4.2 K with presence of CW microwave radiation at ν(D+E) and ν(D-E).
e. Determined from fluorescence onset at 77 K (no microwaves present).
f. Calculated from k_m and p_m measured by method c.

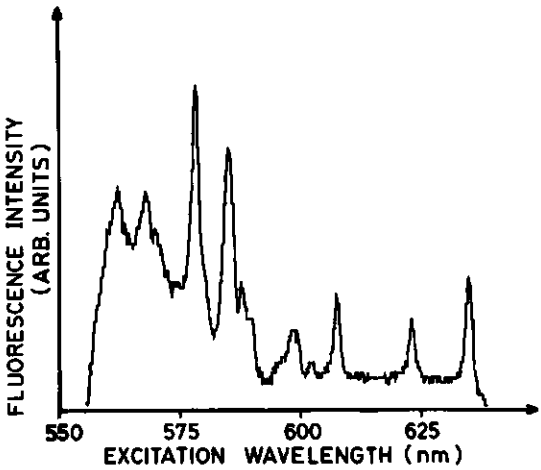

Fig. 5.3.1.3.
Fluorescence excitation spectrum of chlorin free base in a n-octane single crystal at 4.2 K. Excitation bandwidth 1 nm; detection bandwidth 20 nm; detection wavelength 676 nm; scan rate excitation: 12.5 nm/min. The spectrum has been obtained using background-subtraction.

None of the transitions in the D+E region exhibits a significant change of its intensity if microwavepower is increased from 1 to 50 mW. Even at power-levels as low as 1 mW we find considerable saturation broadening. The smallest linewidth was measured at 80 μW to be 6.8 MHz for the D-E transition and 4 MHz for the D+E transition which is the most intense ODMR transition at this power-level. Special care was taken to ensure that intensity measurements were only made under saturating conditions.

Fluorescencespectra were identical to those previously published [1] and did not change during experiments. A fluorescence-excitation spectrum is shown in fig. 5.3.1.3, and exhibits complete wavenumber mirror-symmetry with the fluorescence emission spectrum in the 560-635 nm region (see Table II). As is apparent from this Table, the calculated fluorescence excitation spectrum agrees with experiment to within 1 nm, which was the resolution of the monochromator. The absolute values of wavelengths are accurate to ± .5 nm.

5.3.2 Triplet state kinetics

From time dependent single resonance experiments, saturating either the D+E or D-E transition with a 1-2 msec microwavepulse following the method of Van Dorp *et al.* [3], or with a 50-100 msec microwave pulse following the method of Clarke *et al.* [5], the kinetic parameters of the lowest triplet state T_0 (species 1) were determined as collected in Table III. The data presented in

this Table, column b, were obtained by taking the average of several measurements at frequencies at and close to the maximum of the ODMR profile. In separate experiments at 77 K and 4.2 K, we determined the mean decay time k_T of T_0 by the fluorescence-onset method 3 also given in Table III.
The errors given in Table III for k_i, k_j and k_k were determined from the r.m.s. deviation between the experimental and calculated fluorescence transients. For the k-values, obtained with Van Dorp's method, a regular distribution of residues is obtained if two exponentials are used for fitting the calculated curve to the experimental transient. Using Clarke's method, we have found an instrumental artefact to interfere with our measurements; it consists of an exponential with an apparent decay rate of 50 sec^{-1}, its amplitude increasing with light-intensity. Including this 50 sec^{-1} component in a double-exponential curve-fitting, yielded a regular distribution of residues, and allowed the determination of pure decay rates of spin states. It should be noted, that in the range of excitation rates employed in our measurements, the experimental transients obtained by the method van Dorp can be fitted by double exponential with sufficient accuracy, whereas the curve-fitting of data obtained by Clarke's method could be carried out using a single exponential (in addition to the interfering 50 sec^{-1} component).
Errors in p_i, p_j, and p_k are quoted as standard deviations of the slope of the experimental decay-rates *vs.* light intensity. The errors in n_i, n_j, and n_k have been calculated as the r.m.s. sum of errors in k's and p's. The decay constants at finite light intensity are found to vary somewhat over the profile of the microwave transitions: in a region $\pm$ 3 MHz around the maximum of the profile, decay constants did not vary outside the accuracy of our measurements. At larger distance from the center of the transition, the decay constants eventually decrease to about 50% of the value measured at the top. This may be ascribed to a smaller optical excitation rate for molecules at the edge of the absorption band which also have slightly shifted zero field resonance positions. If this explanation is correct, these shifted resonances arise from molecules in different environments.

5.4 DISCUSSION

The sequence of spectra shown in fig. 5.3.1.1 A-C can be viewed to arise from a slow, light-induced transformation of a chlorin species (1) with resonance-frequencies 1308 and 1085 MHz into a different species (3) with $\nu(D+E)$ = 1246, $\nu(D-E)$ = 1085 MHz.

After long periods of irradiation, both species reach ∿50/50 equilibrium, as judged from their D+E amplitudes in fig. 5.3.1.1 C. A resonance due to a species labeled 2 with smaller amplitude appears to be always associated with the species 1 resonance; its timedependence and spectral characteristics are undistinguishable from those of species 1; a similar satellite at 1289 MHz (species 4) is associated with the species 3 resonance.

Ascribing the different D+E resonances to different chlorin species, we have silently assumed that for a single molecule only three resonances can be observed at $\nu(D+E)$, $\nu(D-E)$ and $\nu(2E)$; the latter is commonly too weak to be observed for photosynthetic pigments. Satellites have been observed in ODMR, arising from nuclear quadrupole interaction [10], but their relative amplitudes do not change with time. Therefore, we assign the different D+E resonances to different species, where species 1 through 4 have D-E resonance frequencies equal to within the ∿10 MHz linewidth at half height of the D-E peak.

For porphin free base in n-octane, similar light induced changes have been observed both by optical spectroscopy [6] and magnetic resonance [7]. There are some striking differences with the behaviour of chlorin, however: for porphin in n-octane at 1.2 K, a quasi-line fluorescence spectrum was observed [7], each fluorescence-"line" being doubled with a splitting of $\sim 65\ cm^{-1}$. The ODMR spectrum [6] exhibits similar doubling of D-E and D+E transitions; the correlation of each separate pair of D-E and D+E transitions and their associated fluorescence-progressions with two physically distinct species (i.e. tautomers) has been convincingly demonstrated [6]. Under broadband excitation, one observes both species by ODMR and fluorescence with almost equal amplitude. Photoinduced transformation of one species into the other can be achieved by *selective* optical absorption of one species, using laser irradiation [11]. This phototautomerism involves a rotation of the H-H axis in porphin free base by 90^{o}, as is confirmed by high field EPR [7].

The possibility to distinguish porphin tautomers by different fluorescence and ODMR transitions is evident from fig. 5.4.1.A, since the crystalfield interacting with either the first excited singlet state (S_1) or the lowest excited triplet state (T_0) has lower than D_{4h} symmetry causing the energy of S_1 and zero field splitting (ZFS) of T_0 of both tautomers to be slightly different. For the groundstate, the energy difference between both tautomers is apperantly so small that they occur in equal statistical weight when a liquid solution of porphin in n-octane is slowly crystallized into a single crystal.

For chlorin free base we have a quite different situation as depicted in fig. 5.4.1.B: the potential energy surface of the chlorin dianion skeleton after

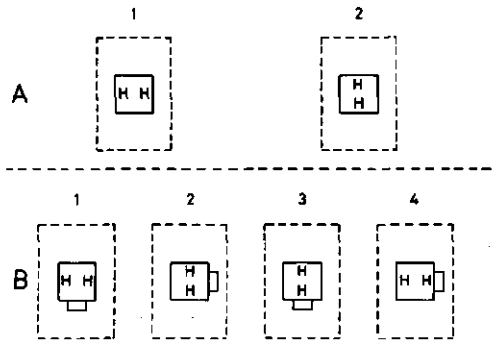

Fig. 5.4.1.
A: Porphin free base in a crystal site with lower than D_4 symmetry; B: Chlorin free base in a similar crystal site. Skeletons of porphin and chlorin free base have been represented by fully drawn lines, the crystal environment by dashed lines. Rotated porphin/chlorin skeletons have been labeled by 1 and 2 in A and B, whereas rotation of protons within the chlorin skeleton results in 3 and 4 in diagram B.

removal of the two inner protons has C_{2v} symmetry, thus making both tautomers to occur with unequal statistical weight in the groundstate if a solution of chlorin in n-octane is slowly crystallized. In fact, a previous study [1] has shown, that the tautomer with the H-H axis parallel to the pyrrole saturated bond is almost exclusively present in fresh samples of chlorin in n-octane single crystals. Now, *broadband* excitation at $\sim$ 400 nm of such a sample induces the transformation to one tautomer into the other, until a 50/50 mixture is reached. Prolonged broadband irradiation leaves this ratio unchanged, as found by comparing ODMR spectra. The constant integrated intensity in the D+E region for different excitation periods relative to that of the D-E transition provides another argument that the single tautomer which was originally present, is transformed into a second one until equilibrium is reached. When the exciting light is turned off, the proton pairs remain fixed in both positions, at least at 4.2 K.

Returning to fig. 5.3.1.1. it can be understood why at least one of the chlorin ODMR resonances (D+E) is split into *four* different peaks after long periods of excitation, in contrast with porphin free base exhibiting only *two* resonances for the D+E as well as the D-E transition; we note that two chlorin dianion skeletons obtained by removing two protons from chlorin free base and rotated by 90° about an axis perpendicular to the chlorin plane, within a crystal site with lower than fourfold symmetry, are physically non-equivalent (cf. fig. 5.4.1.B 1 *vs.* 2, and 3 *vs.* 4); each of the non-equivalent orientations may carry two protons with a H-H axis parallel or perpendicular to the in-plane C_2 axis of chlorin, yielding a total of *four* distinguishable chlorin molecules. The resonances 1-4 of fig. 5.3.1.1. have been assigned to those four different

chlorin molecules in fig. 5.4.1.B, such that the pairs of resonances 1/3 and 2/4 result from a rotation of protons, whereas the pairs 1/2 and 3/4 arise from a rotation of the chlorin skeleton within the crystal lattice. Note that the splitting $\nu_1(D+E) - \nu_2(D+E) = 46$ MHz is very close to $\nu_4(D+E) - \nu_3(D+E) = 43$ MHz, which is expected for the same crystal field acting on structurally similar tautomers.

If the previous assignment is correct, removing the orientational inequivalency of the chlorin skeleton within the crystal lattice by transformation of chlorin into porphin free base would cause the resonances 1 and 4 as well as 2 and 3 to coalesce. For the D+E transitions of chlorin we obtain

$$\tfrac{1}{2}\{\nu_1(D+E) + \nu_4(D+E)\} - \tfrac{1}{2}\{\nu_2(D+E) + \nu_3(D+E)\} = 44 \text{ MHZ}$$

The splitting of the D-E transitions is within the linewidth of $\sim$ 7 MHz. The pronounced difference between both splittings is very similar to that observed for porphin free base: 33 and 4 MHz, respectively [6] and is also found in ODMR spectra of photosynthetic pigments in solid alkane matrices [9]. By inspection of fig. 5.4.1 we may obtain the splitting of the D+E resonances due to rotation of protons alone, i.e. in the absence of crystal field splittings: by rotation of the entire chlorin molecule, including protons in fixed positions, within the crystal site, symbolized by a rectangular box, we observe diagrams 1-4 to be transformed into each other as $1 \leftrightarrow 2$ and $3 \leftrightarrow 4$. Thus, the average values $\frac{1}{2}(\nu_1 + \nu_2)$ and $\frac{1}{2}(\nu_3 + \nu_4)$ represent resonances for which the effect of the orientation of the chlorin molecule within the lattice site, i.e. crystal field splittings, have been eliminated.

The difference $\frac{1}{2}(\nu_1 + \nu_2) - \frac{1}{2}(\nu_3 + \nu_4) = 18$ MHz represents the purely tautomeric splitting of D+E resonances for chlorin structures with the H-H axis parallel and perpendicular to the saturated pyrrole bond.

Averaging over both orientations of the H-H axis in the chlorin skeleton restores D_{4h} symmetry and one expects the molecule to become insensitive to the orientation within the crystalsite. This means that the average $\frac{1}{2}(\nu_1 + \nu_3)$ should approximately coincide with $\frac{1}{2}(\nu_2 + \nu_4)$ which is indeed found from Table I.

The absence of a resolved crystal field splitting in the fluorescence spectrum of chlorin is in striking contrast with the 65 cm^{-1} splitting observed throughout the porphin free base fluorescence spectrum [6]. Such a splitting is also absent in the fluorescence excitation spectrum of chlorin, shown in fig. 5.3.1.3. Probably one of the Q transitions (in our axis system, shown in fig.

5.1.2, designated as Q_y, corresponding to Q_x in Goutermans work [12] hides in the 480 nm region which was not accessible under the conditions of our experiment. The Q_x fluorescence excitation spectrum is an almost perfect mirror image of the fluorescence spectrum. Although the different behaviour of porphin and chlorin free base in n-octane single crystals is not yet understood, there is no doubt that both species previously denoted by 1 and 3, and their respective partners 2 and 4, all have fluorescence spectra coinciding to within experimental error.

Finally, we want to comment on the kinetic data, presented in Table III: The k values quoted in Table III exhibit some differences with previously published results [3,4]. For k_k (= k_z in the molecular axis system of fig. 5.1.1) there is excellent agreement, whereas k_i (= k_y) in Table III is equal within experimental error to the previously reported value. For k_j (= k_x), however, the presently determined value is considerably higher than in ref.[3] and [4]. This is probably due to a 50 sec^{-1} contamination, mentioned above, of the older data.

We cannot exclude that the tabulated decay constants are contaminated by spinlattice relaxation; this contribution can be shown to be small for the extrapolated values $\frac{1}{2}(k_i + k_k)$ and $\frac{1}{2}(k_j + k_k)$ [2]. The mean decay constant $k_T = \frac{1}{3}(k_i + k_j + k_k)$ calculated from the data of Table III following methods b and c does not agree with the value obtained from fluorescence onset experiments at 4.2 and 77 K. The 4.2 K experimental value of k_T, obtained from double-resonance experiments may be too fast if saturation is incomplete, evidence for which has been found in section 5.3.1. For the discrepancy between k_T obtained at 77 K and the caculated value $\frac{1}{3}(k_i + k_j + k_k)$ we do not have a satisfactory explanation.

Finally, we note that the spin state labels i, j, and k can be identified with y, x, and z as in [3].

5.5 REFERENCES

1. S.J. van der Bent. T.J. Schaafsma. Chem.Phys.Lett. 35 (1975) 45-50.
2. S.J. van der Bent. Thesis, Chapter 3.
3. W.G. van Dorp, W.H. Schoemaker, M. Soma, J.H. van der Waals; Mol.Phys. 30 (1975) 1701-1721.
4. S.J. van der Bent, P.A. de Jager, T.J. Schaafsma. Rev.Sci.Instrum. 47 (1976) 117-121.
5. R.H. Clarke, R.H. Hofeldt. J.Chem.Phys. 61 (1974) 4582-4587.
6. W.G. van Dorp, T.J. Schaafsma, M. Soma, J.H. van der Waals. Chem.Phys.Lett. 21 (1973) 47-51.
7. W.G. van Dorp, M. Soma, J.A. Kooter, J.H. van der Waals. Mol.Phys. 28 (1974) 1551-1568.
8. S. Völker, J.H. van der Waals. Mol.Phys. 32 (1976) 1703-1718.
9. S.J. van der Bent, T.J. Schaafsma, in press.
10. A.H. Francis, C.B. Harris. J.Chem.Phys. 57 (1972) 1050-1065.
11. K.N. Solov'ev, I.E. Zalesski, V.N. Kotlo, S.F. Shkirman. J.Exp.Theor. Phys.Lett. 17 (1973) 332.
12. M. Gouterman in: Excited states of matter (C.W. Choppee ed.), Grad. Studies Texas Techn.Univ., 2: 1-74, 27 April 1973, 63-103.

CHAPTER 6

INTERACTION OF LIGHT AND MICROWAVES WITH PHEOPHYTINS

Sievert J. van der Bent and Tjeerd J. Schaafsma
(submitted for publication in Chem.Phys.Lett.)

6.1 INTRODUCTION

Optical spectroscopy of photosynthetic pigments has been frequently used for their identification as well as for defining solute-solute and solute-solvent interactions. Interpretation of the results of such optical studies is complicated, since absorption- and emission spectra usually consist of broad ($\sim$300-400cm^{-1}) overlapping bands, resulting from different species, with different molecular structure or in different environments.
This handicap is particularly troublesome in spectroscopic studies of intact biological systems, such as *in vivo* photosynthetic units, containing a multicomponent mixture of pigments in various environments. In this paper, we want to demonstrate how Optically Detected Magnetic Resonance (ODMR) [1] can be helpful in discriminating photosynthetic pigments in various environments, using pheophytin-a in solid n-octane as an illustration.

In ODMR, transitions between pairs of spin levels of the lowest triplet state T_0 are induced by microwave absorption and detected by their effect on the rate of emission (or absorption) of optical quanta from (or into) any level participating in an optical pumping cycle including T_0. Noting that the triplet zero-field splitting (ZFS) parameters are sensitive to molecular structure, state of aggregation, and molecular environment, we have reversed the usual ODMR procedure by observing only those emissionbands which in our case are part of the fluorescence spectrum, and which are linked to a particular ODMR transition. In this way, microwave-modulated fluorescence spectra with a reduced inhomogeneous linewidth have been obtained from samples exhibiting broad fluorescence bands in the absence of microwave modulation. A similar technique has been developed by El Sayed and his group for decomposing phosphorescence spectra of various traps in doped molecular crystals [2].

As it turns out, increasing pigment-solvent interaction not only changes the magnitude of the ZFS parameters, but also can increase the rate of spin--lattice relaxation (SLR). This phenomenon is important for triplet traps in biological systems which can be coupled to the lattice via electron-phonon

coupling, even at T ∿ 1K. SLR in such *in vivo* units is relatively fast as compared to *in vitro* relaxation [3].

6.2 EXPERIMENTAL

Pheophytin-a (in the following abbreviated as Ph-a) was prepared from chlorophyll [4]. Dry n-octane freed from UV absorbing impurities by chromatography [5] was used as a solvent.

Ph-a in n-octane solution to which ethanol had been added in slight excess of pheophytin was quickly frozen by immersion into liquid nitrogen and then into liquid helium. ODMR spectra at various fluorescence wavelengths were obtained using a set-up, outlined in fig. 6.2.1 and described in detail elsewhere [6]. Microwave modulated fluorescence spectra were recorded by 18 Hz amplitude--modulation of the microwave source (Hewlett-Packard 8690B/8699B) and phase--sensitive detection (Brookdeal 411/422) at the modulation frequency of the a.c. component of the fluorescence emission. An RCA C31034 A photomultiplier was used for fluorescence detection in combination with a Spex Minimate monochromator. Zero-field ODMR spectra were recorded using a Hewlett-Packard 5480 B Signal Analyzer for S/N improvement.

6.3 RESULTS

Fig. 6.3.1 represents an ODMR spectrum of Ph-a in n-octane containing a small amount of ethanol. A strong transition corresponding to a decrease of fluorescence is found at 980 ± 10 MHz; at 1110 ± 5 MHz and 1160 ± 20 MHz the fluorescence intensity exhibits peaks corresponding to a decrease and an increase, respectively. This spectrum is obtained with wide-band fluorescence detection (λ = 665 - 685 nm) covering most of the main emission-band. Close inspection reveals the presence of a small shoulder at 668 nm, a dominant maximum at 675 nm and an unresolved shoulder at ∿ 683 nm (see dotted line in fig. 6.3.3).

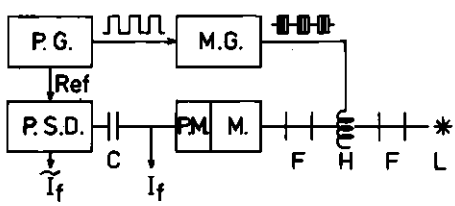

Figure 6.2.1 Experimental set-up for the measurement of microwave-modulated fluorescence spectra; F = filters, lenses; C = capacitor; H = helix containing sample kept at 4.2 K; L = 900 Watt Osram XBO Superhigh pressure xenon arc; P.G. = pulse generator; M.G. = microwave generator; P.S.D. = phase--sensitive detector; P.M./M. = photomultiplier/monochromator; $\tilde{I}_f$ and I_f represent the microwave-modulated and total fluorescence emission, respectively; Ref. = reference signal.

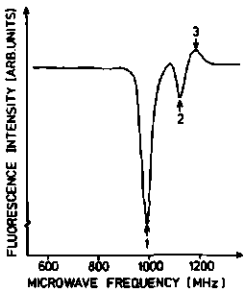

Figure 6.3.1

ODMR spectrum of pheophytin-a (10^{-5}M) in n-octane containing ethanol in slight excess of 10^{-5}M; T = 4.2 K; Sweep-rate 1300 MHz/sec; Fluorescence detection band 675 ± 10 nm; 1 - 3 refer to text. Note that transitions 1 and 2 correspond to a decrease and 3 to an increase of fluorescence intensity.

Monitoring this spectrum at 667.5 nm with a 1 nm detection bandwidth, results in the ODMR spectrum labeled A in fig. 6.3.2, exhibiting two microwave resonances of ∿ 30 MHz width, both of which correspond to a decrease of fluorescence; ODMR spectra, labeled B and C in fig. 6.3.2 were taken at 675 and 683 nm, respectively, with a detection bandwidth of 1 nm. Clearly, a redshift of the fluorescence detection wavelength corresponds to a change of the shape of the ODMR spectrum: the amplitude of the high frequency transition in the 1100 MHz region first decreases and then reverses sign upon a redshift of the fluorescence detection wavelength. Simultaneously, the top of this ODMR peak shifts to higher frequency. The 980 MHz transition does not show such a conspicuous change of amplitude when the fluorescence detection wavelength increases, but shifts to lower frequency.

Similar effects have been observed for pheophytin-b (Ph b) in n-octane, doped with a trace of diethylether. Table I collects the observed ZFS parameters for both compounds. The Ph-b D-value agrees with previous measurements (R.H. Clarke, private communication).

Table I. ZFS parameters of Ph-a and Ph-b in n-octane at 4.2 K.

Compound	D (x $10^4 cm^{-1}$)	E (x $10^4 cm^{-1}$)	Fluorescence detection wavelength (nm) [a]
Ph-a	350±2	20±1	667.5(±.5)
	348±2	25±1	675(±.5)
	353±7	33±3	683(±.5)
Ph-b	361±5	32±3	660(±10)
	366±5	- [b]	660(±10)

a. Number in parentheses indicates fluorescence detection bandwidth.
b. Number uncertain.

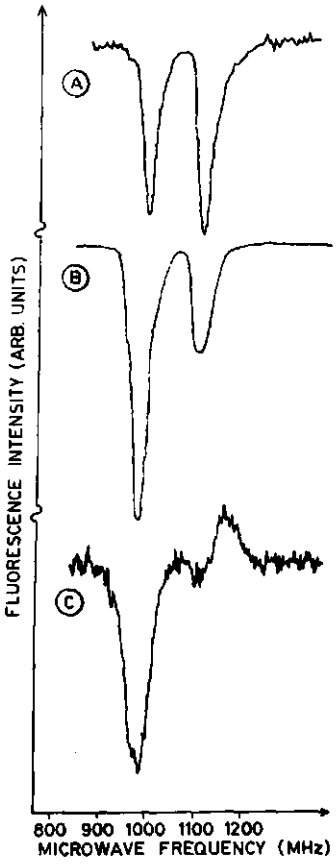

Figure 6.3.2.
Zero-field ODMR spectra of pheophytin-a (10^{-5}M) in n-octane at 4.2 K with fluorescence detection at (A) 667.5 nm, (B) 675 nm, and (C) 683 nm. Detection bandwidth 1 nm; excitation 375 - 475 nm. Spectra A-C have been recorded at different gain. Spectra A and B are the result of 2048 accumulations, whereas C represents 2^{13} accumulations. Sweep-rate: 1300 MHz per second; microwave-power input + 10 dBm.

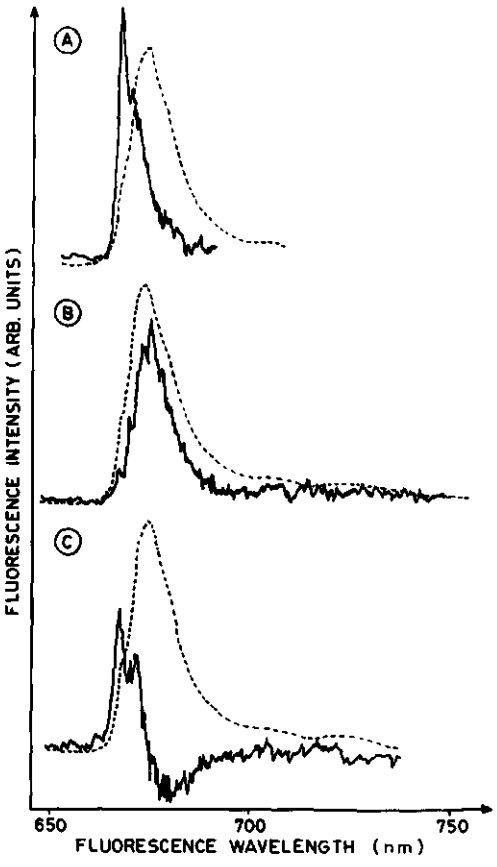

Figure 6.3.3.
Microwave-modulated fluorescence spectra (solid lines), detected by 18 Hz microwave amplitude modulation at 1110 MHz (A), 970 MHz (B), and 1142 MHz (C). Scanning speed 12.5 nm/min. Fluorescence detection bandwidth 1 nm. The dashed line represents the unmodulated fluorescence spectrum.

In a reverse experiment, amplitude-modulated microwave radiation, the frequency of which has been adjusted to a particular region of the ODMR spectrum, is applied to the sample. Using phase-sensitive detection of the fluorescence output at the modulation frequency, we obtain fluorescence spectra of Ph-a corresponding to a particular value of the triplet zero-field splitting. The results of three such experiments are shown in fig. 6.3.3, clearly demonstrating that the weak shoulder in the fluorescence spectrum at 667.5 nm corresponds to a species with ODMR transition at 1110 MHz (fig. 6.3.3.A). Similarly, other components of the fluorescence spectrum can be selectively enhanced by monitoring other regions of the ODMR spectrum (Figs. 6.3.3.B,C). Slow scanning speeds are required to prevent distortion of microwave modulated fluorescence spectra, occurring when the microwave modulation frequency is close to dI_f/dt, the rate of change of fluorescence intensity, when scanning through the fluorescence spectrum. The apparent negative sign of the microwave modulated fluorescence spectrum in the 680 nm region, shown in fig. 6.3.3.C, does not originate from such an instrumental artifact, but is of course related to the opposite sign of the ODMR transition marked with 3 w.r.t. the transitions 1 and 2 (see fig. 6.3.1). Distortions can be almost completely avoided at a scanning speed of 12.5 nm/min. and a modulation frequency of 18 Hz; of course, these numbers cannot be considered to be generally valid, since they depend on the shape of the fluorescence spectrum, the kinetics of the triplet state, and the desired resolution of the microwave modulated spectrum.

Our results provide evidence that both the fluorescence spectrum and the ODMR spectrum are inhomogeneously broadened, the emission maxima occurring at 667.5, 675, and 683 nm, corresponding to pairs of ODMR transitions at $990\pm5/1110\pm5$ MHz, $970\pm5/1120\pm5$ MHz, and $960\pm5/1160\pm20$ MHz.
In order to decide, whether the inhomogeneous broadening of the fluorescence spectrum results from different forms of Ph-a aggregation or from different environments, we increased the amount of ethanol in the n-octane solution. This results in a relative increase of the 675 and 683 nm bands at the cost of the 667.5 transition, indicating that the red-shifted transitions are associated with Ph-a in a more polar environment. Since ethanol is sufficiently polar to cause disaggregation of Ph-a, the relative increase of the intensity of the fluorescence bands at 675 and 683 nm excludes the possibility that these bands arise from pigment in an aggregated state.

All ODMR transitions are from Ph-a since a control absorption spectrum of the n-octane solution after completion of the ODMR experiment completely agrees with published data of the pure compound [7]. Monitoring the fluorescence emission at one of the wavelengths corresponding to ODMR transitions labeled

A-C, and analyzing the timedependence of this emission when a saturating microwave pulse is applied at position 1, 2 or 3 in fig. 6.3.1, approximate values can be obtained for the radiationless decay constants of the individual triplet spinlevels. For the 667.5 nm species, these constants are found to be $k_i \sim 750$ sec^{-1}, $k_j \sim 1000$ sec^{-1}, $k_k \sim 90$ sec^{-1} with a relative error of 40%. At 675 nm these numbers show a roughly fourfold increase, whereas in the far-red wing of the fluorescence (720 nm), we approach again the values obtained at 667.5 nm. As will be discussed below in more detail, spin-lattice relaxation between spin levels contributes to the experimental decay constants.
Except for k_z, these constants were found to depend on the intensity of the exciting light. The values quoted above were obtained by extrapolating to zero light-intensity.

6.4 DISCUSSION

Considering an optical pumping cycle comprising S_0, S_1 and T_0 (see fig. 6.4.1), the fluorescence intensity during continuous optical excitation is given by

$$I_f = k_f \; S_1 \; = \alpha\{N - \; T_0 \;\} \tag{1}$$

where

$$\alpha \equiv \frac{k_f k_{exc}}{k_f + k_{ISC}} \tag{1a}$$

and the rate constants k_f, k_{ISC}, and k_{exc} are defined in the same figure; N, S_0 and T_0 denote the total concentration, and the concentration of ground- and triplet state molecules, respectively. All concentrations are expressed in number per unit volume.

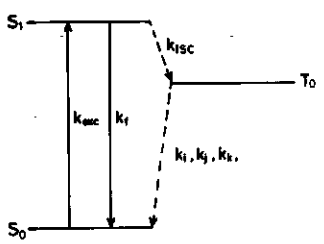

Fig. 6.4.1.
Optical pumping cycle, comprising groundstate S_0, first excited singlet state S_1, and lowest excited triplet state T_0; k_{exc} is the rate constant for optical excitation $S_0 \rightarrow S_1$, k_f is the radiative rate constant for fluorescence, k_{ISC} is the rate constant for $S_1 \rightarrow T_0$ intersystem crossing, and k_i, k_j, k_k are the total decay rates of spin states $|i\rangle$, $|j\rangle$, and $|k\rangle$ of T_0.

The spin states of the lowest triplet state T_0 are labeled $|m\rangle = |i\rangle, |j\rangle,$ and $|k\rangle$ and are non-degenerate for pheophytins lacking any symmetry. Fig. 6.4.2 depicts the situation for the lowest $\pi\pi^*$ triplet state of this compound. By analogy with planar aromatics [8], $|i\rangle$, $|j\rangle$, and $|k\rangle$ correspond to spins moving in the planes $x = 0$, $y = 0$, and $z = 0$, respectively, where x and y axes are arbitrarily oriented in the molecular plane and z is perpendicular to it.

By absorption of microwaves at a frequency $\nu^{mm'}$ resonant with the separation (in frequency units) between $|m\rangle$ and $|m'\rangle$, the concentration of triplets changes by an amount $\Delta\ T_0$, resulting in a change of fluorescence intensity

$$\Delta I_f^{mm'} = -\alpha\Delta\ T_0 \tag{2}$$

In the absence of SLR, it has been derived [9] that $\Delta\ T_0$ is given by

$$\Delta\ T_0 = -\alpha\ (k_i - k_j)\ (k_i + k_j)^{-1}\ (n_i^o - n_j^o) \tag{3}$$

for the transition ν^{ij}, where the decay constants k_i and k_j are defined in fig. 6.4.2, and steady state populations n_m^o are related to populating rates $IP_m\ S_0 \equiv P_m'$ and decay constants k_m by

$$n_m^o = P_m'/k_m\ (m = i,j,k) \tag{4}$$

where the superscript o symbolizes the absence of SLR, I denotes the intensity of the exciting light in dimensionless units, and P_m is the rate constant for populating spinlevel $|m\rangle$ in sec^{-1}.

In the presence of SLR, expressions analogous to (3) can be derived by solving the set of steady state rate equations for n_m of spin states $|m\rangle$, using the symbols k_m, P_m', n_m, and w as defined in fig. 6.4.2:

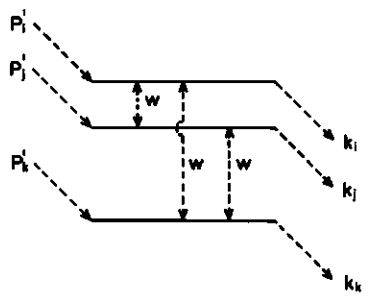

Fig. 6.4.2.
Decay rates constants k_i, k_j and k_k, populating rates P_i', P_j', P_k' and isotropic relaxation rate constants w for spinstates $|i\rangle$, $|j\rangle$, and $|k\rangle$ of the lowest excited triplet state T_0.

$$P'_m - (k_m + 3w)n_m + w \sum_m n_m = 0 \quad (m = i,j,k) \tag{5}$$

where we have made the simplifying approximation that $w_{mm'} = w$, i.e. all relaxation rate constants are taken to be equal. This also implies that $w_{mm'} = w_{m'm}$, thus we do not include Boltzmann equilibrium except in the high temperature limit, where the difference between $w_{mm'}$ and $w_{m'm}$ is the only factor determining the (very small) amplitude of the ODMR signals.

Before solving (5), we note that for unsubstituted dihydroporphin free base, which is a suitable model for the chromophoric group of pheophytin-a, $k_k \ll k_i, k_j$ and $P'_k \ll P'_i$, P'_j.
We distinguish three cases

(i) $w \ll k_i k_j$, w not $\gg k_k$

(ii) $w \gg k_k$

(iii) $w \gg k_i, k_j, k_k$ and $w_{mm'} = w_{m'm} \exp(-\Delta E_{m'm}/kT)$
where $\Delta E_{m'm} = E_{m'} - E_m$ and E_m, $E_{m'}$ denote the energies of spinlevels $|m\rangle$ and $|m'\rangle$,

and impose the conditions $n_i = n_k$ for the transition at D+E, and $n_j = n_k$ for the transition at D-E, in order to obtain the steady-state amplitudes of the zero-field resonance signals ΔI_f (D-E) and ΔI_f (D+E).

In case (i), straightforward algebraic manipulation of (5) with the condition $n_i = n_k$, $n_j = n_k$, respectively, leads to the following expressions at low excitation rate:

$$\Delta I_f(D+E) = -\alpha (k_k + 2w)^{-1} \{k_k(n_i^o - n_k^o) + w (n_i^o - n_j^o)\} \tag{6a}$$

$$\Delta I_f(D-E) = -\alpha (k_k + 2w)^{-1} \{k_k(n_j^o - n_k^o) - w (n_i^o - n_j^o)\} \tag{6b}$$

We note that both transitions for Ph-a have negative sign, implying n_i^o, $n_j^o > n_k^o$, provided $k_k < k_i$, k_j. If also $n_i^o > n_j^o$, ΔI_f (D+E) in the presence of SLR approaches $\frac{1}{2}\{\Delta I_f^o (D+E) - \Delta I_f^o (D-E)\} \equiv \Delta I_f^o$, as follows from (6a,b) and defining ΔI_f^o (D+E) and ΔI_f^o (D-E) as the amplitudes of transitions at D+E and D-E in the absence of SLR; ΔI_f(D-E) approaches $-\Delta I_f^o$ and thus changes sign with increasing SLR. If $n_i^o < n_j^o$, the behaviour of ΔI_f(D+E) and ΔI_f(D-E) is interchanged. Generally, it can be shown, that if D+E and D-E transitions have the same sign (either positive or negative) in the absence of SLR, the weakest transition will change sign, whereas the strongest transition does not, at an increase of w in the regime where $w \ll k_i, k_j, \gg k_k$. By comparison of these predictions with fig. 6.3.2.A-C we may conclude that for Ph-a in n-octane $n_i^o < n_j^o$, if SLR is respon-

exhibit ODMR spectra when dissolved in apolar solvents, such as n-octane. In view of the observed shifts of fluorescence spectra of photosynthetic compounds in polar solvents, it is plausible to assume in such solvents a strong electron-phonon coupling with the lattice, providing an effective SLR mechanism. It appears interesting to study SLR effects in the triplet state of molecules, which are expected to have a strongly anisotropic interaction with a polar solvent; such studies could provide valuable information about the direction and strength of solvent-solute interactions.

We want to make two concluding comments: firstly, there is an alternative explanation for the changes in the ODMR spectra observed when increasingly red shifted fluorescence bands are monitored. If either k_k would gradually decrease w.r.t. k_i and k_j, and/or P'_k would increase w.r.t. P'_i and P'_j, when one traverses the fluorescence spectrum in the direction of longer wavelength, the signs of $n_i^o - n_k^o$ and $n_j^o - n_k^o$, which determine the signs of the D+E and D-E transitions, respectively, might change. Such a change of decay constants and populating rates has no theoretical basis, however, and has not been found for kinetic constants of other photosynthetic pigments in polar glasses as determined by high field ESR [12]. Secondly we note that no mention has been made of the third transition at $\nu^{ij} = 2E$. As is found for all photosynthetic pigments studied sofar [15] $k_i, k_j >> k_k$. Then from (3) it is clear that the factor $(k_i-k_j)(k_i+k_j)^{-1}$ can easily reduce the 2E signal amplitude below the detection limits of our apparatus.

Summarizing, we may conclude, that the combination of fluorescence emission and microwave absorption, such as is realized in fluorescence detected ODMR, and applied to the example of Ph-a in an n-octane host doped with ethanol, provides suitable means to distinguish between various chemically indistinguistable species. Introduction of polar solvent molecules near to the fluorescent solute causes a fluorescence redshift, common for $\pi\pi^*$ transitions, an increase of the frequency difference of the D+E and D-E ODMR transitions, and an increase of SLR rate. Microwave modulated fluorescence spectra obtained by monitoring particular ODMR transitions may be helpful for resolving a composite fluorescence band into its components, corresponding to various physically distinct species. An interpretation of optical and microwave shifts and their relation has been omitted from this report, since it is outside the scope of this study, and has been presented elsewhere for chlorophyll-a [11].

6.5 REFERENCES

1. M.A. El-Sayed in: MTP International Review of Science, Vol 3, Spectroscopy, ed. D.A. Ramsay (Buttorworths, London) 119-153.
2. M.A. El-Sayed, P.S. Tinti, and D.V. Owens, Chem.Phys.Lett. 6 (1970) 395-399.
3. H. Maki and J.A. Zuchlich in: Topics in Current Chemistry, Vol. 54, Managing ed. F. Boschke (Springer-Verlag, Berlin, 1973).
4. J.H.C. Smith and A. Benitez in: Moderne Methoden der Pflanzenanalyse. eds. K. Paech and M.V. Tracey (Springer Verlag, Berlin, 1955) 151-154.
5. E.C. Murray and R.N. Keller, J.Org.Chem. 34 (1969) 2234.
6. S.J. van der Bent, P.A. de Jager and T.J. Schaafsma, Rev.Sci.Instrum. 47 (1976) 117-121.
7. J.C. Goedheer in: The Chlorophylls, eds. L.P. Vernon and G.R. Seely (Academic Press, New York, 1966) 147-184.
8. J.H. van der Waals and M.S. de Groot in: The Triplet State, ed. A.B. Zahlan (Cambridge University Press, London, 1967) 101-132.
9. S.J. van der Bent and T.J. Schaafsma. Chem.Phys.Lett. 35 (1975) 45-50.
10. S.J. van der Bent, T.J. Schaafsma and J.C. Goedheer. Biochem.Biophys.Res. Comm. 71 (1976) 1147-1152.
11. R.P.H. Kooyman, T.J. Schaafsma and J.F. Kleibeuker, in press.
12. J.F. Kleibeuker, Thesis, Wageningen, 1977.
13. S.J. van der Bent, unpublished results.
14. J.F. Kleibeuker, private communications.
15. R.H. Clarke and R.H. Hofeldt. J.Chem.Phys. 61 (1974) 4582-4587.

CHAPTER 7

APPLICATION OF ODMR TO WHOLE ALGAE

7.1 INTRODUCTION

In section 7.3 of this chapter we present a reprint of our previously published paper on ODMR experiments on intact algae. This introduction contains some additional data and comments. On the basis of experimental results, represented in section 7.3.2, we have concluded that the observed signals originate from monomeric chlorophyll-a in antennapigment of photosystem I or II.

In a recent paper by Clarke *et al* [1] , after our experiments has been published, this conclusion was criticized, since the agreement between the ZFS values of the ODMR spectra of *Anacystis nidulans* and *in vitro* chlorofyll-a does not provide sufficient proof that we observe monomeric chlorophyll-a in the alga.

Following Clarke it cannot be excluded that we have observed the reaction center, provided it consists of a parallel pair of chlorophylls oriented as in Fong's model [2] , since exciton theory for a dimeric triplet predicts the ZFS values to remain unchanged w.r.t. those of the monomer, if both monomers have a plane-parallel orientation [1] ; on may add that this criticism only holds if there is no charge transfer between the chlorophylls in Fong's model since otherwise there will be a change of D and E values as compared to those of monomeric chlorophyll.

The fact that we can only observe the zero field signals by monitoring the fluorescence at 713 nm or longer wavelengths is an indication that the signals originate from aggregated chlorophyll [3] . Antenna chlorophyll arranged as in a recent model [4] should have reduced D values compared to *in vitro* monomeric chlorophyll, however. It is clear that further experiments are needed to clarify the exact source of our ODMR spectra in algae.

Concerning the 713 nm emission, there are some necessary comments to make. Firstly, it is not necessary that the triplet signal which we observe in a sample with fast energy transfer between chlorophyll molecules is originating from the triplet state of a molecule of which the fluorescence

is monitored. Secondly in the case of *Anacystis Nidulans* the ODMR spectrum was only observable in the presence of DCMU or dithionite, but for *Chlorella vulgaris* it was possible to observe an ODMR spectrum (although with lower S/N ratio) at 4.2 K without the addition of blocking agents. The reason for this different behaviour is as yet not clear. The fact, that for *Anacystis* signals are only observed in the presence of DCMU provides evidence however, that the signals do not originate from chlorophyll loosened from the algae by sample treatment as suggested by Clarke [1]. Such chlorophyll would not be sensitive for the presence of DCMU.

The ODMR line which we assign to pheophytin-a is not observed monitoring the fluorescence at 740 nm.

Almost simultaneously with our work Nissani *et al* [5] published results on high-field EPR on whole cells of *Chlamydomonas reinhardi*.

7.2 REFERENCES TO SECTION 7.1

1. R.H. Clarke, R.E. Connors, H.A. Frank, and J.C. Hoch, Chem. Phys. Lett 45 (1977) 523-528.
2. F.K. Fong, Appl. Phys. 6 (1975) 151.
3. T. Cotton, Thesis, Evanston, Illinois, 1976.
4. L.L. Shipman, T.M. Cotton, J.R. Norris, and J.J. Katz, J. Am. Chem. Soc. 98 (1976) 8222-8230.
5. E. Nissani, A. Scherz, H. Levanon, Photochem. Photobiol. 25 (1977) 93-101.

7.3 DETECTION OF TRIPLET STATES IN ALGAE BY ZERO-FIELD RESONANCE

Sievert J. van der Bent,* Tjeerd J. Schaafsma,* and Joop C. Goedheer**

*Laboratory of Molecular Physics, Agricultural University,
De Dreijen 6, Wageningen, The Netherlands and
**Biophysical Research Group, Physics Institute,
The State University, Utrecht, The Netherlands

Received June 22,1976

SUMMARY Triplet states have been detected and characterized by zero-field splitting parameters in Anacystis nidulans, Euglena gracilis, Porphyridium cruentum, and Chlorella vulgaris, using fluorescence-detected magnetic resonance in zero-field at 4.2 K. Monitoring the 720 nm photosystem I emission, transitions between triplet spin levels have been assigned to antenna chlorophyll of one of both photosystems; photochemical reactions of chlorophyll are observed in the presence of an inhibitor and strong light, probably resulting in photoreduction and pheophytinization.

7.3.1

INTRODUCTION Triplet states have been detected in several photosynthesizing organisms (1-4) using magnetic resonance methods. The recently developed method of FDMR (5,6) appears to be very suitable to study the primary processes in photosynthesis using the triplet state as an internal probe, by monitoring fluorescence bands assigned to different parts of the PSU. In contrast with singlet states, triplet states are perturbed by (short-range) magnetic- rather than electric fields, and thus reflect molecular properties of pigments in the PSU, more than environmental effects. Here we report FDMR experiments on four types of algae, (blue-green) Anacystis nidulans, (red) Porphyridium cruentum and (green) Chlorella vulgaris and Euglena gracilis. No FDMR signals were obtained for Synechococus cedrorum, Phaeodactylum tricornutum and Visscheria stellata.

METHODS Immediately before experiment, algae were suspended in ethyleneglycol/H_2O 2:1 mixture, forming a glass at 4.2 K by immersion into liquid helium. Blue light (400-525 nm) excites the sample by reflection from a

Abbreviations:
FDMR: fluorescence detected magnetic resonance in zero magnetic field.
PSU: photosynthetic unit

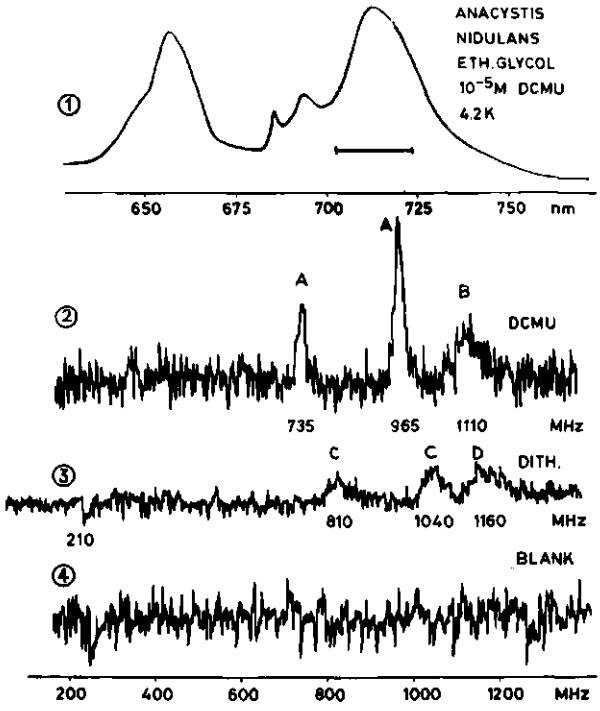

Figure 1 Surface-detected fluorescence spectrum of Anacystis nidulans in ethylene-glycol/H_2O 2:1 glass at 4.2 K in the presence of 10^{-5} M DCMU.

Figure 2 FDMR spectrum of Anacystis nidulans detected at 713 nm Chl fluorescence in the presence of 10^{-5} M DCMU. Detection bandwidth 40 nm.

Figure 3 FDMR spectrum of same alga with DCMU replaced by 10^{-3} M dithionite; other experimental conditions identical to those of Fig. 1,2.

Figure 4 Blank experiment of alga without blocking agent; other experimental conditions identical to those in Figs. 1-3.

dichroic mirror, transmitting fluorescence (> 600 nm) to an RCA 31034 photomultiplier cooled to -35°C, after passing through a .25 m Spex Minimate monochromator. Variable frequency microwave radiation was applied employing a helical slow-wave structure, surrounding the alga sample Fluorescence was monitored when the microwave frequency was swept through the 10-1300 MHz range. For further details, we refer to ref. 7.

7.3.2

RESULTS AND DISCUSSION If the main Chl- fluorescence band (see Fig. 1) of Anacystis nidulans at its maximum at 713.5 nm (with a 20 nm bandwidth) is monitored with microwaves swept from 10-1300 MHz, FDMR spectra were measured

as shown in Figs. 2, 3 if DCMU (10^{-5} M) or dithionite (10^{-3} M) was added before illumination. In the absence of inhibitors, no spectrum was observed (Fig. 4). Table I collects triplet state parameters of Anacystis and three other algae, in additon to those of some relevant compounds in vitro.

With Anacystis, four different types of FDMR spectra can be distinguished. In the presence of DCMU, and monitoring fluorescence at λ_F = 713.5 ± 20 nm, transitions A and B are detected, as shown in Fig. 2; at λ_F = 738 ± 20 nm, only A transitions are observed, whereas no resonances are found at λ_F = 660 nm (phycocyanineband) and λ_F = 685 and 694 nm (bands of P.S. II antenna Chlorophyll (8)). Thus, A and B transitions have a separate origin. It was concluded that resonances at 965 and 735 MHz correspond to D+E and D-E transitions of one and the same species A, whereas the broad transition at 1110 MHz is D+E of a different species B, the D-E transition of which is obscured by the D+E resonance of species A (9). Repeating the experiment with dithionite instead of DCMU eventually leads to disappearance of A and appearance of a similar, but displaced FDMR spectrum, with components C and D (Fig. 3). This may suggest that formation of species C occurs via the triplet state of A. Although the Chl 713 nm fluorescence decreases to roughly half of its original value during irradiation for ∿8 hrs, the species A resonances are completely replaced by B; this means that only those Chl molecules which are observable as triplets, are completely photo-transformed into species B. The latter one is tentatively assigned as photoreduced Chl.

With Chlorella in strong blue light illumination, FDMR spectra of type A were observed even in the absence of DCMU. Prolonged (∿8 hrs) illumination with blue light at 4.2 K and in the presence of DCMU, resulted in a super-position of type A and C transitions, whereas B and D resonances are absent when measured close to the 720 fluorescence maximum. With Euglena (+DCMU),

---

Chl = chlorophyll-a; DCMU = 3-(3,4-dichlorophenyl)-1, 1-dimethylurea; P.S. = photosystem.

Table I. ZFS parameters of algae triple states

Alga[a]		$\|D\| \times 10^4$ cm^{-1}[b]	$\|E\| \times 10^4$ cm^{-1}[b]
Anacystis nidulans			
	A	283	38
	B	348	21
	C	311	38
	D	366	20
Porphyridium cruentum		283	37
Euglena gracilis		297	37
Chlorella	A	288	38
	C	311	38
Chlorophyll-a in			
EtOH		287	36
Pheophytin-a in			
MTHF[c]		341	33

a. Measured at T = 4.2 K; b. ZFS parameters defined as $|D| = \frac{3}{2}|Z|$, $E = 1/2|X - Y|$, where X, Y, Z define energies of triplet spin states in zero magnetic field; c. MTHF = 3-methyltetrahydrofuran.

type A resonances were detected only in the early stages of the experiment, the final result being of the C type, but without D.

By comparison with in vitro ZFS values (Table I), the transitions A found in Anacystis are assigned to monomeric Chl, being part of the P.S. I or II antenna pigment, since reaction center Chl is expected to have smaller ZFS parameters due to spin delocalization in a special Chl pair or oligomer, analogous to bacterial reaction centers (1,2). Since no resonances are observed at 685 and 695 nm, known to be associated with P.S. II antenna

ZFS = zero field splitting

chlorophyll, whereas on the other hand these bands are enhanced by DCMU (10), further experiments should decide in which part of the PSU species A is located. Species B may be pheophytin-a, resulting from known photoconversion of Chl (11), in view of its in vitro ZFS parameters (Table I). In the presence of a strong reductant, such as dithionite, triplet state Chl (species A) may be photoreduced to a compound with unknown structure, emitting fluorescence at 620, 651 and 731 nm (12), and thus observable as species C in the monitoring fluorescence band (700 ± 40 nm in this experiment). If C is photoreduced Chl, it can be readily pheophytinized to D (12). Further work on isolated chlorophyll-protein complexes is in progress.

ACKNOWLEDGEMENT One of the authors (T.J.S.) thanks Dr. Govindjee for a stimulating discussion.

7.3.3

REFERENCES

1. Dutton, P.L. and Leigh, J.S., Reed, D.W. (1973) Biochim. Biophys. Acta, 292, 654-664.

2. Uphaus, R.A., Norris, J.R., Katz, J.J. (1974) Biochem. Biophys. Res. Commun., 61, 1057-1063.

3. Clarke, R.H., Connors, R.E., Norris, J.R., Thurnauer, M.C. (1975) J. Am. Chem. Soc., 97, 7178-7179.

4. Hoff, A.J., Van der Waals, J.H. (1976) Biochim. Biophys. Acta, 423, 615-620.

5. Van Dorp, W.G., Schaafsma, T.J., Soma, M., van der Waals, J.H. (1973) Chem. Phys. Lett., 21, 221-225.

6. Clarke, R.H., Hofeldt, R.H. (1974) J. Chem. Phys., 61, 4582-4587.

7. Van der Bent, S.J., de Jager, A., Schaafsma, T.J. (1976) Rev. Sci. Instr., 47, 117-120.

8. Papageorgiou, G. (1975) in Bioenergetics of Photosynthesis, Chapter 6, Acad. Press, New York, ed. Govindjee.

9. Van der Bent, S.J., unpublished results.

10. Goedheer, J.C. (1964) Biochim. Biophys. Acta, 88, 304-317.

11. Seely, G.R. (1966) in The Chlorophylls, Chapter 6, Acad. Press, New York, ed. Vernon, L.P. and Seely, G.R.

12. Gachkovskii, V.F. (1959) Biofizika, 4, 19-26 (Engl. transl: (1959) Biophysics, 4, 16-23).

APPENDIX I

In this Appendix, we define yields as used in Chapter 3; fig. 1 contains all relevant levels and is identical to fig. 3.2.1. of Chapter 3. The fluorescence yield $\phi_f(\ell)$ is defined as the number of photons emitted per second, divided by the number of $S_0 \rightarrow S_\ell$ ($\ell = 1,2,\ldots$) excitations per second *in the absence of T-T absorption*. We use the definition of parameters $I, I', k_{\ell\ell'}, n_\ell$ and states $|\ell\rangle$ from Chapter 3, if necessary labeled with spin index $m = i,j,k$. When the $S_1 \rightarrow S_0$ process is purely radiative, which is assumed to be valid in our case, we find

$$\phi_f(1) \equiv \frac{k_{21}n_2}{Ik_{12}n_1} \qquad \text{for } S_0 \rightarrow S_\ell \text{ excitation} \tag{1a}$$

Furthermore

$$\phi_f(2) \equiv \frac{k_{21}n_2}{Ik_{13}n_1} \qquad \text{for } S_0 \rightarrow S_2 \text{ excitation} \tag{1b}$$

We define the yield $\phi^m_{ISC}(\ell)$ as the number of molecules formed per second in the state $T_o|m\rangle$ divided by the number of $S_0 \rightarrow S_\ell$ excitations per second *in the absence of T-T absorption*. Assuming conservation of spin orientation w.r.t. the molecular frame during IC in the triplet manifold (i.e. taking all SLR rates in excited triplet states (except T_0) to be small compared to IC and ISC rates) it follows that

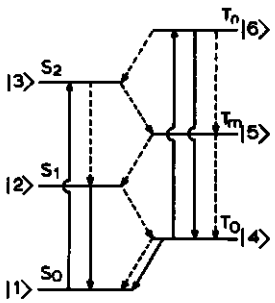

Fig. 1
Level diagram of the relevant singlet states S_0, S_1, S_2, triplet states T_0, T_m, T_n, and deactivation pathways involved in an optical pumping cycle; levels are numbered $|1\rangle$ through $|6\rangle$; fully drawn lines denote optically allowed transitions; dashed lines mark radiationless transitions

$$\phi^m_{ISC}(1) \equiv \frac{k^m_{24} n_2}{I K_{12} n_1} \tag{2a}$$

$$\phi^m_{ISC}(2) \equiv \frac{k^m_{24}\, n_2 + k^m_{54}\, n^m_5}{I k_{13}\, n_1} \tag{2b}$$

In order to eliminate the populations n_1, n_2, and n_5 from eqns. (1) and (2) we consider the steady state solution for eqns. (1a - f) from Chapter 3 with I' = 0 which for $S_0 \rightarrow S_2$ excitation are

$$- I k_{13}\, n_1 + k_{21}\, n_2 + k_{41}\, n_4 = 0 \tag{3a}$$
$$- (k_{21} + k_{24})\, n_2 + k_{32}\, n_3 + k_{52}\, n_5 = 0 \tag{3b}$$
$$- (k_{32} + k_{35})\, n_3 + I k_{31}\, n_1 = 0 \tag{3c}$$
$$- k_{41}\, n_4 + k_{24}\, n_2 + k_{54}\, n_5 = 0 \tag{3d}$$
$$- (k_{52} + k_{54})\, n_5 + k_{35}\, n_3 = 0 \tag{3e}$$
$$n_6 = 0 \tag{3f}$$

and analogue expressions for $S_0 \rightarrow S_1$ excitation

Where $k_{35} = \sum_m k^m_{35}$; $k_{24} = \sum_m k^m_{24}$; $k_{52} = \frac{\sum_m k^m_{52} n^m_5}{n_5}$; $n_4 = \sum_m n^m_4$; $n_5 = \sum_m n^m_5$,

and k_{46} is assumed to be spin-independent, since it corresponds to an optically allowed transition within a manifold of the same multiplicity. Combining eqns. (1c), (3b), (3c) and (3e) for ϕ_f (2) and following an analogous elimination of the populations n_1 and n_2 from (1a), we obtain

$$\phi_f(1) = \frac{k_{21}}{k_{21} + k_{24}} \tag{4a}$$

$$\phi_f(2) = \frac{k_{32} + \sum_m k_{35}\, k^m_{32}\, (k^m_{52} + k^m_{54})^{-1}}{k_{32} + k_{35}} \tag{4b}$$

Defining

$$\Delta\phi_f \equiv \frac{\phi_f(1) - \phi_f(2)}{\phi_f(1)} \tag{5}$$

this parameter can be expressed as

$$\Delta\phi^m_f = \frac{1}{k_{32} + k_{35}} \cdot \frac{k^m_{35} + k^m_{52}}{k^m_{52} + k^m_{54}} \tag{6a}$$

$$\Delta\phi_f \equiv \sum_m \Delta\ \phi_f^m \tag{6b}$$

The relation between $\Delta\phi_f$, $\phi_f(1)$, and $\phi_f(2)$ is given by

$$\phi_f(2) = \phi_f(1)\ .\ (1 - \Delta\phi_f) \tag{7}$$

$\Delta\phi_f$ represents a parameter describing the deviation from Vavilov's law which states that the fluorescence yield is independent of the excitation wavelength. In our case, a non-zero value of $\Delta\phi_f$ can only be caused by a difference in the total ISC rate to the triplet manifold for $S_0 \rightarrow S_\ell$ excitation and excitation, where $\ell = 1,2,3...;S_0 \rightarrow S_1$ (v) labels the electronically excited state and v denotes the vibronic state. Note that $\phi_f(\ell)$ can be also regarded as the probability of a molecule to decay from the state S_ℓ with the emission of a photon at the $S_1 \rightarrow S_0$ transition; the decay may involve $S^* \dashrightarrow T^* \dashrightarrow S'^*$ ISC processes, apart from IC within the singlet manifold.
From (1), (2), and (3a, d) we find

$$\phi_f(\ell) + \sum_m \phi_{ISC}^m\ (\ell) = 1 \tag{8}$$

This leads to

$$\phi_{ISC}^m\ (\ell) = \frac{k_{24}^m + \Delta\phi_f^m\ k_{21}}{k_{21} + k_{24}} \tag{9}$$

$\phi_{fT}^m(\ell)$ is defined as the probability for a molecule to decay from the state $T_\ell|m\rangle$ to S_0 via IC and ISC processes with emission of a photon at the $S_0 \rightarrow S_1$ transition;
$\phi_{ISC}^{mm'}(\ell)$ is defined as the probability for a molecule to decay from the state $T_\ell|m\rangle$ to $T_0|m'\rangle$ via IC and ISC processes; analogously $\phi_{TT}^m(\ell)$ refers to the transition $T_\ell|m\rangle$ to $T_0|m\rangle$ via IC processes only. Note that m,m' = i,j,k, From the steady state solutions of eqns (1a - f) in Chapter 3 it follows that

$$\phi_{fT}^{m}(\ell=m) = \frac{k_{52}^{m}}{k_{52}^{m} + k_{54}^{m}}\,\phi_f(1) \tag{11a}$$

$$\phi_{fT}^{m}(\ell=n) = \frac{k_{63}^{m}}{k_{63}^{m}+k_{64}^{m}+k_{65}^{m}}\,\phi_f(2) + \frac{k_{65}^{m}}{k_{63}^{m}+k_{64}^{m}+k_{65}^{m}} \cdot \frac{k_{52}^{m}}{k_{52}^{m}+k_{54}^{m}}\,\phi_f(1) \tag{11b}$$

$$\phi_{ISC}^{mm'}(\ell=m) = \frac{k_{52}^{m}}{k_{52}^{m} + k_{54}^{m}}\,\phi_{ISC}^{m'}(1) \tag{12a}$$

$$\phi_{ISC}^{mm'}(\ell=n) = \frac{k_{63}^{m}}{k_{63}^{m}+k_{64}^{m}+k_{65}^{m}}\,\phi_{ISC}^{m'}(2) + \frac{k_{65}^{m}}{k_{63}^{m}+k_{64}^{m}+k_{65}^{m}} \cdot \frac{k_{52}^{m}}{k_{52}^{m}+k_{54}^{m}}\,\phi_{ISC}^{m'}(1) \tag{12b}$$

$$\phi_{TT}^{m}(\ell=m) = \frac{k_{54}^{m}}{k_{52}^{m}+k_{54}^{m}} \tag{13a}$$

$$\phi_{TT}^{m}(\ell=n) = \frac{k_{64}^{m}}{k_{63}^{m}+k_{64}^{m}+k_{65}^{m}} + \frac{k_{65}^{m}}{k_{63}^{m}+k_{64}^{m}+k_{65}^{m}} \cdot \frac{k_{54}^{m}}{k_{52}^{m}+k_{54}^{m}} \tag{13b}$$

It can be shown straightforwardly that

$$\phi_{fT}^{m}(\ell) + \sum_{m} \phi_{ISC}^{mm'}(\ell) + \phi_{TT}^{m}(\ell) = 1 \tag{14}$$

Combining (1) and (11) the fluorescence intensity $I_f(\ell)$ is found to be

$$I_f(\ell) = Ik_{13}n_1\phi_f(\ell) + I'k_{46} \sum_{m} \phi_{fT}^{m}(\ell)\, n_4^{m} \tag{15}$$

The fluorescence intensity is now completely determined by experimentally accessible parameters Ik_{13}, $I'k_{46}$, n_1, n_4^m, $\phi_f(\ell)$, $\phi_{fT}(\ell)$.
We can make a further simplification based on the following argument: Under normal experimental conditions the rate of the optical excitation processes $S_0 \rightarrow S_2$ and $T_0 \rightarrow T_n$, as well as the decayrate of the $T_0 \dashrightarrow S_0$ process, are much smaller than all other ISC and IC processes, i.e.

$$Ik_{13},\ I'k_{46},\ k_{41} \ll k_{\ell\ell'} \quad (\ell\ell' \neq 41,13,46)$$

Then

$$n_\ell \ll n_1, n_4 \text{ for } \ell = 2,3,5,6 \tag{16}$$

and

$$n_1 + n_4 = 1 \tag{17}$$

to a high degree of approximation.
Therefore

$$I_f = Ik_{13}\,\phi_f\,(1-n_4) + I'k_{46}\,\sum_m \phi_{fT}^m\, n_4^m \tag{18}$$

In steady state, the sum of all rates leaving a particular spinstate $T_0|m\rangle$ equals the sum of all rates entering this state including SLR processes. Therefore we can write

$$\begin{aligned} 0 = {} & -k_m n_4^m - I'k_{46} n_4^m + \sum_{m'\neq m} w_{m'm} n_4^{m'} \\ & - \sum_{m'\neq m} w_{mm'} n_4^m + Ik_{13}\,\phi_{ISC}^m\,(1-\sum_m n_4^m) + \\ & I'k_{46}\,\phi_{TT}^m\, n_4^m + I'k_{46}\sum_m \phi_{ISC}^{m'm}\, n_4^{m'} \end{aligned} \tag{19}$$

When we sum over $m = i,j,k$ we get:

$$\begin{aligned} 0 = {} & -k_{41} n_4 - I'k_{46} n_4 + Ik_{13}\,\phi_{ISC}\,(1-n_4) \\ & + I'k_{46} \sum_m (\phi_{TT}^m n_4^m + \sum_{m'} \phi_{ISC}^{m'm}\, n_4^{m'}) \end{aligned} \tag{20}$$

Since eqn (14) is valid, we have

$$\sum_m (\phi_{TT}^m n_4^m + \sum_{m'} \phi_{ISC}^{m'm}\, n_4^{m'}) = \sum_m n_4^m - \phi_{fT}^m n_4^m$$

For sake of convenience we define $\bar{\phi}_{fT}$ by

$$\bar{\phi}_{fT} \equiv \frac{1}{n_4} \sum_m \phi_{fT}^m\, n_4^m \tag{21}$$

Note that $\bar{\phi}_{fT}$ is dependent on the presence of microwaves and light-intensity. We can solve eqn. (20) for the total T_0 population

$$n_4 = \frac{Ik_{13}\,\phi_{ISC}}{Ik_{13}\,\phi_{ISC} + k_{41} + I'k_{46}\,\bar{\phi}_{fT}} \tag{22}$$

Combined with (6), (10), and (18) we find:

$$I_f = \frac{Ik_{13}\,k_{21}\,(1-\Delta\phi_f)\,(k_{41}+I'k_{46}\bar{\phi}_{fT}) + Ik_{13}I'k_{46}\bar{\phi}_{fT}\,(k_{24}+\Delta\phi_f k_{21})}{Ik_{13}\,(k_{24}+\Delta\phi_f k_{21}) + (k_{21}+k_{24})\,(k_{41}+I'k_{46}\bar{\phi}_{fT})} \tag{23}$$

This is eqn. (6) from Chapter 3.

SUMMARY

In this Thesis the results of investigations on the lowest excited triplet state of photosynthetic pigments and some model compounds are presented, partly as reprints of published papers.
Most of the experiments are carried out using ODMR (Optically Detected of Magnetic Resonance), detecting microwave-induced changes in the populations of the spin states of the lowest excited triplet state, via induced changes in the fluorescence emission.

10^{-6}-10^{-7}M chlorin free base incorporated as a guest in a n-octane single crystal proved to be a very attractive model for the study of the zero-field-splittings and the decay rate constants of the lowest excited triplet state. Contrary to naturally occurring compounds such as pheophytins and chlorophylls, chlorin can be easily studied without effects of polar solvents and aggregation. Since chlorin has the same conjugation pathway as the chromophoric group of chlorophyll-a and b and the corresponding pheophytins, it is interesting to determine its properties.
As already has been found for porphin free base by other groups, chlorin exhibits photoinduced rotation of the two central protons at 4.2 K, but at a much slower rate than porphin. *In vitro* studies of pheophytins-a and -b have learned that the ODMR technique can be fruitfull in unraveling optical emission spectra of systems containing molecules in different solvated states, which have overlapping optical absorption and emission bands.
The results suggest a correlation between the red shift of the fluorescence emission and the spin-lattice-relaxation rate of molecules in polar environments. A exploratory study has been made of the application of the ODMR technique to *in vivo* photosynthetic systems such as intact algae. Although hindered by spin-lattice-relaxation at 4.2 K causing a poor signal-to-noise ratio, the technique is promising for the study of whole algae.
Since in biological systems both spin-lattice-relaxation and triplet-triplet absorption may cause difficulties in determining the kinetic constants of the lowest excited triplet state, a detailed computer analysis is made of the possible influence of these effects on the measured decay rate constants

and populating rates. This analysis indicates the importance of including higher excited singlet and triplet states into the optical pumping cycle for the understanding of ODMR results.

SAMENVATTING

In dit proefschrift worden de resultaten van onderzoekingen aan de laagste aangeslagen triplet toestand van fotosynthetische pigmenten en enige model verbindingen beschreven, deels als herdrukken van gepubliceerde artikelen.

De meeste experimenten zijn gedaan met ODMR (Optische Detectie van Magnetische Resonantie) waarbij veranderingen geïnduceerd door microgolven in de populaties van de spintoestanden van de laagste aangeslagen triplet toestand, via geïnduceerde veranderingen in de fluorescentie-emissie gedetecteerd worden.

10^{-6}-10^{-7}M chlorine vrije base ingebouwd als een gast in een n-octane één-kristal bleek een aantrekkelijk model te bieden voor de bestudering van de nulveld splitsingen en de vervalsnelheidsconstanten van de laagste aangeslagen triplet toestand. In tegenstelling tot in de natuur voorkomende verbindingen zoals die van het feofytine en chlorofyll-type, kan chlorine gemakkelijk bestudeerd worden zonder effecten van polaire oplosmiddelen en aggregatie, omdat chlorine hetzelfde conjugatie pad heeft als de chromofore groep van chlorofyll-a en b en de overeenkomstige feofytines, is het interessant om de eigenschappen ervan te bestuderen.
Zoals reeds door andere groepen gevonden voor porfine vrije base is heeft chlorine ook een licht-geïnduceerde rotatie van de twee centrale protonen bij 4.2 K, maar met een veel lagere snelheid dan porfine.

In vitro studies van feofytine-a en b hebben geleerd dat de ODMR techniek vruchtbaar kan zijn voor het ontrafelen van optische emissie spectra van systemen die moleculen bevatten in verschillende gesolvateerde toestanden, die overlappende optische absorptie en emissie banden hebben. De resultaten suggereren een verband tussen de roodverschuiving van de fluorescentie emissie en de spin-rooster-relaxatie snelheid van moleculen in een polaire omgeving.

Een verkennende studie is gedaan naar de toepassing van de ODMR techniek op *in vivo* fotosynthetische systemen m.n. intacte algen. Hoewel spin-rooster-relaxatie bij 4.2 K een slechte signaal-ruis verhouding veroorzaakte,

houdt de techniek beloftes in voor de studie van intacte algen.

Omdat in biologische systemen zowel spin-rooster-relaxatie als triplet-triplet absorptie moeilijkheden kunnen veroorzaken bij de bepaling van de snelheids constanten van de laagste aangeslagen triplet toestand, is m.b.v. computersimulaties een gedetailleerde analyse gemaakt van de mogelijke invloed van deze effecten op de gemeten verval- en bevolkingssnelheidsconstanten. Deze analyse wijst op het belang om hoger aangeslagen singlet en triplet toestanden mee te nemen voor het begrijpen van de resultaten van ODMR.

CURRICULUM VITAE

Na het slagen van het Gymnasium-β examen aan het Revius Lyceum te Doorn begon ik in 1966 met de studie wis- en natuurkunde aan de Rijksuniversiteit te Utrecht. In 1973 slaagde ik voor het doctoraal examen Experimentele Natuurkunde, met bijvakken Medische-fysica en Biofysica.

Sinds april 1974 ben ik als wetenschappelijk-assistent in dienst van de Landbouwhogeschool te Wageningen, waar ik onder leiding van Prof. Dr. T.J. Schaafsma aan het promotieonderzoek werkte dat geleid heeft tot het tot stand komen van dit proefschrift. Een deel van het onderzoek is gedaan in samenwerking met Dr. J.C. Goedheer, van de afdeling Biofysica in Utrecht, bij wie ik afstudeerde.

Tijdens mijn promotie onderzoek werd ik in de gelegenheid gesteld internationale congressen te bezoeken, waarbij over mijn onderzoek gerapporteerd is.